The SCARPE procedure

Conceptual design and validation of a continuous force mechanism to reduce post-operative pain in repair of Pectus Excavatum.

S.H.G. Ackermans

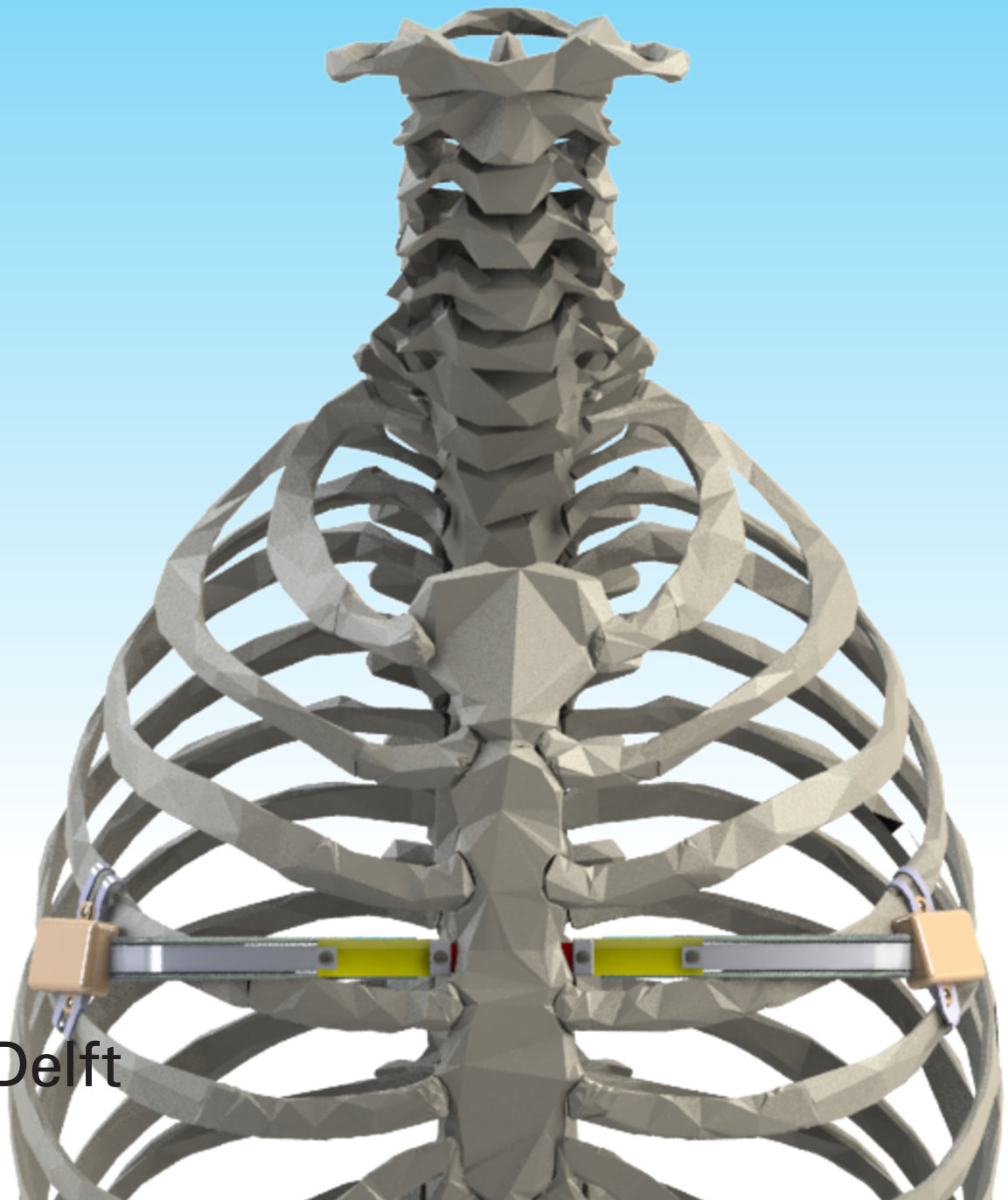

Delft University of Technology

TU Delft

The SCARPE procedure

by

S.H.G. Ackermans

to obtain the degree of Master of Science
at the Delft University of Technology,
to be defended publicly on Monday January 30, 2023 at 9:45 AM.

Student number: 4494733
Project duration: Februari 1, 2022 – January 30, 2023
Thesis committee:

Prof. dr. ir. P. Breedveld,	TU Delft
Dr. ir. G. Smit,	TU Delft
PJ. Van Huistee MD,	Haga Ziekenhuis

TU Delft

Preface

It has been a privilege to work on this master thesis. Together with Pieter Jan van Huijstee, a surgeon from the Haga Hospital in The Hague, we started a journey to developing something new. Something that has not been done before. I got the privilege of attending multiple of his surgeries in the OR. I would lie if I said that I was not a little scared at first. It felt like visiting a secret place, off-limits to the rest of the world. But I could only watch in awe, to see the ease and coordination of the medical staff performing surgery. And even in the back office, the amount of effort every doctor puts into every patient is enormous.

As a mechanical engineer one does not often get the opportunity to change a persons life. Engineering is often about making a bigger machine, more efficient usage or cheaper production. Therefore, I enjoyed it all the more to try and develop a more sophisticated device. I consider this thesis as my contribution to the health care system. It doesn't matter if this study is groundbreaking research, or just a simple step into the right direction. I hope my technical knowledge can one day improve the life of the people.

S.H.G. Ackermans
Delft, January 2023.

Abstract

Pectus Excavatum (PE) is a common deformity of the thoracic wall, characterized by a depression of the sternum. In the current golden standard for surgical correction of PE, the deformity is instantaneously corrected, causing severe and prolonged post-operative pain. The goal of this study is to design and validate a novel implant to slowly correct PE over time and minimize post-operative pain. A new procedure was developed called SCARPE: spring-loaded continuously actuated repair of pectus excavation. During the SCARPE procedure, an implant continuously applies a small force on the posterior surface of the sternum. The continuous force is just large enough to stimulate cartilage remodeling and correct the deformity in two years. The SCARPE implant uses two symmetrically located tape springs as force generator. A tape spring is a thin sheet of metal with a constant cross sectional radius. When subjected to sufficient bending, a tape springs starts to buckle and applies a constant bending moment. The resultant force can be controlled by adjusting the fold location of the buckled tape spring. Adjustments are non-invasively actuated by an external drive mechanism that creates a rotating magnetic field.

A proof-of-concept experiment was performed to investigate the force displacement relationship (FDR) of a tape spring mechanism in various conditions. It was found that the elevation force increased with spring size, number of layers and thickness. Furthermore, the FDR of the tape spring mechanism showed a unique curve for each fold distance, but was equal for the number of spring layers. Only the three layered tape springs, with layers fixed together, applied an average elevation force large enough to correct the PE deformity in two years. None of the tape spring configurations, however, could adhere to all requirements simultaneously.

Although the tape springs could achieve a constant force within the force boundaries, some challenges arose. Mainly, the small margin towards the lower force boundary, delamination and anatomical constraints pose a problem. In its current form, the SCARPE implant is not yet suited for clinical application, but is to be considered as a novel approach towards PE repair. Several recommendations are presented for optimization, as well as alternative design proposals for future research.

Contents

1 Introduction **1**

Introduction **1**

1.1 Pectus Excavatum . . . 1
1.2 Treatment of Pectus Excavatum . . . 1
1.3 Minimally Invasive Repair of Pectus Excavatum . . . 2
1.4 Alternative surgical approaches & drawbacks . . . 3
1.5 Goal of the study . . . 4
1.6 Structure of the paper . . . 4

2 Structural analysis **5**

2.1 Anatomical analysis . . . 5
2.2 Mechanical analysis . . . 5
2.2.1 Simplified model . . . 5
2.2.2 Load case . . . 6
2.3 Biomechanical analysis . . . 8
2.3.1 Cartilage remodeling . . . 8
2.3.2 Correction rate . . . 8
2.4 Progressive load case . . . 9
2.5 Force & displacement boundaries . . . 10

3 Design requirements **12**

3.1 Introduction . . . 12
3.2 Functional requirements . . . 12
3.3 Size & manufacturing requirements . . . 12
3.4 Clinical requirements . . . 12

4 Conceptual design **14**

4.1 Concept selection . . . 14
4.2 Mechanical analysis of tape springs . . . 16
4.2.1 Introduction . . . 16
4.2.2 Directional dependent behavior . . . 16
4.2.3 Steady state behavior . . . 17
4.3 Tape spring placement . . . 18
4.4 Tape spring as force generator . . . 18

5 Final concept **20**

5.1 The SCARPE procedure . . . 20
5.2 General layout . . . 20
5.3 Middle segment . . . 21
5.4 Fold distance control . . . 21
5.5 Actuation box . . . 22

6 Evaluation **25**

6.1 Proof-of-principle experiment . . . 25
6.1.1 Goal . . . 25
6.1.2 Variables . . . 25
6.1.3 Experimental setup . . . 25
6.1.4 Experimental procedure . . . 27

6.2 Experimental results . . . 28
6.2.1 Introduction . . . 28
6.2.2 Experiment 1 - Spring dimension . . . 29
6.2.3 Experiment 2 - Number of free layers . . . 29
6.2.4 Experiment 3 - Number of fixed layers . . . 30
6.2.5 Experiment 4 - Fold distance . . . 30
6.2.6 Experiment 5 - Hysteresis . . . 32

7 Discussion **33**
7.1 Experimental discussion . . . 33
7.1.1 Experiment 1 - Spring dimension . . . 33
7.1.2 Experiment 2 - Number of free layers . . . 33
7.1.3 Experiment 3 - Number of fixed layers . . . 33
7.1.4 Experiment 4 - Fold distance . . . 34
7.1.5 Experiment 5 - Hysteresis . . . 34
7.2 Bending moment . . . 35
7.3 Assessment of functional requirements . . . 35
7.3.1 Force bandwidth . . . 35
7.3.2 Adjustable correction rate . . . 36
7.3.3 Achieve & maintain full correction . . . 36
7.3.4 Failure safety . . . 37
7.4 Assesment of size & manufacturing requirements . . . 37
7.4.1 Maximum bar dimensions . . . 37
7.4.2 Maximum box dimensions . . . 37
7.4.3 Simplicity & producibility . . . 37
7.5 Assessment of clinical requirements . . . 37

8 Recommendations for future work **38**
8.1 Methods for increasing the elevation force . . . 38
8.1.1 Tape spring dimensions . . . 38
8.1.2 Alternative materials . . . 38
8.2 Asymmetrical PE correction . . . 39
8.3 Alternative force control mechanisms . . . 39

9 Conclusion **41**

A Usage of the SCARPE procedure **47**
A.1 Usage . . . 47
A.1.1 Post-operative adjustments . . . 49
A.1.2 Removal procedure . . . 49

B Iterations of the middle flexure **51**

C Validation of sample size **53**

D Matlab files **54**
D.1 Usage . . . 54
D.2 Import.m . . . 54
D.3 CentralFile.m . . . 56
D.4 Function Files . . . 56
D.4.1 ThickComp.m . . . 56
D.4.2 LayerComp.m . . . 58
D.4.3 WidthComp.m . . . 60
D.4.4 DistanceComp.m . . . 61
D.4.5 LoadComp.m . . . 63

E Experimental graphs **65**
E.1 Experiment 1 - Width . . . 65
E.2 Experiment 2 - Number of layers . . . 66
E.3 Experiment 3 - Number of fixed layers . . . 67
E.4 Experiment 4 - Fold distance . . . 67
E.5 Experiment 5 - Hysteresis . . . 68
E.5.1 Discrete measurements . . . 68
E.5.2 Continuous measurements . . . 70

F Force values **72**
F.1 Spring geometry . . . 72
F.2 Number of spring layers . . . 72
F.3 Fold distance . . . 73

G Including peak force in the force bandwidth **74**

H Alternative load case **76**
H.1 Alternative concept design . . . 76
H.2 Matlab scripts . . . 79
H.2.1 Pulltech.m . . . 79
H.2.2 ForcesBoia16m.m . . . 80

Nomenclature

Abbreviations

3MP	Magnetic mini-mover procedure
ESB	Equal sense bending
FDR	Force displacement relation
MIRPE	Minimally invasive repair of pectus excavatum
MOVARPE	Minor open videoendoscopically assisted repair of pectus excavatum
OSB	Opposite sense bending
PCHIP	Piecewise Cubic Hermite Interpolating Polynomial
PCPB	Progressively corrected pectus bar
PE	Pectus Excavatum

Definitions

Continuous correction	Correction of PE distributed over time in infinitely small steps. A constant force is imposed to the sternum
Gradual correction	Correction of PE distributed over time in finite steps. A displacement is imposed on the sternum
Instantaneous correction	Correction of PE performed instantaneously. A displacement is imposed on the sternum
Progressive correction	Correction of PE distributed over time. Can be both gradual or continuous correction but not specified which

Variables

α	Subtended angle	[rad]
δ	Instantaneous displacement	[mm]
δ_{min}	Minimal instantaneous displacement	[mm]
δ_{peak}	Instantaneous displacement after snap back	[mm]
λ	Distance between the fold and the supported end of a tap spring	[mm]
θ	Bending angle	[rad]
CR	Correction rate	[days/mm]
CR_{av}	Average correction rate at 10N	[days/mm]
d	Fold distance	[mm]
$F_{\perp}$	Perpendicular force	[N]
F_e	Elevation force	[N]
F_r	Reaction force of the thorax	[N]

F_{eq}	Equilibrium force after snap back	[N]
F_{max}	Maximal force boundary	[N]
F_{min}	Minimal force boundary	[N]
F_{peak}	Peak force	[N]
F_{step}	Step force during gradual correction	[N]
h	Corrected height	[mm]
h_{eq}	Equilibrium height after snap back	[mm]
h_{tot}	Total height to be corrected/pectus depth	[mm]
l_s	width of the sternum	[mm]
M	Bending moment	[Nmm]
M^*	Steady state moment	[Nmm]
M_+	Bending moment for opposite sense bending	[Nmm]
M_-	Bending moment for equal sense bending	[Nmm]
n	number of free stacked layers	-
n_d	number of days for total correction	[days]
n_t	number of fixed stacked layers	-
R	Radius of a tape spring	[mm]
r	arm length/effective length of the free end of a tape spring	[mm]
R_l	Longitudinal radius of the fold of a tape spring	[mm]
R_t	Transverse radius of a tape spring	[mm]
t	Thickness of a tape spring	[mm]
t_{total}	Thickness of a stack of fixed tape springs	[mm]

1 Introduction

1.1. Pectus Excavatum

Pectus Excavatum (PE) is the most common congenital anomaly of the thoracic wall, accounting for 87-90% of all chest wall deformities [1, 2, 3, 4]. PE occurs in roughly 1 in 300-1000 births and predominantely affects men with a ratio of 4:1 [1, 4, 5]. Already present at birth, PE characterizes in patients as a depressed sternum into the thoracic cavity (Figure 1.1). Disproportionately rapid growth of the cartilaginous section of the ribs (or costal cartilage) cause the sternum to extend inward. PE usually progresses during growth and noticeably worsens during the growth spurt in adolescent years. In mild cases of PE, patients can go their entire life without experiencing any discomfort. In moderate and severe cases, however, the depressed sternum causes a diminished ventrodorsal diameter of the thorax. As a result, the volume in the thoracic cavity decreases and patients may suffer from compromised pulmonary and cardiac function and chest pain [6, 7, 8]. Symptoms generally become most apparent during labor or exercise [8]. Moreover, the patient's divergent aesthetic may cause a reduced self-image, reduced psychosocial health and in some cases even lead to depression [9].

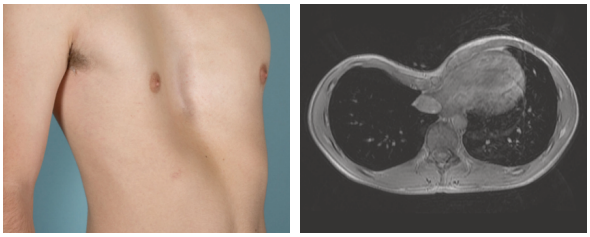

(a) *Picture of the external appearance of the thorax.*

(b) *CT-scan of the thorax at the deepest point of the deformity.*

Figure 1.1: *Adolescent patient suffering from Pectus Excavatum (PE), showing a depression of the sternum. [10]*

1.2. Treatment of Pectus Excavatum

In the past seventy years, a variety of treatment options have been developed to treat both the physiological and psychological symptoms of PE. Mild severity PE can be treated by sufficient exercise and posture program [11]or non-invasive treatment with, for example, the vacuum bell [12, 13, 14]. The vacuum bell is a cup shaped suction device that can be placed over the deformed sternum (Figure 1.2). With a small pump the air can be removed from the cup. The resulting negative pressure will generate a corrective force, pulling the sternum outward. Moderate and severe cases of PE are usually treated surgically. Presently, the two most widely applied surgical methods are the modified Ravitch procedure [15] and the Nuss procedure [16]. The latter is more generally known as minimal invasive repair of Pectus Excavatum (MIRPE). Both the modified Ravitch procedure and MIRPE force the sternum outward instantaneously during surgery and fix the sternum in the corrected position by a metal bar [17].

The Ravitch procedure was first introduced in 1949 by Mark Ravitch [18]. Modifications have been made in the decades thereafter to increase safety and satisfaction [15, 19]. In the Ravitch procedure, a long vertical incision is made over the sternum. The pectorales muscles are dissected to expose the costal cartilage. With a scalpel, the surgeon incises the perichondrium and carefully removes 4-5cm cartilage segments from the perichondrial sleeve in the ribs spanning the deformity [20]. After removal of the cartilage, the posterior side of the sternum is separated from the soft tissue. If the mobilization of the sternum is still insufficient, a wedge osteotomy is performed to alter the shape of the sternum itself. During a wedge osteotomy, a wedge is cut out of the sternum and the cut surfaces are sutured together. Finally, the sternum is fixated in the corrected

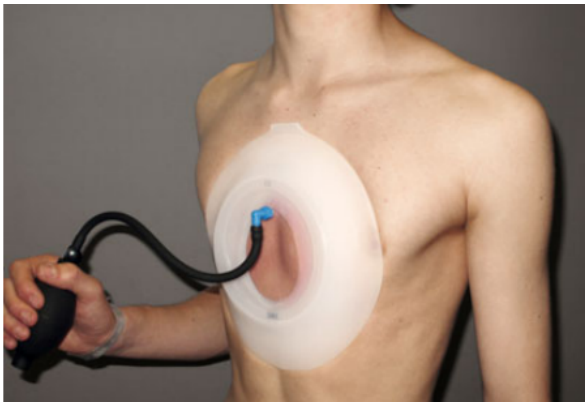

Figure 1.2: *Vacuum bell on the chest of an Pectus Excavatum (PE) patient [21]. The PE deformity can be corrected by creating a negative pressure in the suction cup with a hand pump.*

potition by a metal bar. The metal bar is left in place for at least a year, after which it is removed.

The modified Ravitch procedure is especially useful for treating PE in adults. During the aging process, the cartilaginous part of the ribs ossifies and becomes stiffer [22]. By resection of costal cartilage the thorax becomes malleable and is easier to correct [19]. As a result, post-operative stress in the thorax is reduced. Post-operative pain is mostly from healing of the wounds. Patients are discharged as early as three days after surgery. In spite of good results, the modified Ravitch procedure requires open surgery, which is prone to infection and other risks. Large visible scar tracts remain after surgery. Since PE surgery is partly cosmetic, this can be an eyesore for many patients.

1.3. Minimally Invasive Repair of Pectus Excavatum

In 1998 Donald Nuss published MIRPE as a less invasive alternative for correcting PE [16]. During MIRPE, a slender steel bar (so-called pectus bar) is curved along the desired circumference of the thorax (Figure 1.3). Two small bilateral incisions are made in the on either side of the thorax (Figure 1.4a). A third incision is made slightly inferior on the right to introduce a thoracoscope for video-assisted guidance (Figure1.4b). To improve sight, surgeons often deflate the right lung and induce an artificial pneumothorax. Before the pectus bar is implanted, a substernal tunnel is made using an introducer (Figure1.4c). The introducer is a long rigid long tool with a handle on one side and a slight s-curve on the other. The tip of the s-curve is relatively sharp to penetrate the fascia. The introducer enters on the right side of the thorax. The introducer travels subdermally, but only enters the thoracic cavity slightly medial of the highest point of the deformity. The tip is then forced through the fascia point down. The introducer slowly advances splitting the soft tissue from the sternum.

Figure 1.3: *Pectus bar curved conform to the desired circumference and placed on top of the thorax of a PE patient. [23]*

When the introducer exits the opposing incision, umbilical tape or a thorax drain is attached to the tip. The introducer is then carefully retracted, leaving the thorax drain in the substernal tunnel. The pectus bar is connected to the drain at the right side and pulled in place through the tunnel, the concave side facing anterior (Figure1.4d). The pectus bar is supported on the ribs at the entrance sites of the thoracic cavity. To finally correct the deformity, the pectus bar is flipped 180° from concave to convex using one or two bar flippers (Figure1.4e). The flipper is a surgical tool with a metal handle which slides on the ends of the pectus bar. Occasionally, the pectus bar-ends are slightly bent by the flippers to better suit the shape of the thorax.

Flipping the pectus bar forces the sternum outward, into the desired position, correcting the entire deformation instantaneously. Stabilizers are attached at the bar-ends to increase width of the pectus bar and prevent dislocation (Figure1.4f). Once the bar is in place, the thoracoscope taken out, the excess air is removed using an airlock and the incisions are stitched. The pectus bar is left in place for 2-3 years after which the bar is surgically removed. For long PE deformities or stiff thorax walls, multiple bars are implanted. Sometimes even up to four bars are required to obtain the optimal result.

Although MIRPE shows excellent results and patient satisfaction [24] and is less invasive compared to the modified Ravitch procedure, still post-operative pain is a major problem. Forces on

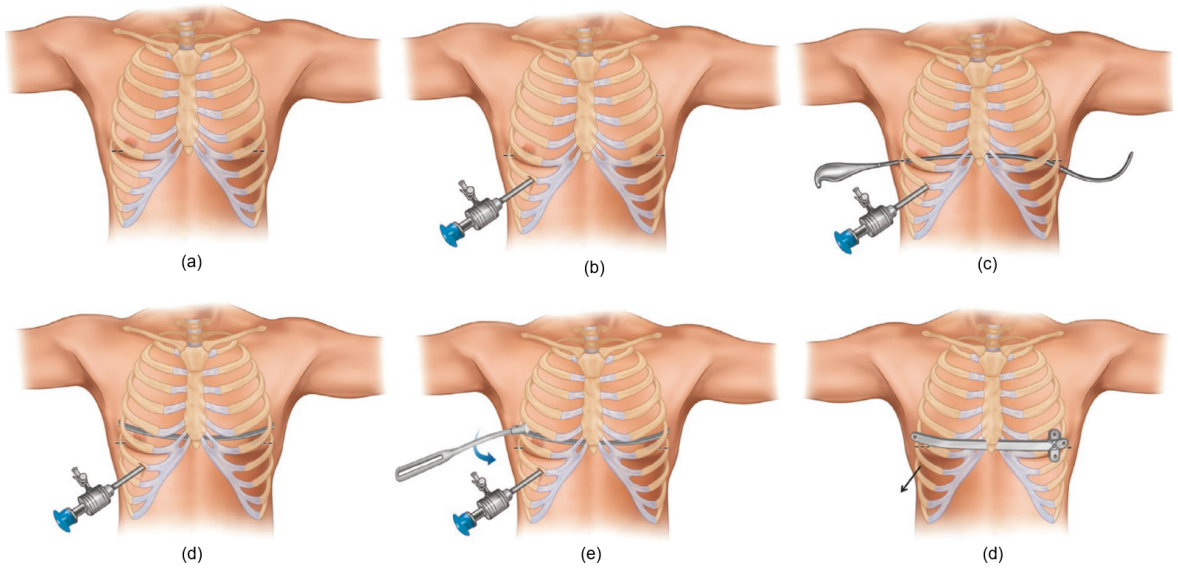

Figure 1.4: *Schematic procedure of minimally invasive repair of Pectus Excavatum (MIRPE) in steps [20]. (a) Two small bilateral incisions are made along the dashed lines. (b) A third incision is made slightly inferior to the right incision to introduce a thoracoscope. (c) An introducer is moved from right to left to make a substernal tunnel. (d) A curved pectus bar is pulled in the substernal tunnel, concave side facing up. (e) The bar is rotated 180°. Convex side facing up. (f) One or two Stabilizers are fixed to the pectus bar to prevent dislocation. The thoracoscope is removed and all the incisions are closed.*

the pectus bar create large stresses in the thoracic wall [25]. This stress is experienced by the patient as severe and long-lasting pain. On average, patients stay hospitalized for 5 days, mainly to apply epidural analgesic for pain management. But depending on the patient, hospital stay can range anywhere from 3 to 10 days [1, 16, 26, 27]. Older patients tend to stay longer because of a more rigid thorax [27]. During recovery, it takes up to 2-3 weeks before patients may return to school or work, 4-6 weeks before resuming normal routine and light sporting activities and 8-12 weeks before lifting heavy objects and participating in competitive sports [28, 29]. Chest pains can be persistent for an even longer time. Kim et al. documented 54% that of adult PE patients experience pain up to 6 months after surgery [30]. Therefore, it is desirable to perform MIRPE in children and adolescents, while the thorax is still malleable. The more stresses are applied to the thorax during correction, the more severe and prolonged pain the patient experiences.

1.4. Alternative surgical approaches & drawbacks

Although modifications have been made over the last two decades such as shorter bars, new surgery tools and smaller incisions, MIRPE still remains largely unchanged. The problem of MIRPE is best described by this quote by researchers Jashidi and Harrison (2007): ”clearly, the existing solutions to the problem are inadequate and a new treatment is required: one that is less painful and less radical.” [31]. In current advances, researchers try to combine MIPRE with a strategy for reduction of post-operative pain. In general, post-operative pain in PE can be mitigated using one of three strategies.

1. Suppressing the pain experienced
2. Reduce stress in the thorax by resection
3. Replace the instantaneous correction with a series of smaller corrections

The first strategy is the strategy currently applied in MIRPE. Physicians try to suppress post-operative pain with heavy analgesics. The epidural administration of medication is the primary reason for the long hospital stay after surgery. As an alternative, a recent study proposes the use of neural cryoablation during MIRPE surgery to block the sensation to pain. Local freezing of nerve bundles above and below the pectus bar offer a temporarily pain relieve. Although use of cryoablation reduces hospital stay [32], there is no significant difference in the amount of epidural medication and pain severity. Using this first strategy is, therefore, only temporarily fixing the problem. Both epidural analgesics and cryoablation are effective at treating pain as a symptom, but are not solving the root of the problem.

The second strategy to reduce pain is applied now in open surgery during the modified Ravitch procedure. Del Frari and Schwabegger combined the Ravitch and Nuss procedure into an semi-open approach called minor open videoendoscopically-assisted repair of Pectus Excavatum (MOVARPE) [24, 33]. This hybrid procedure follows the same protocol as MIRPE, only before introducing the pectus bar, two additional incisions are made, presternally for males and submammary for females. Using these extra incisions, resection of the costal cartilage can be performed similar to the modified Ravitch procedure (Section 1.2). Removing costal cartilage reduces the effective stiffness of the thorax. When bar placement is now performed conform to MIRPE, post-operative stress of the thoracic wall is reduced, as well as both immediate and long-term pain [33]. In addition, satisfaction rates are higher with MOVARPE than with MIRPE [24]. The downside of MOVARPE are increased operative times due to a more complicated procedure. Furthermore, MOVARPE is more invasive because it requires more and longer incisions.

The third strategy is the application of gradual or continuous correction. Instead of correcting the entire deformity instantaneously, the correction is broken up into a series of smaller corrections performed over time. This strategy is, for example, applied in dental braces. By breaking up the instantaneous correction in steps, there is less strain on the costal cartilage per correction step. Therefore, the stress levels of the thoracic wall remain lower. A procedure that applies this strategy in PE is the magnetic mini-mover procedure (3MP) [31]. In this procedure, a permanent magnet is implanted anterior to the sternum. PE patients are instructed to wear a brace, housing several electromagnets. The correction is performed due intermittent bracing. The attractive forces between the internal and external magnets produce a correction force on the sternum. By limiting the strain in each correction, the pain experienced has been reduced significantly with the use of the 3MP. But, recent study trails have shown mixed results in terms of efficacy [34, 35]. Because of a small sample size, no control group and device breakage, studies of the 3MP could not show a significant difference between pre- and post-treatment pectus depth. Moreover, PE patients using the 3MP have to be committed to wearing a brace daily, which requires routine use even if experiencing discomfort.

To clarify some nomenclature used in the next sections, in this study the progressively corrected pectus bar (PCPB) was designed. *Progressive correction* is a stepwise correction over time and can be done by either finite sized steps (*gradual correction*) or infinitely small steps (*continuous correction*). The term progressive correction is used as contrast to the entire correction performed at once(*instantaneous correction*), but does not specify if the correction is performed gradual or continuous. If the type of progressive correction is specified, it will be stated as either gradual correction or continuous correction.

The third strategy seems the most promising strategy to apply in this study. Replacing the instantaneous correction in MIRPE by a series of smaller corrective steps allows for a more technical approach on post-operative pain management. Recent advancements such as 3MP show that progressive correction is possible. Still, treatment relies on external bracing and issues with efficacy remain.

1.5. Goal of the study

The goal of this study is to present the conceptual design of a novel progressive correction implant in order to reduce post-operative pain of PE repair, without need of external bracing. Moreover, we want to experimentally evaluate the conceptual design to draw conclusions about its feasibility. In consideration of time, this study is focused on the force application mechanism for gradual or continuous correction. The actuator and implantation procedure are treated in less detail.

1.6. Structure of the paper

In Chapter 2 an extensive analysis is performed and a simplified model for progressive PE repair is presented. Chapter 3 states a list of requirements, used during concept design. In Chapter 4 the best correction method is selected from gradual and continuous correction. Moreover an analysis of tape springs is presented in the selected concept. Chapter 5 presents the conceptual design of the SCARPE implant. In Chapter 6 the method for evaluation of the proof-of-principle experiments is given. The results of the experiments are presented in the same section. Chapter 7 presents a discussion of the experimental results. Furthermore, Chapter 7 contains a discussion to assess the final concept, according to the design requirements. In Chapter 8 some recommendations are stated for future research. Conclusions from the evaluation and discussion are presented in Chapter 9.

2

Structural analysis

2.1. Anatomical analysis

During MIRPE, the surgeon makes two incisions on the left and right side of the patient. During insertion, the pectus bar is guided through subcutaneous tunnel through the tissue layers of the thoracic wall. All the tissue layers present are shown in Figure 2.1. Entering through the right incision, the pectus bar first travels between the superficial fascia and the costal muscles and rib cage, until it reaches the entrance location (Figure 2.2a). The entrance location is located slightly medial of the highest point of the deformity (Figure 2.2b). The pectus bar enters the thoracic cavity through a hole in the costal muscles and the endothoracic fascia. Once inside the thorax, the pectus bar goes underneath the (deepest point of the) sternum through the pleural cavity in the anterior mediastinum. The pectus bar exits the thoracic cavity at the exit site on the opposite side of the thorax; medial of the highest point of the deformity. The final part of the tunnel is again underneath the superficial fascia over the ribs. At the left incision the bar emerges from the body.

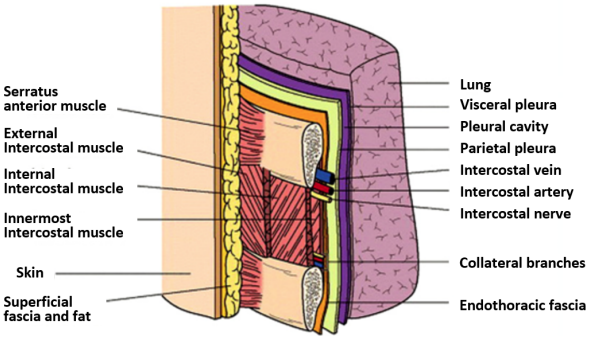

Figure 2.1: *Layers present in the thoracic wall [36].*

To correct the deformity, the bar is flipped in place. As a consequence, the sternum is forced outward by pressure on the anterior side of the sternum. The elevation force (F_e) of the pectus bar to the sternum is supported on the ribs at the highest points on both sides (Figure 2.3). The elevation force is a result of the strain on the costal cartilage. Because the stiffness of bone ($E = 11.5 - 15.7GPa$) [22, 25] is much larger than the stiffness of cartilage ($E = 5.5 - 17.7MPa$) [22, 25, 37], only the costal cartilage deforms during PE correction. The deformation in the bony segments of the ribs is considered negligible.

PE deformities come in all shapes and sizes. Each deformity ranges in length, width, depth, shape, asymmetry, steepness, flaring and location [38].Each PE deformity requires a different shape of the pectus bar [27]. With MIRPE, pectus bar curvature is determined by the surgeon in the operating room. A template is placed on the deformed thorax and curved in what the surgeon considers as the desired configuration. A straight steel pectus bar is curved according to the template using a table top bender. Often the bar is curved to result in a slight overcorrection to accomplish the best result. To design a device that is applicable to all different PE geometries may be troublesome and time consuming. In the scope of this thesis it was therefore decided to treat one simplified approach as a first approximation. Within the simplified model, the complex variety of deformities are generalised to represent one standard situation which can be evaluated in an experimental setting.

2.2. Mechanical analysis

2.2.1. Simplified model

In order to generalise all PE deformities, the anatomical situation is represented as a simplified model. In the simplified model we assume the device has only to respond to one standard situation. Before implementing the model, some assumptions are made. First of all, PE is treated as a two-dimensional problem. In the model we consider the deformity only in the transverse plane. Secondly, only symmetric deformities are considered. Although asymmetrical PE is

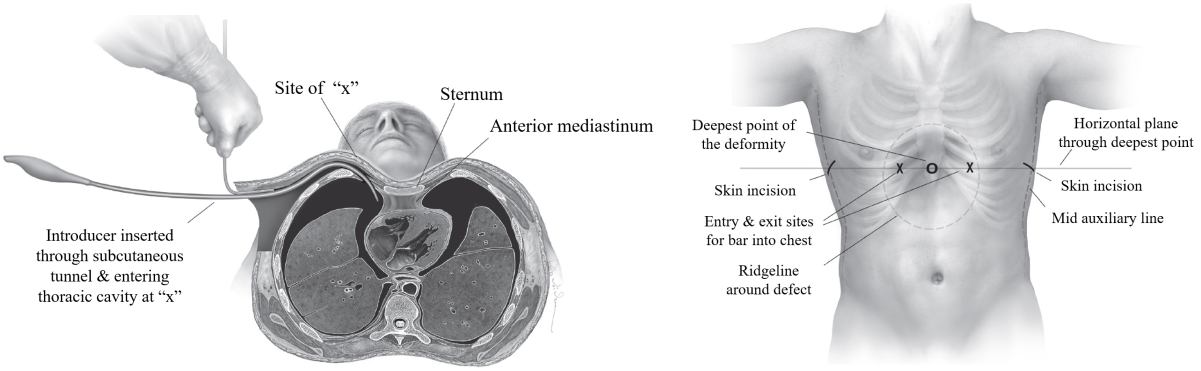

(a) *Anterior view of the thorax* (b) *Transverse view of the thorax*

Figure 2.2: *Drawings of important anatomical landmarks during tunnelling of MIRPE [11]*

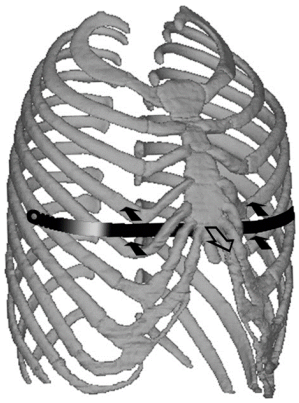

Figure 2.3: *Pectus bar in place with the induced forces on the thoracic cage [25]. The open arrow represents the elevation force F_e. the solid arrows represents the costal forces F_c.*

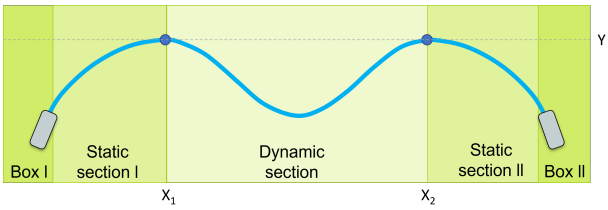

Figure 2.4: *Different sections of the pectus bar in the simplified model.*

not uncommon, the majority of thoracic wall deformities are classified as symmetrical PE (76%) [3]. Finally, the dimensional properties of the deformity are known. The choice of the dimensional properties is based on the median values determined by Coorens et al. [38]. The deepest point is located 40mm below the highest point. The width between the two high points is 140mm.

The pectus bar is modelled as a simple slender beam with a known curvature. The beam can be divided in three sections as shown in Fig. 2.4. The dynamic section is the section of the bar with an adjustable curvature that corrects the deformity. The dynamic section is located in the middle of the bar and should follow the shape of the thorax closely during correction. Located at either side of the dynamic section is a static section for which the length and curvature are fixed. The static sections having a fixed length entails the dynamic section to decrease in length, in order to follow the shape of the thorax during correction. The static sections supply stiffness to the implant. The different sections are separated at the support points X1 and X2. The support point is a representation of the position where the beam exits the thorax and is supported on the ribs. The x and y-coordinates of each support point are fixed.

In Figure 2.4 a box is depicted on both sides of the beam. This box houses the actuation mechanism to facilitate the elevation force of the dynamic section. The box is located outside of the static sections. The selection of the box is closely related to the working principle of the dynamic section and can therefore not be chosen freely. During the design of the PCPB, the actuation mechanism is initially considered a "black box". The black box can supply either a translation or rotation to actuate the beam, but the internal mechanism which produces this motion is left out of consideration. Only after the dynamic section of the beam is decided, the internal mechanism of the box will be chosen.

2.2.2. Load case

The elevation force F_e, is the force required to raise the sternum a certain distance δ. The bar is supported by the ribs at the points X1 and X2. To satisfy for equilibrium the support force F_s on either side is equal to $0.5F_e$. In reality the bar is often placed over two ribs on each side (Figure 2.3). Because of the symmetry of the standard

situation, the load case is also symmetric. The force on each rib F_c is, therefore, evenly distributed among the two ribs on each side.

$$F_e = 2F_s = 4F_c \tag{2.1}$$

[25] Three studies tried to quantify F_e during correction of PE. Fonkalsrud et al. [39] and Weber et al. [40] measured the forces required for elevation of the sternum. They attached a spring balance to the sternum during surgery and measured the force required for complete elevation. Boia et al. [41] modelled the force-displacement relationship (FDR) of PE based on experimental results. By pushing on the sternum of healthy children anterior to posterior, Boia et al. measured the force required for a certain displacement. Table 2.1 presents the elevation force for complete elevation in different age groups and genders, based on these three studies.

Table 2.1: *Mean of instantaneous elevation force (F_e) required for complete elevation of the sternum per age group and gender in different studies. * Complete elevation is considered as 30mm. ** only data for 15 and 16 years old.*

Author	Gender	Age				Unit
		<10	11-14	15-18	>19	year
Fonkalsrud[39]	Male	68.1	144.6	139.7	183.3	N
	Female	-	-	-	-	-
Weber [40]	Male	181			231	N
	Female	153			200	N
Boia* [41]	Male	97.0	104	175**	-	N
	Female	91.9	93.6	185**	-	N

Based on the values in Table 2.1 we can conclude that, just like PE deformity, F_e is patient specific. The FDR varies by factors such as age, gender, muscle mass and severity of PE. Even between the groups of each study large deviations could be seen. Because we are interested in progressive correction, the relationship between force and displacement is important in the behavior of the system. Boia et al. presented a model to describe the FDR of instantaneous correction of PE [41]. Boia et al. found that the FDR of the sternum can be represented as a second-order polynomial.

$$F_e = a_1\delta + a_2\delta^2 \tag{2.2}$$

Where δ is the displacement of the sternum and a_1 and a_2 are linear and quadratic coefficients respectively. These coefficients change linear with age (Figure 2.5). Using the model of Equation 2.2 and the coefficient values from Figure 2.5, the required elevation force can be found for PE patients of different ages. Figure 2.6 shows the FDR of different age groups. The PCPB should be able to perform

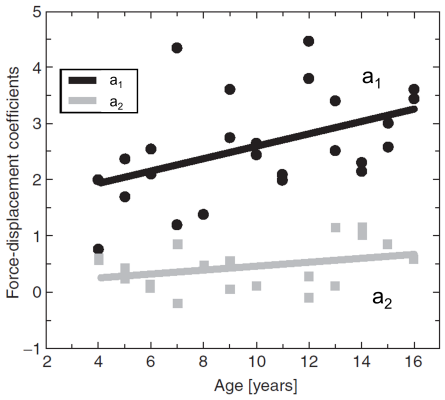

Figure 2.5: *The linear force-displacement coefficient (a_1) and quadratic force-displacement coefficient (a_2) plotted against patient age in males [41].*

corrections on all patients within the target group. Because the target group on whom MIRPE is generally performed are boys between 13-16 year [42]. Furthermore, the elevation force for female subjects is generally lower than for male; especially for small displacements. Therefore, the load case of a 16-year-old male is applied in this study.

It should be mentioned that the FDR changes after adolescent years. The ossification of the costal cartilage is stagnating, so the stiffness of the thorax is reaching a constant value. Stagnation of the stiffness is not taken into account in the model of Boia et al. (Equation 2.2) [41]. For example, we can linearly extend the coefficients a_1 and a_2 to represent a forty-year-old patient. Then a 40mm correction would require an elevation force of 500N (dashed line in Figure 2.6). But, according to the measurements of Weber et al. [40] full

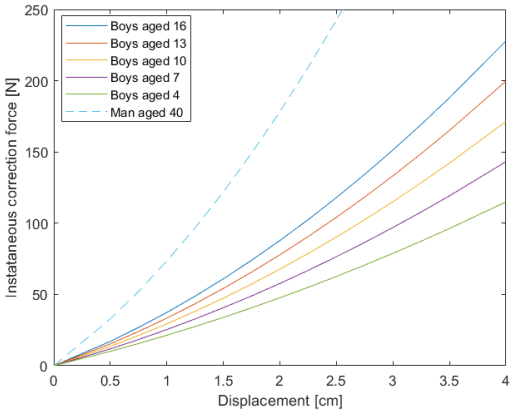

Figure 2.6: *Instantaneous force-displacement relationship (FDR) of the thoracic wall based on the model of Boia et al. [41]. This graph illustrates the effect of aging on the elevation force F_e.*

correction of a male adult only required 231N. The in-vivo measurements of Weber et al. are more likely to describe reality than the model in Equation 2.2. Therefore it can be concluded that Equation 2.2 is not applicable to adults. Nevertheless, the model of Boia et al. is a good first approximation of the FDR in children and adolescents. Still, the three studies quantifying elevation forces of PE performed measurements during instantaneous displacement. For progressive correction, the model needs to consider an extra unit not yet treated in literature: time.

2.3. Biomechanical analysis

2.3.1. Cartilage remodeling

In progressive correction of PE, a distinction can be made between gradual correction (in which a position is imposed to the sternum) and continuous correction (in which a force in imposed to the sternum). Both correction methods use bone remodeling to correct the thoracic wall over time. The relation to bone remodeling, however, differs slightly for the two correction methods. Both gradual and continuous correction could be used in the PCPB.

With gradual correction, an elevation force F_e, imposes a small displacement to the sternum. This displacement strains the costal cartilage and introduces internal stress in the cartilage. The stress results in a reaction force F_r, equal in magnitude and opposing to F_e. Initially, F_e has a damped elastic response to the displacement. Due to the visco-elastic properties, relaxation of the cartilage causes F_r decreases towards a lower steady state within minutes [43]. Both cartilage and bone have the tendency to evolve towards a stress free state [44]. In PE, the stress free state is reached by elevation of the sternum. In several weeks, the sustained stress, induced by F_e, slowly causes remodeling of the cartilage. Cartilage remodeling results in a decrease of F_r. The remodeling is complete when F_r reaches zero. This process is repeated for every step of displacement until complete elevation.

With continuous correction, the imposed F_e on the sternum is kept constant. The thoracic wall has to generate sufficient reaction force F_r to stimulate cartilage remodeling. Initially, F_e causes displacement of the sternum, until F_e and F_r find equilibrium. During remodeling of the cartilage, the stress in the thoracic wall, and thus F_r, tends to decreases. Because F_e is kept constant, the sternum continuously moves outward to preserve the force equilibrium and keep the stress in the thorax constant. After reaching the desired shape of the thorax, the force should be removed to prevent overcorrection. By use of continuous correction, the entire deformity can be corrected by subjecting the sternum to a small, but constant force.

2.3.2. Correction rate

The remodeling rate of cartilage must be known, in order to make an estimation on the number of required displacement steps (gradual correction), or the magnitude of the constant elevation force (continuous correction). The remodeling rate is the amount of time it takes for F_r to reach zero after a displacement step. The remodeling rate for costal cartilage is unknown and difficult to measure. The correction rate is a related parameter easier to measure; the average number of days per millimeter correction. To get an indication of the remodeling rate in PE, the correction rate of two PE repair procedures were studied: the vacuum bell treatment and the 3MP.

For example, during the vacuum bell treatment, the suction cup supplies a median negative pressure of 173-186 mbar [42]. That roughly translates to 259-276N. On average, applying the vacuum bell for 1.8 hours per day, a sternum depth of 27mm could be corrected in 20.5 months [13]. This equals an average correction rate of 23 days per mm at this elevation force.

In contrast, the 3MP used a substantially lower elevation force (43.7N) [31], compared to the vacuum bell. Replying to a question about duration of the correction, the inventor M. Harrison (2007) simply responded: ”We don’t know. ... Our best estimate from other ways to think about remodeling cartilage is a 6-month to 1-year range.” [17]. Wearing the brace for 16 hours per day and using the expected correction duration as mentioned by Harrison, would result in a correction rate of 5-10 days [34, 35].

Table 2.2 shows an overview of important characteristics for each procedure. Comparing the correction rate of the vacuum bell procedure with 3MP, it seems that the application time has a larger influence on the remodeling rate than the elevation force. Still, a large elevation force can increase the remodeling rate. Inasmuch as the PCPB will be operational 24 hours per day, the remodeling rate in this instance will be closest to the remodeling rate of the 3MP. Unfortunately, there is no data available to support the claim of Harrison on the correction time. In the latest study trail the magnet remained implanted for 24 months [34]. However, there is no documentation about time to complete correction or average pectus depth.

Therefore, a conservative value is taken for the

Table 2.2: *Procedural characteristics of the vacuum bell (VB)[42], the Magnetic mini-mover procedure (3MP)[31, 17] and minimally invasive repair of Pectus Excavatum (MIRPE)[40].*

	VB	MIRPE	3MP	unit
Elevation force	266-286	181	45	N
Application time	1.8	24	16	h/day
Correction time	20.5	24	6-12	months
Correction rate	23	18	5-10	days/mm

correction rate in this study. The correction rate is estimated to be in between the vacuum bell and 3MP. For a step size of 2.0mm (gradual correction) or a constant elevation force of 10N (continuous correction), the correction is assumed to be equal to 17 days/mm. Of course, changing the step size or elevation force would influence the correction rate.

2.4. Progressive load case

The elevation forces in progressive correction should be estimated to make a good approximation of the remodeling rate. Compared to the instantaneous correction during MIRPE, progressive correction has a clear advantage. During progressive correction the required elevation force is substantially smaller. The FDR for progressive correction is not yet modelled in literature. The forces for gradual and continuous correction can be defined based on Equation 2.2.

In order to determine the required elevation force for a gradual correction step, the FDR of instantaneous correction should be broken up in finite steps. A displacement δ is imposed in Equation 2.2. Starting at zero, the required F_e for each step is denoted by F_{step}.

$$F_{step,i} = F_{e,i} - F_{e,(i-1)} \tag{2.3}$$

Where i is the number of steps performed. To simulate weeks of cartilage remodeling, the graph was shifted downward to $F_e = 0N$ after one displacement step. Subsequently, an equal displacement step can be imposed starting from zero to find F_{step} for the second step. This process is repeated until complete correction is achieved.

The step force F_{step} increases linear with the displacement, because of the increasing stiffness of the thorax. As was illustrated in the FDR of the thorax (Figure 2.6), the stiffness profile is not purely elastic. During cartilage remodeling, the cartilage remodels to a stress-free state. Simultaneously, the cartilage remodels itself to increase the stiffness in the direction opposing the step force, to prevent future stresses.

Figure 2.7 shows F_{step} for three different step sizes. The increasing slope of F_{step} is dependent on the size of each step. It is suspected that the linear increase of F_{step} in reality has a smaller slope or could even be horizontal. Periodic cycles of loading cause the thorax to adapt to the correction. For example, in vacuum bell treatment the pressure to elevate the sternum 10mm was reduced by 55.6% after only three months of usage [42]. The costal cartilage becomes more compliant during correction and flattens the linear increase in F_{step}.

The size of each displacement step affects the remodeling rate. Taking smaller steps means more steps are required for the same correction and results in a longer correction time. Larger steps induce a larger strain on the cartilage and stimulate faster remodeling and positively influences the correction time. At the same time, taking larger steps increases F_{step}. Therefore, finding the optimal step size is a trade-off between force and correction time.

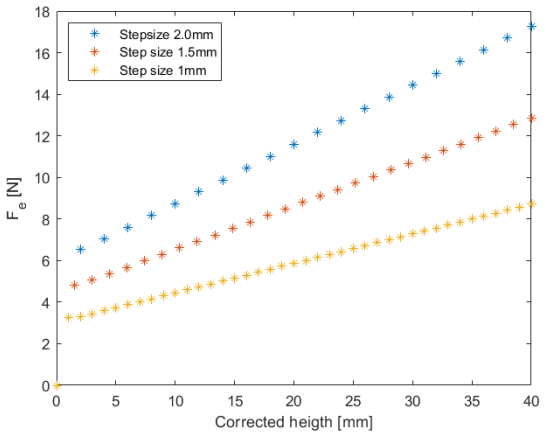

Figure 2.7: *Required step force for gradual correction of PE, based on different step sizes. Load case represents a 16-year-old male.*

In continuous correction F_e is constant, but the remodeling rate decreases during correction. The decrease is again caused by the increasing stiffness of the thoracic wall as is illustrated in Figure 2.6. With an increasing stiffness, a constant force causes the remodeling rate to decrease over time. Elevation of the sternum will happen more slowly as correction progresses. If F_e is chosen too low, a low correction rate would require the implant to remain implanted for several years, which is undesirable. It is, thus, important to choose F_e sufficiently large.

A prediction of the continuous correction rate of the sternum can be made using the same approach as for gradual correction. Figure 2.8 shows the decrease in δ for constant $F_e = 5N$ and

$F_e = 10N$. The decrease in remodeling rate can clearly be seen. In reality continuous correction does not displace the sternum in steps but results in a slow continuous displacement over time. The fitted line through the data points in Figure 2.8 presents the estimate of the correction rate for a continous correction. If continuous correction is used in the PCPB, the decreasing correction rate should be accounted for when choosing the magnitude of the constant elevation force.

The magnitude of the elevation force also influences the correction rate. The total correction time decreases when a larger constant force applied. For now, assume that the remodeling rate scales with the elevation force. Then comparing 5N with 10N, a decrease of 4.1% is found in total correction time. Similarly, doubling the elevation force yields a 4.3% decrease in total correction time (between 10N and 20N). Therefore, the correction rate decreases by approximately 4% over the relative change in elevation force. But as shown in Figure 2.8, the remodeling rate does not scale linearly with the elevation force. Instead, the remodeling rate relatively decreases compared to the increase in elevation force. The effect of the remodeling rate on the correction rate is estimated to be an additional 10%. The correction rate is predicted to decrease by 14% over the relative change in elevation force. The change in correction rate is used to determine the lower force boundary.

2.5. Force & displacement boundaries

The displacement step size or elevation force magnitude should fit within a certain bandwidth.

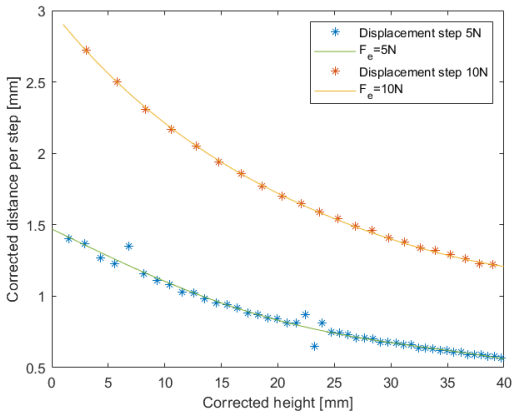

Figure 2.8: *A prediction of the decreasing correction rate as result of the chest wall subjected to a constant elevation force of 5N and 10N.*

For instance, during continuous correction, F_e should remain somewhat constant. Yet, whether this force is 0.5N more or less is indifferent for the patient. There are, however, boundaries to what forces are acceptable. For gradual correction, it is equivalent for a displacement bandwidth. The force and displacement bandwidths are on the upper boundary constrained by patient comfort and on the lower boundary by total treatment time.

When attempting to reduce post-operative pain, patient comfort is an important requirement for the upper force boundary. It is acceptable for the patient to experience some pressure during the procedure, but pressure should not result in pain. Pain tolerance in children and adolescents is once again patient specific. In the study trails of the 3MP, 86% of the patients occasionally experienced pain [34], with elevation forces of 45N. The upper force boundary should be significantly lower than the forces applied in the 3MP to prevent pain. Consequently, in this study, the maximum force value is set at $F_{max} = 20N$ for continuous correction. For gradual correction roughly translates to a maximum displacement step size of $\delta_{max} = 6.5mm$.

The lower displacement boundary δ_{min} and lower force boundary F_{min} are constraint by treatment time. The total treatment time may not surpass the treatment time of MIRPE; approximately three years [26, 45]. After full correction is achieved, the PCPB should remain stationary for one year to prevent relapse. Hence, the correction time is limited to two years. If the correction rate is too low, the implant is required to remain implanted for longer than is desirable. In addition, with a low correction rate it takes a long time until a patient experiences noticeable results of the surgery; negatively affecting patient satisfaction. The displacement or elevation force should be sufficiently large to ensure complete correction of the deformity within two years.

In calculation, δ_{min} and F_{min} are reliant on each other. The displacement boundary δ_{min} can be found by calculating the minimum required step size, to reach full correction within the maximum correction time of $n_{day} = 730days$.

$$\delta_{min} = \frac{h_{max} * CR}{n_{day}} \tag{2.4}$$

Where h_{max} is the pectus depth to be corrected in mm. The correction rate CR is dependent of the elevation force. To find the CR for F_{min}, we use the average correction at 10N: $CR_{av} = 17days/mm$ (Section 2.3.2). Next we relate CR_{av} to the relative change in elevation force.

$$CR = CR_{av}\left(1 + 0.14\frac{F_{min} - 10N}{F_{min}}\right) \quad (2.5)$$

Equation 2.5 is then substituted in Equation 2.4 to find the resulting expression for δ_{min}. Then to find F_{min}, the model for the FDR of PE is applied as in Equation 2.2.

$$\delta_{min} = \frac{h_{max}CR_{av}\left(1 + 0.14\frac{F_{min}-10}{F_{min}}\right)}{n_{day}}. \quad (2.6)$$

$$F_{min} = a_1\delta_{min} + a_2\delta_{min}^2 \quad (2.7)$$

The coefficients a_1 and a_2 relate F_{min} to patient age and gender, as depicted in Figure 2.5. Substituting Equation 2.6 in Equation 2.7 gives us the complete expression for F_{min}. The solution of the lower force boundary is found by iterative solving of Equation 2.7 for F_{min}. With a value for F_{min}, we can finally solve Equation 2.6 and determine the lower displacement boundary δ_{min}.

If the minimum correction time is known, the lower force boundary is completely determined by patient related parameters such as: age, gender and pectus depth. For this study we use the coeficients belonging to the target group of our simplified model (a 16-year old male with a pectus depth of 40mm). Solving results in the lower force boundary $F_{min} = 3.72N$ (for continuous correction) and the lower displacement boundary $\delta_{min} = 1.13mm$ (for gradual correction).

To include some margin the lower boundary, F_{min} and δ_{min} are be rounded up. In this study, the force bandwidth for continuous correction ranges from 4N to 20N. The displacement bandwidth for gradual correction ranges from 1.5mm to 6.5mm.

3

Design requirements

3.1. Introduction

This study describes the conceptual design of a progressive correction pectus bar (PCPB). The design of the PCPB should meet certain requirements. All requirements that are presented in this chapter are split into three categories: functional requirements, size & manufacturing requirements and clinical requirements. The functional and size & manufacturing requirements are used for assessment of several concepts during concept selection. The clinical requirements are taken into account for the final concept design. All requirement are used for validation of the PCPB.

Each requirement is based on key principles the PCPB should contain. The primary principle is of course to minimize post-operative pain. Furthermore, The PCPB should be suited for minimally invasive implantation and the treatment time must not exceed the maximum of three years. If adjustments are done during treatment, a physician should always be in control. Adjustments should also not introduce large internal stresses in the implant, because failure under large internal stress is a safety hazard.

3.2. Functional requirements

1. *Force and displacement bandwidth*. To adhere to the maximum treatment time, bandwidths of force and displacement are required. When applying gradual correction, the displacements must be within 1.5mm and 6.5mm. When applying continuous correction, the force may not exceed the bandwidth of 4N to 20N.
2. *Adjustable correction rate*. The correction rate should be controllable to increase or decrease the speed of the correction.
3. *Achieve & maintain full correction*. The deformity should be fully corrected to achieve an aesthetically pleasing result. To prevent overcorrection, the correction should be stopped once correction is completed and maintain that final position.
4. *Failure safety* Failure or breakage of the PCPB should not be hazardous for the patient.

3.3. Size & manufacturing requirements

1. *Maximum bar dimensions*. The cross-sectional dimensions of the bar should not exceed 13x3 mm. The size requirement is based on the current pectus bar to allow minimal invasive implantation. The length of the bar may vary depending on patient size.
2. *Maximum box dimensions*. The cross-section dimensions of the actuation box should not exceed 25x15 mm. The box is implanted subdermally, but does not enter the thoracic cavity. The dimensions can therefore be larger than for the bar. The length of the box is constrained to 40 mm.
3. *Simplicity & producibility*. The PCPB should be designed to be as simple as possible, as complex as necessary. Parts should be designed to be cheap and producible.

3.4. Clinical requirements

1. *Non-invasive adjustment*. When the adjustment of the PCPB is required during implantation, adjustments should be performed in a non-invasive manner.
2. *Malleability of the static section*. The PCPB should be suitable to a range of thorax shapes and sizes. The static section should be malleable to allow adaptability to different curvatures.
3. *Curve conformity* The dynamic section should follow the shape of the thoracic wall

during correction and cannot lose contact with the sternum.

4. *Materials fit for implantation*. Components in the PCPB should be suited for sterile operation, be non-toxic and allow safe actuation.
5. *No sharp or serrated edges*. Sharp or serrated edges could damage the soft tissue in the thorax and should be prevented.

4

Conceptual design

4.1. Concept selection

In order to explore the possible solutions for the design of the PCPB, the ACRREx method was used. ACRREx stands for Abstract, Categorize, Reflect, Reformulate and Extend [46]. The ACRREx method is a creative design method to explore a design space containing all possible solutions to the problem. The problem was described as *"Correction of the thoracic wall by a posterior to anterior force applied on the posterior side of the sternum"*. This problem description implies the concept should be a slender bar-like device placed behind the sternum for which a certain force application strategy (main group), results in a certain displacement deployment (subgroup). Some initial brainstorm sessions led to the design of several concepts. For each concept the working principle was defined. Then, each concept was appropriately categorized based on its working principle. From the resulting tree diagram, the voids were identified and filled with concepts that should fit inside the void. See Figure 4.1 for the final tree diagram. Three main groups were found, each with three subgroups.

The main groups, based on force application strategy, were:

- Instantaneously preloaded force
- Gradually preloaded force
- Continuous force

Each main group can theoretically be subdivided in three subgroups, based on displacement.

- Instantaneous displacement
- Gradual displacement
- Continuous displacement

From the nine subgroups, two were dismissed as they were considered impossible (*Gradually preloaded force → Immediate displacement* & *Continuous force → Immediate displacement*). The group Continuous force → Gradual displacement was dismissed as it would over-complicate the design. The resultant was three main groups, with six subgroups (Figure 4.1).

From the created design space the best strategy was selected for the design of the PCPB. Located on left side of the tree-diagram is the current golden standard, MIRPE. An instantaneously applied force directly results in a large displacement of the sternum. The large displacement is accompanied by large strain on the thorax. Moving from left to right in Figure 4.1, level of strain on the thorax decreases, as well as the intensity of post operative pain. The decreasing strain on the thorax could be considered as an increasing degree in desirability. Still, there was one more aspect to be considered from this tree: level of control. Gradual displacement had the highest level of control, compared to instantaneous and continuous displacement. A high level of control was interpreted in the high adjustability of the correction rate and the position of the sternum. A large potential strain was interpreted as the ability to minimize the displacement per ”step” (continuous displacement having infinitely small steps). In choosing the best design strategy, a correct balance should be found between potential strain and level of control.

Aside from level of control and potential strain, one more requirement was important in evaluating the concepts: safety. The safety of the concepts was assessed on the level of internal stress. Generally, application of the force should directly be followed by a displacement. Otherwise, the energy introduced in the PCPB through force application is be stored in the form of material stress. This could result in large internal forces in the PCPB. Breakage or failure of the PCPB accompanied by large internal forces is a safety hazard and could have severe consequences for the well being of the patient.

First, the concepts within each design strategy were evaluated. After, the design strategies

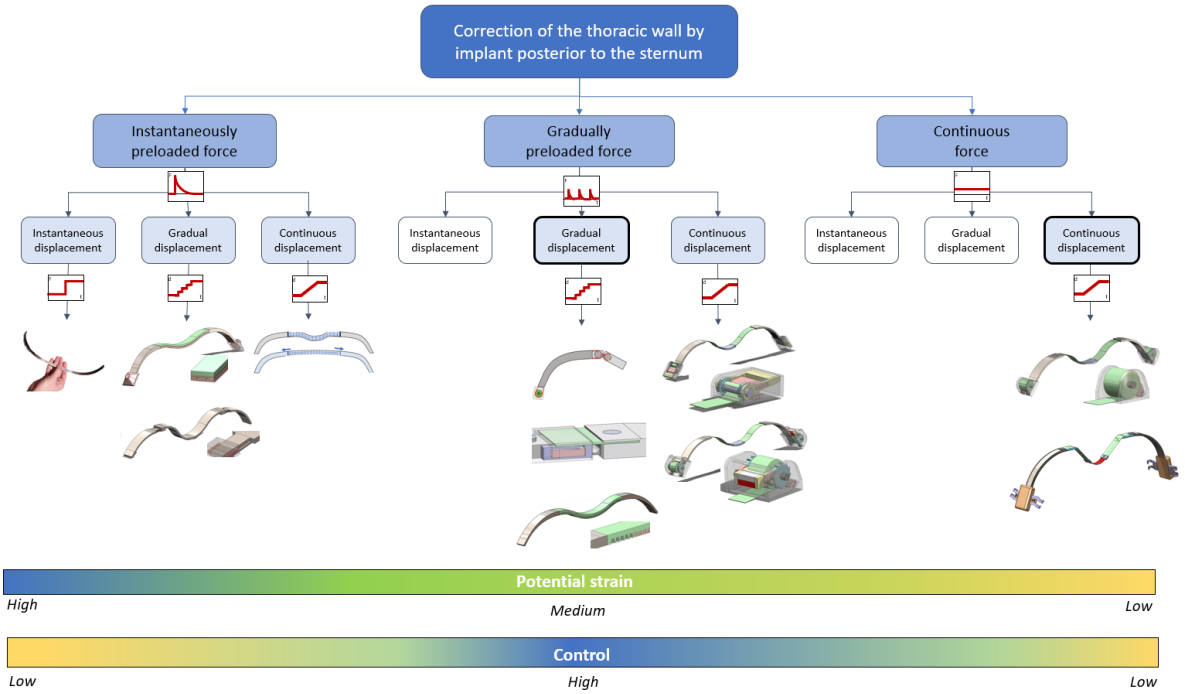

Figure 4.1: *Tree diagram creating a solution space. The red graphs present a schematic visual representation to make the diagram more intuitive. The pictures underneath each subgroup are categorised concepts.*

were compared with each other to select the best design strategy. The majority of the concepts were dismissed, because of high risk of internal stress. Only the concepts in the middle group and last group of Figure 4.1 remained. The two remaining groups are outlined in black. From these two remaining groups, the concepts were scored based on level of control and potential strain. The concepts in the *Gradual displacement* group had scored best, primarily on level of control. For potential strain the *Continuous displacement* group scored slightly higher, although the differences were minimal. Therefore, the concepts in the *Gradual displacement* group were explored further.

After a prolonged process of working on several detailed concepts, every concept in the *Gradually preloaded force* group was evaluated and eventually dismissed because it was not suited for PE correction. Many of the detailed concepts required large actuation forces, large currents, high temperatures or simply would not fit within the size requirement. Eventually, the decision was made to step away from the *Gradually preloaded force* group and reconsider the *Continuous force* group.

We tried to explore the possibilities of a continuous force mechanism for which, the magnitude of the force is controllable. The reason the *Continuous force* group was initially disregarded was the lack of control. Controllability is one of the functional requirements and must be present in the PCPB. By controlling the magnitude of the continuous force post-operatively, physicians have control over the correction rate, whereas the continuous force still results in a continuous displacement. During a search of springs with a controllable, constant force, we came across tape springs. A tape spring is most commonly applied in tape measures or carpenters tape (Figure 4.2). Tape springs have the ability to apply a constant bending moment, with a controllable resultant force. Therefore, continuous correction is selected as the most promising design strategy and tape springs are selected as constant force actuators in the PCPB.

Figure 4.2: *Tape springs are often used in tape measures.[47]*

4.2. Mechanical analysis of tape springs

4.2.1. Introduction

A tape spring is a special type of flexure with a constant transverse radius of curvature R_t. Tape springs have an unique set of properties suitable for continuous correction. The bending of a tape spring creates a fold with a constant longitudinal radius R_l. In the folded state (Figure 4.3a), the tape spring tends to return to the straight state (Figure 4.3b) with a constant bending moment M. The thickness t, transverse radius R_t and subtended angle α can be used as variables to influence the bending moment. Moreover, the bending moment remains constant independent of bending angle θ [48, 49].

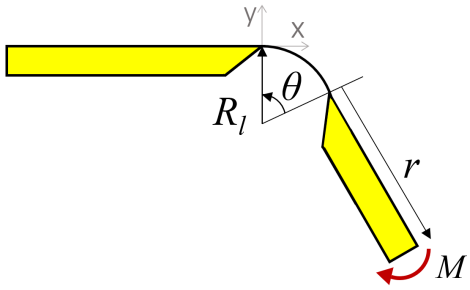

(a) *Folded state*

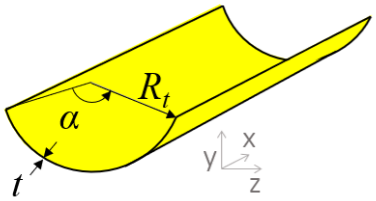

(b) *Straight state*

Figure 4.3: *Parameters of a tape spring.*

In this chapter we consider the situation in which one end of the tape spring is rigidly supported (supported-end), the other end is free and subjected to M (free-end). For low values of M, the tape spring initially deflects similar to a cantilever. The bending moment increases linearly with θ until, at a certain point, the tape spring snaps through, creating a localized fold. The snap through is similar to the buckling of a beam and is therefore often referred to as buckling [49].

In the folded state, the fold region and the straight region behave differently. The straight region of a tape spring is very stiff with respect to its t. In the straight region $R_l = 0$, and R_t is uniform. In the fold region the transverse radius R_t disappears. The fold region in the tape spring elastically deforms to $R_t = 0$, and an uniform R_l over the fold [50]. Material in the fold behaves more like a flat plate and becomes compliant. So as a result of the buckling behavior, a tape spring is compliant in the fold region, while the straight regions remain stiff.

The radius in the fold region remains constant during bending and is not influenced by θ. In a normal situation, with the fold away from supported-end, R_t and R_l are equal [49, 51].

$$R_t = R_l = R \tag{4.1}$$

4.2.2. Directional dependent behavior

After buckling, the relation between M and θ shows specific behavior, dependent on the bending direction. To explain the directional dependent behavior of a tape spring, the sign convention is important [51]. A positive applied bending moment (M_+) produces a fold on the opposite side of the transverse curvature of the tape spring. This is defined as opposite sense bending (OSB) (Figure 4.4a). Similarly, a negative applied bending moment (M_-) creates the fold on the same side as the transverse curvature. This is known as equal sense bending (ESB) (Figure 4.4b). When controlling the bending angle between the free-end and the supported-end, the required bending moment follows an unique pattern [49] as shown in Figure 4.4c.

With loading in OSB (blue curve), starting at O, the bending moment increases proportional with the bending angle until reaching the peak moment M_+^{max}. At this instance, buckling of the tape spring occurs (point A). The bending moment jumps to a lower steady state moment M_+^* at point B. After buckling, the steady state moment remains constant, even if θ is increased further towards point C.

Regarding controlled unloading in OSB (red curve), the bending moment is still equal to the steady state moment, even if the bending angle is decreased past point B. Snap back only occurs at point D, when the moment jumps back to the blue curve (point E). After snap back, the tape spring is in a deformed straight state without a fold. The different values of θ when buckling and snap back occur, show some energy has dissipated during the loading-unloading cycle. This hysteresis phenomenon provides self-locking in the straight state [48].

During loading in ESB the negative bending moment initially decreases, proportionally with the negative bending angle, through point O (green curve). The stiffness is equal to loading in OSB.

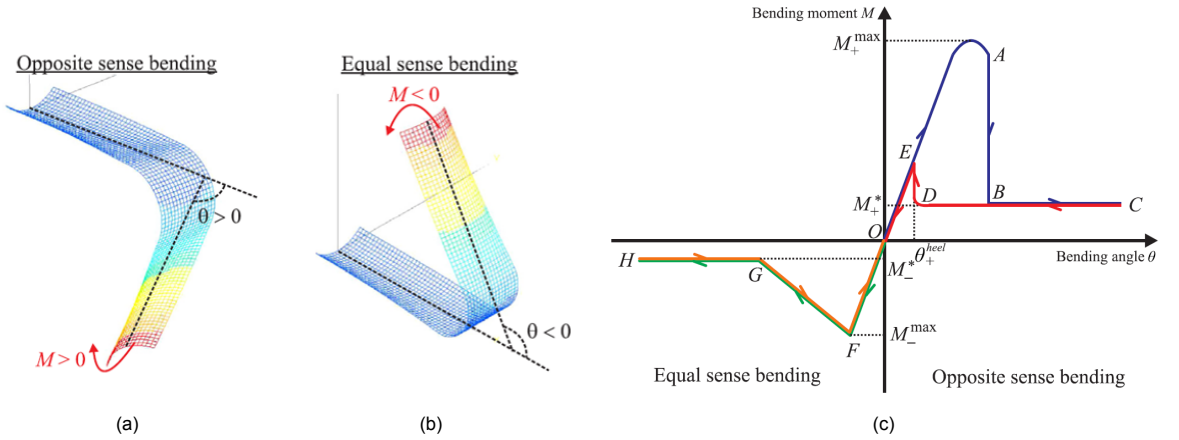

Figure 4.4: *Sign convention and behavior in the bending of tape springs [48]. (a) Buckling as a result of a positive bending moment is known as opposite sense bending. (b)Buckling as a result of a negative bending moment is known as equal sense bending. (c) The behavior of the bending moment has a direction dependent relationship with the bending angle [48]*

After reaching the peak force of ESB M_{-}^{max} (point F), the tape spring starts to buckle. However, the tape spring does not immediately form a complete fold. At first, two asymmetric torsional folds are formed. For decreasing values of θ, the two torsional folds grow larger and move toward each other, while $M_{-} < 0$ slowly decreases. When the torsional folds meet, the two torsional folds merge to form one symmetric longitudinal fold (point G). For all values of θ beyond point G, the moment remains constant at the steady state value M_{-}^{*}. Unloading in ESB (orange curve) is superimposed to loading.

4.2.3. Steady state behavior

The steady state behavior is most interesting for design of a constant force mechanism, because the bending moment remains constant. To make an estimation of the elevation force of a tape spring, we first derive an expression for the bending moment in steady state M^{*}. The same formula can be used for $M*$ in both OSB and ESB. In steady state the bending moment can be estimated by multiplying the bending stiffness of a tape spring D by the transverse arc length $R_t\alpha$ and the change in curvature from transverse and longitudinal curvature [50].

$$D = \frac{Et^3}{12(1-\nu^2)} \tag{4.2}$$

$$M^{*} = DR_t\alpha\left(\frac{1}{R_l} \pm \frac{\nu}{R_t}\right) \tag{4.3}$$

Where E is the Young's modulus and ν is Poisson's ratio. Substituting Equation 4.1 and 4.2 in Equation 4.3 results in the following expression for the steady state moment.

$$M^{*} = \pm\frac{Et^3(1 \pm \nu)}{12(1-\nu^2)}\alpha \tag{4.4}$$

The plus-minus signs uses '+' for OSB and '-' for ESB. The fact that M^{*} in Equation 4.4 can be determined independently of θ, confirms that M^{*} is constant in steady state.

The constant bending moment also shows that the fold has virtually zero stiffness. Moving the fold along the spring requires, thus, little to no force. An unconstrained fold can travel freely along the length of the tape spring, while the free-end stays subjected to M. The location of the fold and the bending angle can not be uniquely determined [50, 49] (Figure 4.5). Therefore, the steady state bending moment is not dependent on bending angle and fold location.

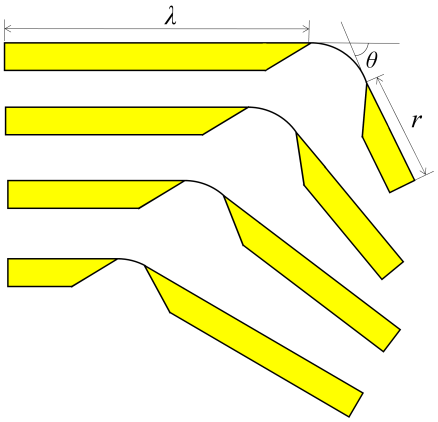

Figure 4.5: *Location of the fold and the bending angle θ cannot be uniquely determined because the fold has virtually zero stiffness*

At the supported-end, the transverse radius R_t of the tape spring is constrained. When a moving fold approaches the supported-end, the constrained R_t causes end-effects on the tape spring. As a result, longitudinal radius of the fold R_l becomes non-uniform. The fold radius on the supported-end r_1 is smaller than the fold radius on the free-end r_2 (Figure 4.6). The non-uniformity of the fold causes an inequality in bending moment between the two sides of the fold ($M_1^* < M_2^*$). Where M_1^* and M_2^* are the steady state bending moments subjected to end-effects, on the supported-end and free-end respectively. Within the PCPB, end-effects increase the bending moment applied on the sternum, when the distance λ between the fold and the support adheres to the following equation [49]

$$\lambda < 1.5R\alpha^2. \tag{4.5}$$

To ensure M^* stays constant during steady state behavior, the fold should be sufficiently far away from the supported-end. In some instances it may not be feasible to ensure λ is large enough to prevent end-effects. To minimize the end-effect, the supported-end of the tape spring should be clamped such that it constraints R_t minimally.

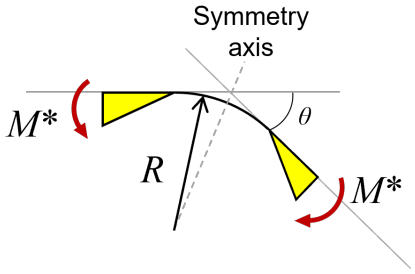

(a) *Uniform fold with constant R*

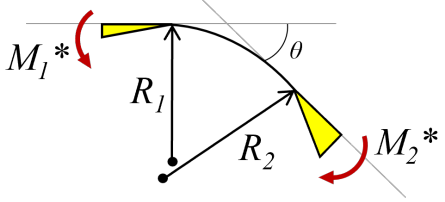

(b) *Non-uniform fold with $r_1 \neq r_2$*

Figure 4.6: *The fold of a tape spring. (a) As long as the fold is sufficiently far away from the supported-end (left in each the figure) the fold is uniform. (b) When the fold approaches the supported-end t he fold radius becomes non-uniform and the steady state bending moment becomes unequal*

4.3. Tape spring placement

In the conceptual design of a tape spring mechanism, the first design choice was to decide the optimal placement for the tape spring. In this study, OSB was preferred over ESB. Looking at Figure 4.4c, the steady state bending moment in OSB is larger than in ESB. This was confirmed by comparing the absolute value of M_-^* with M_+^* derived from Equation 4.4.

$$\left|-\frac{Et^3(1-\nu)}{12(1-\nu^2)}\alpha\right| < \left|\frac{Et^3(1+\nu)}{12(1-\nu^2)}\alpha\right| \tag{4.6}$$

Because the Poisson's ratio is always positive for materials used in tape springs and E, t, and α are equal on both sides of the equation, Equation 4.6 always holds. Therefore, the steady state bending moment in OSB is always larger than in ESB.

Moreover, the self-locking properties of OSB are beneficial after complete correction. Once correction is complete, a rigid bar needs to remain in place to prevent relapse of the sternum. Supporting the sternum after correction is equivalent to a retainer being placed after removal of dental braces [17]. Self-locking makes the tape spring become more stiff to provide support and stability to the thoracic wall. Utilizing snap back is only possible if the peak force stays within the force bandwidth. As long as the peak force is lower than the upper force boundary the patient should not experience pain during self-locking. Finally, the formation of torsional folds during ESB is undesirable. The torsional folds rotate the PCPB and could cause dislocation of the bar.

The formation of torsional folds also makes it unreasonable to produce the entire dynamic section from one long tape spring. If the long tape spring would go down underneath the sternum and up again to resurface from the thorax, the tape spring makes at least three folds. At least one of these folds is in ESB and forms a torsional fold. Therefore, it was decided to use two tape springs. One tape spring on each side of the deformity. Following the same line of thinking, each tape spring can only make one localised fold, as depicted in Figure 4.7. Other configurations, such as z-shaped folded tape springs, again introduce torsional folds. The two tape springs should be connected through a middle segment to support the sternum and prevent relative movement.

4.4. Tape spring as force generator

A variety of properties make tape springs very attractive for use in a medical implant. The self-locking and self-actuating properties, combined with low cost, no backlash, no required lubrication and no small parts, have already been utilized for compliant hinges. Currently, the primary

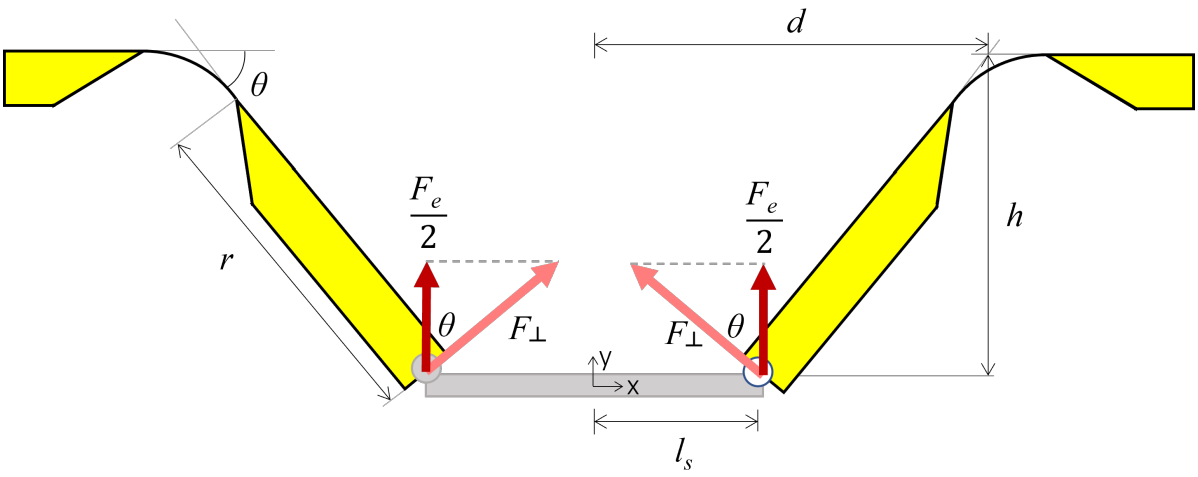

Figure 4.7: *Schematic drawing of a two tape spring mechanism symmetrically placed in the optimal orientation. All dimensions and forces are shown.*

use of tape springs in literature is in the field of deployable space structures [48, 52, 53, 54]. There is little described in literature about the use of a tape spring as force generator. To link the literature about PE (expressed as a force in newton) with the literature about tape springs (expressed as a moment in newton millimeter), the bending moment is expressed as a resultant force in newtons. The following expression is used to achieve this

$$F_{\perp} = \frac{M^*}{r}. \tag{4.7}$$

$$F_e = 2F_{\perp}cos(\theta). \tag{4.8}$$

Here, r is the effective length between the fold and the free-end and $F_{\perp}$ is the perpendicular force. The pependicular force is the resultant force, perpendicular to the symmetry axis of the transverse curvature. Equation 4.8 describes the summation of the projections of $F_{\perp}$ on the y-axis of each tape spring. Because we consider a symmetric situation, $F_{\perp}$ is equal on both sides and the projection of $F_{\perp}$ can be multiply by two. The bending angle θ is equal to the angle between F_e and $F_{\perp}$. Figure 4.7 shows all the parameters within the mechanism.

In Section 4.2 we proved that the steady state bending moment is constant irrespective of the fold location. As long as M^* is constant, $F_{\perp}$ is inversely proportional to the change of r. The length of r can be controlled by changing the location of the fold (Figure 4.5). The magnitude of $F_{\perp}$ can thus effectively be controlled by controlling the fold distance d.

Controlling the d does not only change r, but also the bending angle θ. In other words, by decreasing d, $F_{\perp}$ increases, but simultaneously decreases its projection on the y-axis. Therefore, the contribution of $F_{\perp}$ to F_e decreases. Especially large values of θ could be limiting the growth of F_e. The increase in $F_{\perp}$ is expected to be stronger than the decrease by its projection, but should be carefully investigated in a proof-of-concept experiment.

The full expression of is $F_{\perp}$ and θ are

$$F_{\perp} = \frac{M^*}{r} = \frac{M^*}{\sqrt{(d-l_s)^2+h^2}} \tag{4.9}$$

$$\theta = \quad arctan\left(\frac{h}{d-l_s}\right) \tag{4.10}$$

Where, h is the height until reaching complete elevation and l_s is half of the sternum width. Substituting Equation 4.9 & 4.10 in Equation 4.8 yields the complete expression of F_e

$$F_e = \frac{2M^*cos\left(arctan\left(\frac{h}{d-l_s}\right)\right)}{\sqrt{(d-l_s)^2+h^2}}. \tag{4.11}$$

As long as M^* is known, the elevation force can be entirely determined by geometrical parameters.

5

Final concept

5.1. The SCARPE procedure

The final concept presents the continuous correction implant of the SCARPE procedure. SCARPE stands for: Spring Continuously Actuated Repair of Pectus Excavatum. The SCARPE implant (previously stated as PCPB) uses two tape springs to exert a continuous and relatively constant force on the sternum, to correct PE. A schematic overview of the SCARPE implant can be seen in Figure 5.1. This chapter describes the detailed design of main components of the SCARPE implant and explains some of the design choices. See Appendix A for the surgical implantation, control and removal procedures.

5.2. General layout

The SCARPE implant uses two tape springs, one on either side of the deformity, placed conform to Section 4.3. Each tape spring only makes one fold in OSB. The tape springs are connected through a middle segment. A fold lever underneath the tape springs is used to impose the required fold distance. Together the tape springs, middle segment and fold lever form the dynamic section. On either side of the dynamic section is a bar-end connected. The lateral side of the tape springs are connected to the bar-ends using a clamp and fastened using a small bolt. The bar-end is a slender steel bar that is initially straight, but can be curved along the circumference of the thorax during surgery. The bar-ends are rigid to supply support to the SCARPE implant. Adjacent to the bar-ends runs a transmission that connects the fold lever to an actuator. The transmission together with the bar-ends forms the static section. The actuator is located in a casing and contains rib clamps on the sides. The actuator, casing and rib clamps together form the actuation box.

Since the effective length of a tape spring changes during correction, the lateral side of the tape spring should facilitate translation. The change in effective length during correction ranges from 4.5 to 7.6 mm per spring, depending on the fold distance. In order to comply with the change in effective length, each tape spring is connected to the rigid bar-end via a coil spring. The coil spring loads the tape spring in tension and allows passive displacement during the correction. The tension force of the coil spring does slightly increase the total elevation force. Inasmuch as the tension is perpendicular to the elevation force, its contribution is small and considered negligible, especially nearing the end of the correction. The function of the coil spring is purely to allow passive displacement during the correction.

Clamping the tape spring spring could influence the elevation force due to end-effects.

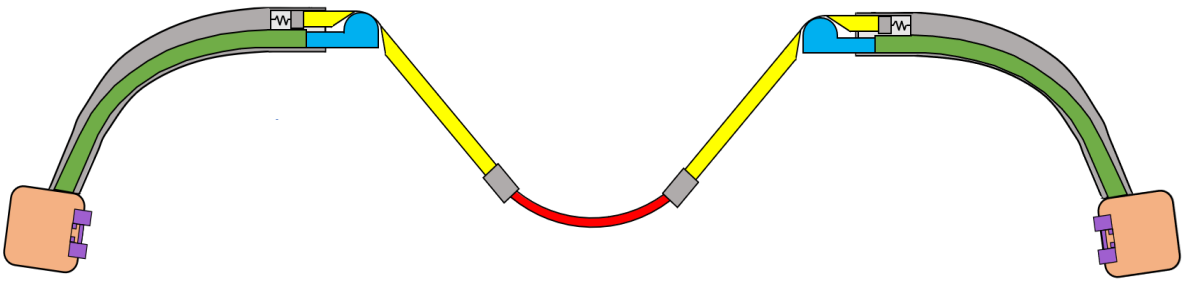

Figure 5.1: *Schematic drawing of the final concept, with the tape springs (yellow), middle segment (red), fold lever (blue), SMA rod (green), bar-ends (dark gray), the box (orange) and the rib clamps (purple). Note that the figure is not on scale.*

End-effects arise when the clamp constrains the radius of the tape spring and the fold is too close to the supported end. In order to minimize the end-effects, the clamp between the coil spring and the tape spring has two convex contact surfaces. The clamp constrains the fold as little as possible and thereby reducing the end-effects if the fold comes too close to the supported end.

5.3. Middle segment

After deciding on the use of two symmetrically applied tape springs, the need arose to connect both springs with a middle segment. Multiple options were evaluated to find the optimal middle segment. Initially the idea was to place a rigid middle segment between the tape springs, connected by compliant joints. After building a quick prototype, however, it became apparent that a system with a rigid middle segment was highly unstable when it was parallel to the sternum. Having a joint on both sides of the middle segment, virtually results in a trapezoidal four-bar linkage with the straight region of the tape springs. In this configuration, both tape springs applied an opposite bending moment to the middle segment. A minor distortion of symmetry made the middle segment tend towards one of two stable positions. This is explained and illustrated in Appendix B, as well as some preliminary alternative concepts. To prevent instability, the middle segments should make only one ”joint” with the tape springs.

In the SCARPE implant, the middle segment is designed as a thin flexure. Because of its compliance, a flexure is stable, follows the shape of the sternum closely and maximizes the contact surface to the sternum. Nevertheless, the bending stiffness of the flexure also applies a non-constant force to the sternum. The total elevation force is increased, and the FDR becomes non-constant. However, some bending stiffness is required to achieve full correction. The contribution of the flexure is considered minimal. As long as the total elevation force remains within the force bandwidth, we accept the contribution of the flexure stiffness.

The compliance of the flexure is a benefit during correction, but has some drawbacks after correction. When the tape springs are in the straight state, the flexure is still subjected to three point bending. The flexure finds an equilibrium position, always slightly deformed. The position of the sternum is therefore always lower than the ends of the tape spring. If the flexure is too compliant, the implant causes undercorrection. If the flexure is too rigid, its shape is not conform to the sternum and may cause instability. The bending stiffness of the flexure should therefore be carefully evaluated. To minimize the residual deformation, the flexure is mounted above the tape springs in a connection block (Figure 5.2). The best flexure should be chosen as short as possible to further reduce residual deformation.

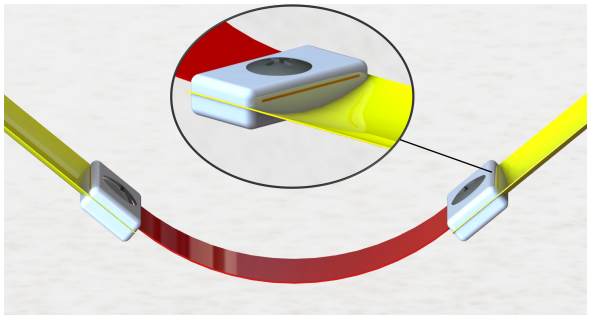

Figure 5.2: *Thin flexure as middle segment in the final concept (red). The flexure is connected above the tape springs (yellow) in a connection block (enlarged view within the circle).*

5.4. Fold distance control

To impose a specific fold distance to the SCARPE implant, the fold is constrained on the inside of the longitudinal radius by a stiff fold lever (Figure 5.3). The tape spring uses the fold lever as a hinge point and buckles around the protruding surface of the fold lever. It is beneficial to maximize the fold distance as much as is anatomically possible. If the fold lever is far away from the clamped end, the elevation force is maximized and end-effects are minimal.

The fold lever is actuated to translate underneath the tape spring (Figure 5.4). The maximum thickness of the bar is too small to also include an actuator inside the steel bar-ends. The actuator is therefore placed in a box at the extremities of the bar-ends. The driving force is transferred through a linear transmission. Two SMA rods connect the fold lever to the actuator

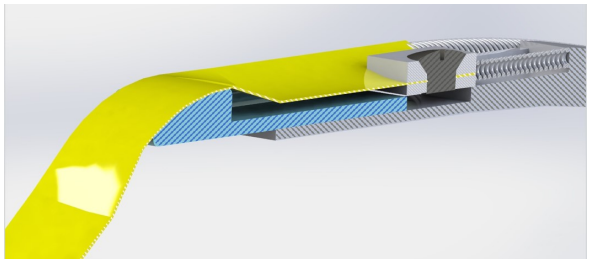

Figure 5.3: *Cross-sectional view of the fold lever (blue) underneath a tape spring (yellow). Through a connection block (gray), the lateral end of the tape spring is connected to a coil spring to passive translation during correction. The cut surfaces are shaded.*

(a) *Fold lever at d50*

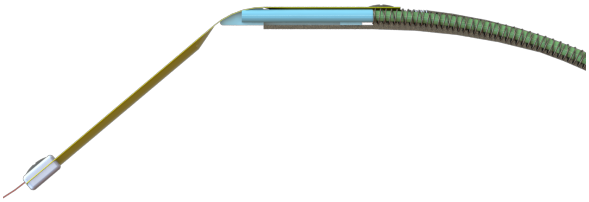

(b) *Fold lever at d70*

Figure 5.4: *Side view of the fold distance control mechanism in two different positions of the fold distance*

and are located adjacent on both sides of each bar-end. Translation of the SMA rod directly changes the position of the fold lever.

The SMA rods are made from nitinol. Nitinol is a nickel titanium alloy with superelastic properties. This specific material is chosen such that the actuation wire can follow a variety of shapes of the bar-end, while keeping its function. To prevent buckling, the SMA rods are packed inside flexible tubes of multi-layered helical wires (Figure 5.5). These tubes are covered by a sterilizable sleeve to prevent bacteria from settling within the wires (not shown). The flexible tube is stiff enough to impose the curvature of the bar-end to the SMA rod, but it is still compliant enough to adapt to a variety of shapes. The outer diameter of the flexible tube is smaller than the thickness of the bar-end. A standard table top bender (similar as used in MIRPE, see Appendix A) can be used to change the curvature without interfering with the transmission. The metal bar-end is therefore free to take any desired shape during operation.

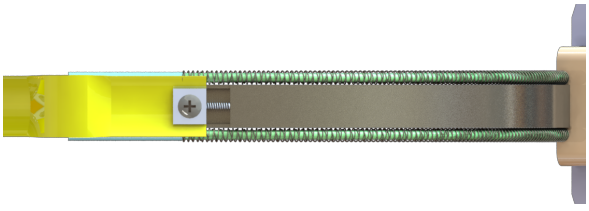

Figure 5.5: *Top view of the static section of the SCARPE implant showing the SMA rods (green) inside a flexible tube (gray), connecting the box (orange) and fold lever (blue).*

5.5. Actuation box

Actuation of the fold lever is done in the box at the far end of the SCARPE implant. The box applies a linear motion to drive the SMA rods. In order to meet the functional requirements, post-operative actuation must be controllable. To comply to the clinical requirements, the actuator must be controlled non-invasively and require no large voltage or current or rely on large pressure. The box does not need to move through the intercostal space, so the outside dimensions of the box are not restricted by the size requirements of the bar.

The outside of the box facilitates fixation to the rib cage. Because a tape spring carries the same bending moment on both sides of the fold, the implant might lift the bar-ends instead of the sternum. To allow fixation of the bar-ends, two flaps are attached on the sides of the box (Figure 5.6a). The flaps enable the application of various fixation procedures. The simplest procedure is to fix the implant to the ribs with sutures or surgical steel wire. Bar fixation by sutures is a familiar technique used in MIRPE for over twenty years [27, 55, 56]. Moreover, the flaps allow for a set of rib clamps to be attached to the bar (Figure 5.6b).

A rib clamp has one or two hooks that wrap around the ribs, for sutureless fixation to the rib cage. After grasping the ribs above and below the box, the rib clamps can be tightened with a small bolt. The ribs can have many different orientations. Therefore, various types of rib clamps are supplied as supplements for the SCARPE implant. The rib clamp in Figure 5.6b has two hooks perpendicular to the box. However, the ribs are rarely running parallel to the bar. For example, grips with one

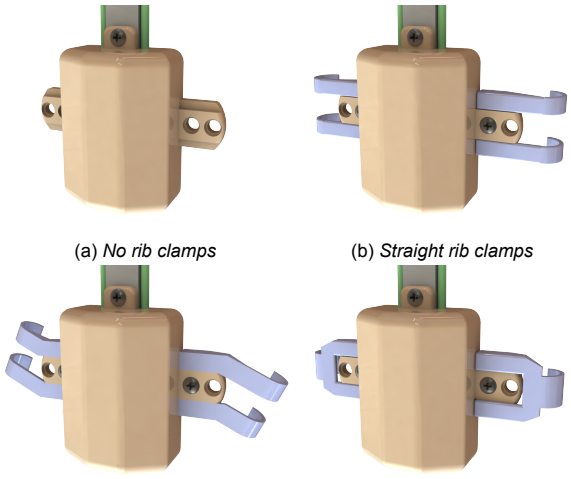

(a) *No rib clamps* (b) *Straight rib clamps*

(c) *Angled rib clamps* (d) *Rib clamps with one hook*

Figure 5.6: *Box attached to the bar-ends with different means of fixation*

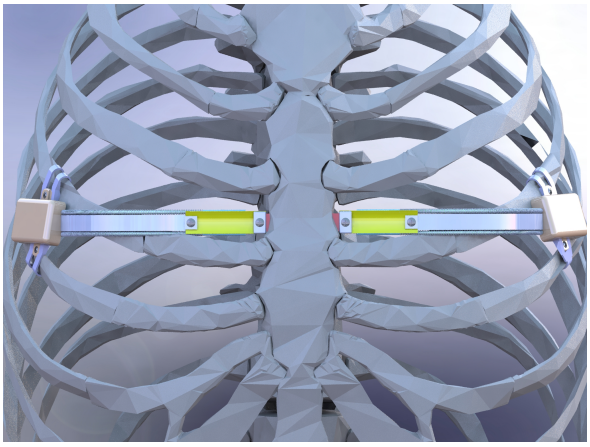

Figure 5.7: *Frontal view of the SCARPE implant, implanted in the thoracic cage. The SCARPE implant is in corrected configuration*

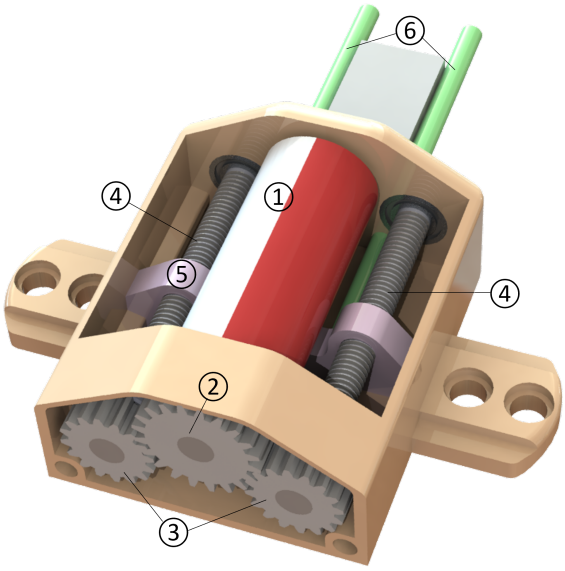

Figure 5.8: *Orthogonal view of the box with parts of the casing removed, showing the actuation mechanism. It shows the cylindrical magnet (1), drive gear (2), gearbox (3), screw spindles (4), driving plate (5) and SMA rods (6).*

hook (Figure 5.6c) or hooks at different angles (Figure 5.6d) can be better suited. A surgeon can select the best combination of two rib clamps to suit the patient specific anatomy of the ribs.

An example of the SCARPE implant connected to the thorax can be seen in Figure 5.7. A combination of two different angled rib clamps with two hooks and one angled rib clamps with one hook was used to suit this specific anatomy.

Inside the box is a remotely adjustable actuator, utilizing permanent magnets. Remotely adjustable means the actuator can be driven from location outside the human body. In order to drive the actuator non-invasively, a rotating magnetic field is used. Figure 5.8 shows a renders of the box with part of the casing removed. A cylindrical, diametrical magnet (1) is located in the middle of the box. The magnet is suspended between two bearings. The bearings are integrated in the casing. On one end, the magnet is also connected to a spur gear (2). The spur gear drives two other gears, in a small gearbox (3). The output of the gear box drives two screw spindles (4). The screw spindles are also suspended between bearings so they are free to rotate, but cannot translate. The driving plate (5) contains two threaded hols that convert the rotation of the screw spindles into translation. The SMA rods (6) are directly connected to the driving plate. In this assembly, rotation of the magnet results in translation of the SMA rods to actuate the fold lever.

In order to drive the cylindrical magnet, an external drive mechanism is required (Figure 5.9). This external drive mechanism supplies a rotating magnetic field to the box. A simple electric motor (1) is connected to two cylindrical diametric magnets (2), through a gear box (3). The electric motor drives both magnets with the same angular velocity, only the poles of each magnet are facing in opposite directions. In this way, the external drive mechanism creates a rotating magnetic field. Keeping the external drive mechanism in close proximity to the box, The cylindrical magnet in the box can be rotated to drive the fold lever. During adjustments the external drive mechanism can be directly placed on the skin. The actuator can move in two directions, by changing the direction of the rotating magnetic field. The direction can be controlled by pressing one of two switches (4) on top of the external drive mechanism. The number of rotations of the magnet in the box is measured and converted to the translation distance of the fold lever. The translation distance is shown on a small screen (5) to allow easy and intuitive usage.

Using a rotating magnetic field to drive adjustments to a medical implant is not something new. This method of actuation has already been successfully applied in correction of early onset scoliosis [57], and telescopic nailing [58]. The device shown in Figure 5.9 is based on an patented device, invented by Pool et al. [59, 60]. Using a similar device in the SCARPE procedure may, therefore, not be possible.

In an alternative embodiment of the remotely adjustable actuator, the cylindrical magnet inside the box, could be replaced by an electric motor that requires a low power. In that instance, the box should also house a battery, or induction pads to transfer currents transcutaneous.

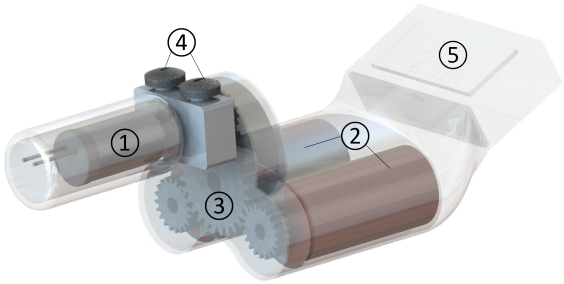

Figure 5.9: *External drive mechanism creating a rotating magnetic field with transparent casing showing the electric motor (1), two cylindrical magnets with opposite facing poles (2), gearbox (3), switches (4) and a screen (5).*

Including electrical components in the box would increase its complexity and pose problems with certification. Using magnetic actuation is the preferred embodiment, because it moves all electronics outside of the human body.

6 Evaluation

6.1. Proof-of-principle experiment

6.1.1. Goal

A proof-of-concept experiment has been performed to investigate the FDR of the tape spring mechanism within the SCARPE implant. The constant bending moment of tape springs is extensively studied in scientific literature. However, in most literature the constant moment principle is described in the context of a deployment mechanism. The experiment performed in this study, investigated the tape spring mechanisms used as constant force actuator. The main goal of this experiment was to establish proof that the tape spring mechanism, as described in the final concept, can be used as a constant force actuator for PE repair. Moreover, by measuring the elevation force, it is investigated if the FDR of the tape spring mechanism is suited for continuous correction of PE.

6.1.2. Variables

A series of five experiments were performed. Each experiment had its own subgoal with its own set of variables. A list of used variables with their annotations is shown in Table 6.1. Note that spring size is indicated by a single variable. It was not possible to evaluate all dimensions separately, because the tape springs used in the experiments were cut from off-the-shelf tape measures. Therefore, the variable width w is used to represent all dimensions of a tape spring. Furthermore, the independent variable height h is chosen to indicate the corrected distance. The variable h is similar to pectus depth, but it makes the evaluation of the data easier. For definition, the maximum pectus depth of 40mm is equal to $h = 0mm$ and a fully corrected, flat chest is equal to $h = 40mm$ (Figure 6.1). The right column in Table 6.1 indicates which variable is chosen as the dependent variable in each experiment of Section 6.1.4.

Table 6.1: *List of variables and their annotation. The right column states the number of the experiment in which that variable was considered as the dependent variable.*

Variable	Term	Unit	Explanation	Dependent
Height	h	mm	Corrected distance	-
Elevation force	F_e	N	Force applied by the tape springs	-
Spring size	w	mm	Spring geometry of the different springs used. Indicated by width	1
Layers	n	-	Number of free spring layers	2
Thickness	n_t	-	Number of fixed spring layers	3
Fold distance	d	mm	distance from the fold to the line of action of the elevation force	4
Loading	lo, ul	-	Direction of the measurement: Unloading $h_1 \rightarrow h_{end}$ or Loading $h_{end} \rightarrow h_1$	5

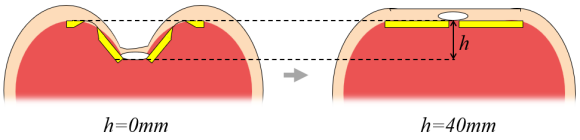

Figure 6.1: *Schematic drawing of an thorax with two tape springs. By definition, $h = 0mm$ is the height before correction has taken place and the springs are bent, $h = 40mm$ is the height after full correction when the springs are straight.*

6.1.3. Experimental setup

The experimental setup has been designed to measure the elevation force in different conditions, at discrete values of the corrected height h. The experimental setup can be found in Figure 6.2. The tape springs (1) used in this experiment, are segments cut from an off-the-shelf tape measure. Two spring sizes were considered. For the smallest tape spring, 120mm segments were cut from the Stanley Powerlock® 3M tape measure (Stanley Black & Decker, Inc., Connecticut, NE, USA). The larger tape springs were segments of the same length cut from the Stanley Powerlock® 5M tape measure (Stanley Black & Decker, Inc., Connecticut, NE, USA). Symmetrically on either side of the experimental setup, a tape spring was fixed in a spring clamp (2). The tape spring was

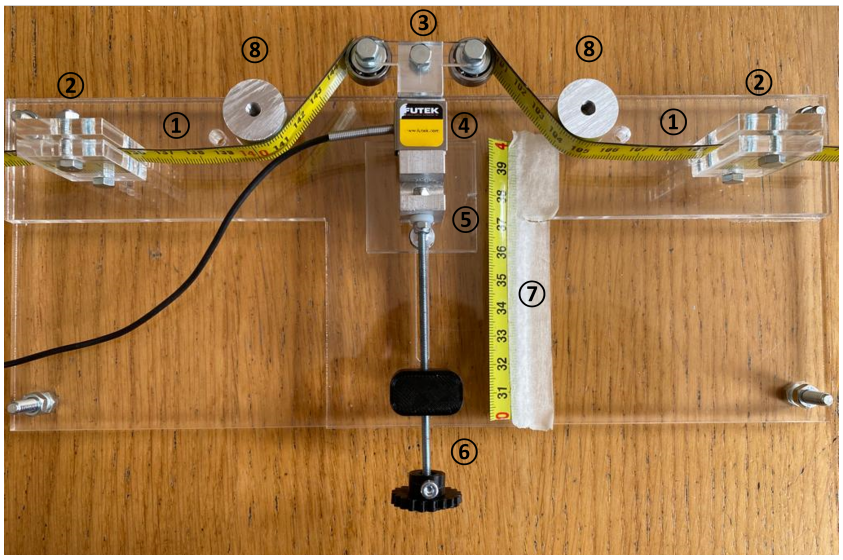

Figure 6.2: *The experimental setup consisting of: tape spring (1), spring clamp (2), sternal block (3), load cell (4), slider (5), leadscrew (6), measuring tape (7), fold rod (8).*

clamped between two plates and fastened with two bolts.

Bending of the tape springs was done by the sternal block (3). The sternal block represents the movement of the sternum during PE correction. The middle segment was omitted to prevent distortions of the force measurements by the stiffness of the thin flexure (Section 5.3). The sternal block consisted of an aluminum block between two PMMA plates, with a Koyo open miniature ball bearing (4x16x5mm)(Jtekt, Osaka, Japan) on each side. The ball bearings were introduced to minimize contact friction between the free ends of tape spring and the sternal block. Grease in the ball bearings was removed using bio-ethanol (95%) and a small brush. The bending moment of the tape springs exerted perpendicular force on the ball bearings of the sternal block. The elevation force of the two tape springs was measured by the LSB200 Miniature S-Beam Jr. Load Cell (Futek, Irvine, CA, USA) (4).

The sternal block and the load cell were connected to a slider (5). To simulate correction of the sternum, the slider could translate to move the loadcell. The elevation force was measured for different values of h. The slider was actuated with a leadscrew (6) to allow accurate placement. The M3 threaded wire used in the leadscrew has a pitch of 0.5. A full rotation of the leadscrew thus resulted in 0.5mm translation of the slider. A piece of measuring tape (7) was connected to the bottom plate as extra verification of the position. The fold distance could be predetermined by two cylindrical fold rods (8). On either side of the setup, three holes were cut at fixed positions. To change the location of the fold, the fold rods could be inserted at the required holes. The load cell in the experimental setup (9) was connected to a DAQmx terminal (National instruments corp., Austin, TX, USA) (10). NI LabVIEW ((National instruments corp., Austin, TX, USA) software was used to display and store the measured data on a HP Zbook Studio G5 (Hewlett-Packard, Palo Alto, CA, USA)(11) (Figure 6.3).

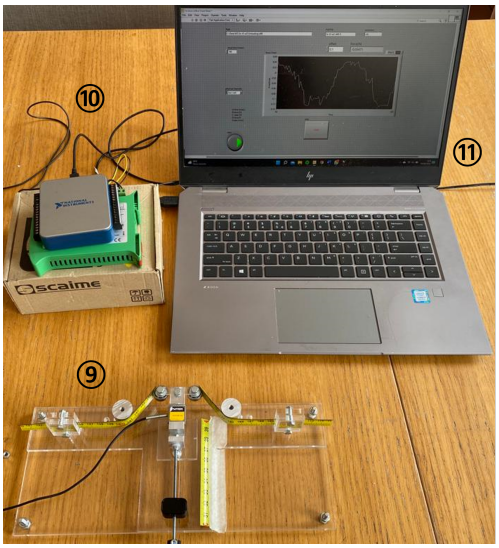

Figure 6.3: *Complete Experimental setup consisting of the experimental setup (9), DAQmx terminal (10) and HP Zbook Studio G5 laptop (11) running NI LabVIEW*

6.1.4. Experimental procedure

Before starting the measurement, the tape springs were fixed at the spring clamps. The fold rods were inserted symmetrically in the required hole. Most measurements started at the ”deformed” position at $h = 0mm$, as shown in Figure 6.2. This corresponds with a pectus depth of 40mm.During one correction cycle, the elevation force was measured at eight different values of h: 0, 10, 20, 30, 32.5, 35, 37.5 and 40mm. After each measurement, the data was stored and the load cell was moved to the next height. After $h = 30mm$, the step size between subsequent values of h has been reduced from $10mm$ to $2.5mm$. The tape spring approaches the straight configuration after $h = 30mm$. By decreasing the step size, the snap back behavior is captured more accurately. At $h = 40mm$, the tape springs are completely straight and the elevation force should be equal to zero. The measurement at $h = 40mm$ was used as reference value to investigate if the load cell was calibrated correctly. All data is imported to MATLAB (MathWorks, Natick, MA, USA) for analysis

The load cell had a finite accuracy. The measured force fluctuated within a certain bandwidth, as can be seen in the laptop screen in Figure 6.3. To find the mean force value, the load cell was kept stationary at the same value of h for a measurement time of 25s. The sample frequency was set to 10 Hz, resulting in 250 data points per measurement. See Appendix A**??**for justification of the measurement time. The result after one correction cycle, is a data set consisting of eight measurements (of 25s), each with 250 data points. The dependent variable was changed between each data set. In order to evaluate all dependent variables individually, five experiments were performed. Each experiment consists of several data sets. The five experiments are listed below.

1. *Spring dimension*. The goal of the first experiment was to establish the FDR for different tape springs. Two tape springs (spring w1 and spring w2) were used to measure the influence of the different dimensional properties: radius of curvature R, subtended angle α and thickness t (Figure 6.4b). Because the evaluated tape springs were segments cut from off-the-shelf tape measures, R, α and t could not be evaluated separately. Therefore, all dimensional properties are represented in one dependent variable, spring size w. The influence of w, was investigated for all possible tape spring configurations.
2. *Number of free layers*. The goal of the second experiment was to investigate the magnitude of the elevation force when tape spring layers were stacked on top of each other. The dependent variable was the number of layers n. The elevation force has only been measured for one layer, two layers and three layers stacked directly on top of each other ($n = 1, 2,$ or 3). The tape springs were not fixed together to allow interlayer sliding. Stacks of both springs w1 and w2 were evaluated, but only tape springs of the same dimensions were used within one stack. The results of this experiment were compared with the results of Experiment 3 to find the optimal technique to increase the elevation force.
3. *Number of fixed layers*. The goal of the third experiment was to investigate the magnitude of the elevation force if the total thickness would increase. The dependent variable was number of fixed layers n_t. Tape springs of the same thickness were stacked and fixed together to prevent interlayer sliding. Bison kit universal contact glue (Bison International, Goes, The Netherlands) was used for fixation. The elevation force has only been measured for two layers and three layers fixed together ($n_t = 2$ or 3). Stacks of both springs w1 and w2 were evaluated, but only tape springs of the same dimensions were used within one stack. The results of this experiment were compared with the results of Experiment 2 to find the optimal technique to increase the elevation force.
4. *Fold distance*. The goal in the fourth

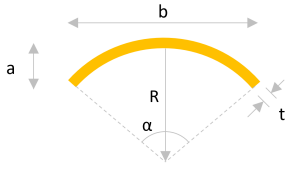

(a)

	a [mm]	**b** [mm]	**t** [mm]	**R** [mm]	α [rad]
w1	1.45	12.7	0.12	14.6	0.900
w2	2.45	15.5	0.15	13.5	1.1

(b)

Figure 6.4: *Parameters and the dimension of the cross section of the two different tape springs used in this study.*

experiment was to investigate the influence of the fold distance d, on the FDR. The measured elevation forces were compared for different positions of the fold rod. Three different fold distances were evaluated: d70, d60 and d50, where d stands for distance and the number stands for the distance to the central axis of the load cell, in millimeters (Figure 6.5). The measured forces at the three fold distances were compared within the same tape spring configuration.

5. *Hysteresis*. The goal of the final experiment was to investigate the impact of hysteresis in the tape spring mechanism. The dependent variable was the loading direction. The tape spring mechanism was first loaded, by decreasing h from 40mm to 0mm and thereafter unloaded, by increasing h from 0mm to 40mm. The hysteresis was measured in all tape spring configurations. For convenience the measurements in this experiment were only collected at fold distance d70. For each tape spring configuration, the measured forces between loading and unloading were compared to determine the energy dissipation in the tape spring mechanism.

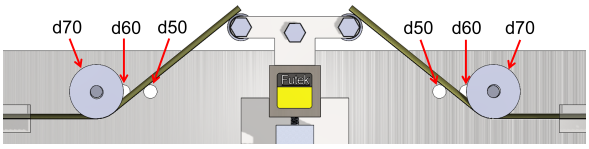

Figure 6.5: *Top view the experimental setup with the fold rod in d70, indicating the three possible fold distances in this study.*

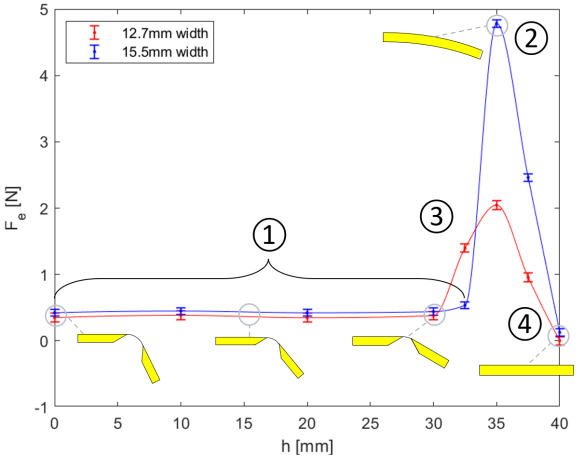

Figure 6.6: *General form of the force-displacement relationship (FDR) of the tape spring mechanism, with on the x-axis is the height h in millimeters and on the y-axis is the measured elevation force F_e. The overall shape of the FDR shows: steady state behavior (1) (where the force remains constant in the folded state), peak force (2), Partitioned peak force (3) (where snap back occurred between two measurements), return to zero (4). The tape springs in yellow illustrate the shape of the tape spring at various moments during correction.*

6.2. Experimental results

6.2.1. Introduction

In all tape spring configurations, 250 data points were obtained for every value of h. For every 250 data points, the mean and standard deviation were calculated using MATLAB. The mean and standard deviation of each measurement were plotted to obtain the FDR of that specific tape spring configuration. Figure 6.6 shows the general form of the FDR of the tape spring mechanism. The overall shape of the FDR is in accordance with findings in literature [61].

Between $h = 0$ and $h = 32.5mm$ steady state behavior was observed (1). During steady state behavior the tape spring is in the folded state and the elevation force remains relatively constant. After $h = 32.5mm$ snap back occurs and a large peak force is observed (2). For some tape springs, the snap back height is located between two values of h. In the FDR this can be seen as a partitioned peak (3), for which the peak is spread out over multiple measurements. At $h = 40mm$ the tape spring is straight and F_e returns to zero (4). See Appendix D for the Matlab-scripts used to calculate the mean of each measurement and plot the results.

It should be noted, that the fit is not part of the measurements. The elevation force in the experiments was only measured at eight discrete heights. The mean over the 250 data points at every height is displayed as a point in the graph, with the standard deviation as error bars. A smooth curve has been fitted through the points for clarity. Although the fit is not part of the measurements, it serves to illustrate the FDR. The fitted model was a Piecewise Cubic Hermite Interpolating Polynomial (PCHIP). This model was able to capture both the peak force and the steady state behavior.

In this section, the results of each experiment are accompanied by a figure showing two typical examples that illustrates the outcome of that experiment. One example for a free tape spring stack, and one example for fixed tape spring stack is shown. Which tape spring configuration is used in the example is shown with a small symbol on the top-left of the graph (Table 6.2). The spring size is indicated above the symbol with w1 or w2. The only exception are the figures in Section 6.2.2. No spring size is indicated above

the symbol because w1 is compared with w2. See Appendix E for the figures of all other results and Appendix F for tables presenting the analyzed data per experiment.

Table 6.2: *Meaning of the symbols illustrating the tape spring configuration in the graphs.*

# of layers	Free/fixed	Symbol
1	Free	
2	Free	
2	Fixed	
3	Free	
3	Fixed	

6.2.2. Experiment 1 - Spring dimension

In the first experiment, the FDR of the two tape springs, w1 and w2, were compared to investigate the influence of tape spring geometry on elevation force. Figure 6.7a shows that the FDR of both tape spring configurations follow the same shape during steady state behavior, for any number of free layers. For w2, F_e was slightly larger than for w1. The tape spring configurations were compared, using the relative force increase f_{rel}[%]. Which was defined as:

$$f_{rel} = \frac{F_{w2} - F_{w1}}{F_{w2}} \cdot 100. \tag{6.1}$$

Where F_{w1} and F_{w2} are the means of the measured elevation force for different values of h, for w1 and w2 respectively. During the steady state behavior, the relative force increase was 14.4% (range, 11.1-18.7%). The largest increase in the elevation force was found in a stack of three spring layers 15.5% (range, 13.7-17.7%) and the smallest increase in two spring layers 12.4% (range, 11.1-13.4%).

For all fixed tape spring stacks, the increase in elevation force between w1 and w2 was larger compared to the free tape spring stacks. Figure 6.7b clearly illustrates the difference between free and fixed tape spring stacks. The FDRs of both fixed tape springs tends to diverge for increasing values of h. During the steady state behavior, the relative force increases by 2.1% (range, -9.5-22.8%) and 19.2% (range, 14.6-26.9%) for two and three fixed layers respectively. Negative value means the elevation force decreased when spring dimensions increased. A decrease in elevation force only occurred in spring w2 with two fixed layers.

The peak force of w2 was estimated to increase by approximately 100% with respect to w1, for $n = 1, 2$ and 3. Because snap back

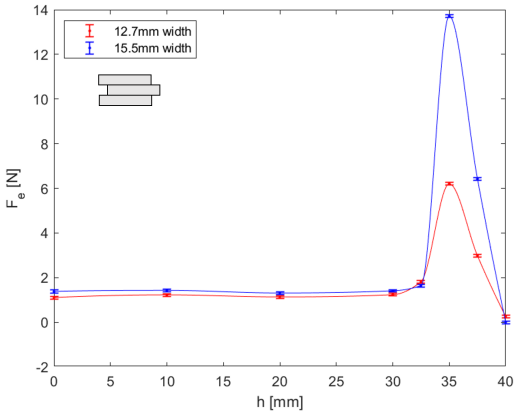

(a) *Free tape spring stack*

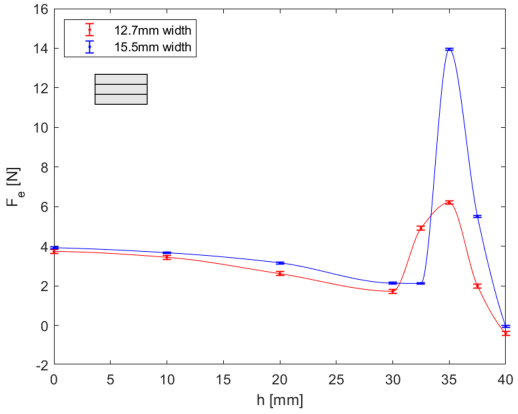

(b) *Fixed tape spring stack*

Figure 6.7: *Force-displacement relationship (FDR) comparing spring w1 and w2 of a three layered stack ($n = 3$) at d70. (a) The FDR for free tape spring stacks. (b) the FDR for fixed tape spring stacks.*

sometimes occurred between two values of h, the maximum peak force was not always captured. Therefore, it was difficult to accurately quantify the peak force. For example, for a stack of two free spring layers, the measured peak force of spring w1 and w2 springs roughly had the same height (Figure 6.8). This is in contrast with other findings in this study. An estimation of the true peak force was made by extrapolating the line between $h = 40mm$ and $h = 37.5mm$, until $h = 35mm$. For both free and fixed layers, and all spring sizes, the peak force increased by approximately 100% (104.2%, range 84.4-130.0%) for each added layer.

6.2.3. Experiment 2 - Number of free layers

In the second experiment the goal was to compare the influence of the number of spring layers on the magnitude of the elevation force. Overall, increasing the number of layers increased the measured F_e.

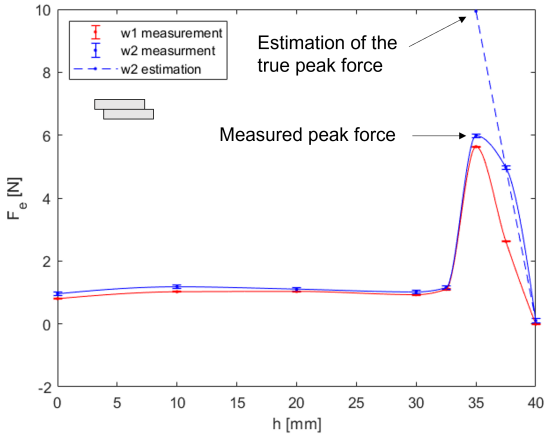

Figure 6.8: *The measured data for spring w1 and w2 for two free layers. The dotted line indicates the estimation of the peak force for spring w2.*

Stacks free tape springs follow the principle of superposition (Figure 6.9a). Stacking spring w1, each added spring layer increased the elevation force by a little over 100% (113.4%, range 96.8-141.4%), during steady state behavior. The elevation force increase for stacking layers w1 was slightly smaller than compared to w2 (112.1% and 114.8%, respectively). Each added layer also increased the peak force by approximately 100% for both stacks of w1 and w2. The increase in F_e was independent of h.

Interplay between the layers is the reason the force increase was larger than 100%. Because the tape spring layers were directly in contact with each other, the layers on the inside of the longitudinal radius were constrained and compressed by the outside layer [62]. A smaller fold radius for the inside layer caused an increased amount of strain in the fold [63]. The additional strain energy in the fold caused a larger bending moment and was measured as a larger elevation force in the experiment.

6.2.4. Experiment 3 - Number of fixed layers

By fixing the stacked layers in Experiment 3, the increase in F_e is larger than for stacking free layers. The FDR showed converging behavior on top of superposition (Figure 6.9b). When fixing the tape spring stacks, each layer increased the measured F_e during steady state behavior by 303% (range, 132.84-419%). The increase in spring w1 was slightly lower compared to spring w2 (296.6% and 310.3%, respectively). For the fixed tape spring stacks the increase in F_e was dependent on h. The measured F_e was largest at the start of the correction and smallest just before snap-back.

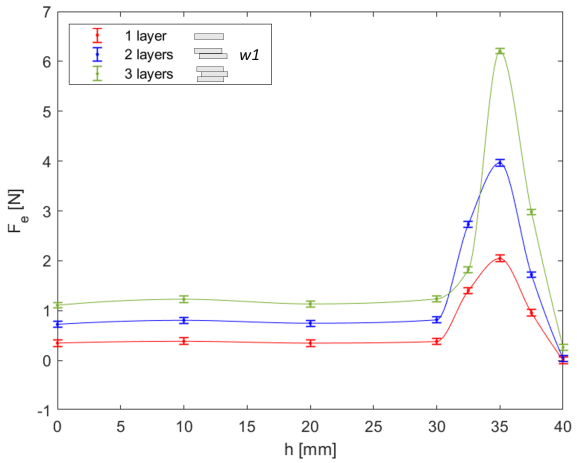

(a) *Free tape springs stacks*

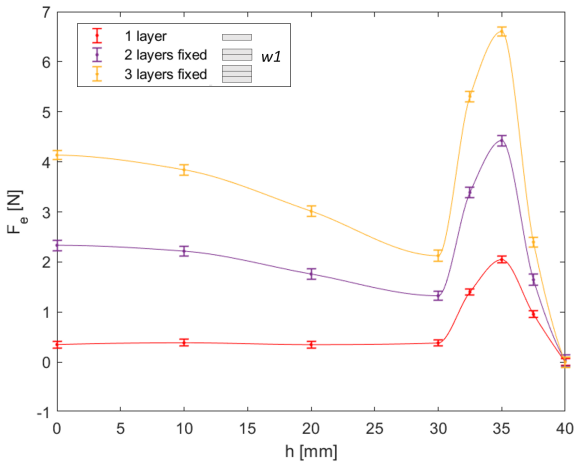

(b) *Fixed tape springs stacks*

Figure 6.9: *Force-displacement relationship (FDR) of spring w1 at d70, comparing different numbers of free and fixed tape spring layers. (a) The FDR for free tape spring stacks, (b) the FDR for fixed tape spring stacks.*

When fixed together, a stack of individual tape spring layers act like one solid layer with a thickness of $t_{total} = n_t t$. When the thickness becomes too large, the fold stops acting like a flat plate. The fold region was not a zero stiffness joint anymore, but contained the bending stiffness of a beam with thickness t_{total}. The introduced bending stiffness caused the decreasing slope for fixed tape spring stacks in Figure 6.9b.

6.2.5. Experiment 4 - Fold distance

In the fourth experiment the FDR was investigated for different values of the fold distance d. Figure 6.10a shows the the steady state behavior of spring w1, for three different fold distances. We observed a relatively constant elevation force for d60 and d70. For d50 the measured elevation

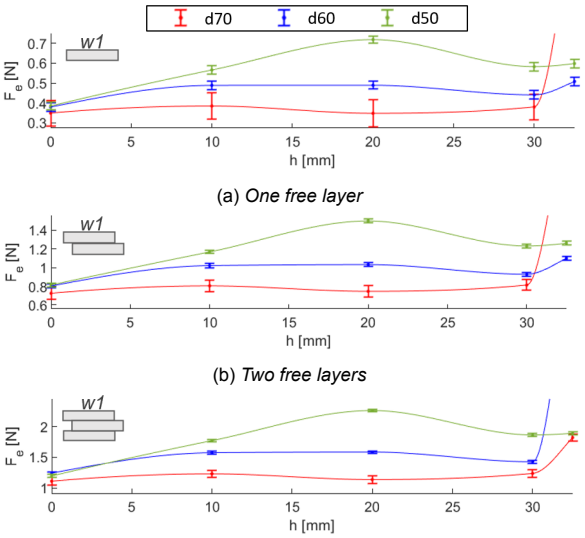

Figure 6.10: *Force-displacement relationship (FDR) for the three different fold distances in the folded state. Each graph is spring w1 with ascending stacked layers: one layer (a); two free layers (b); and three free layers (c).*

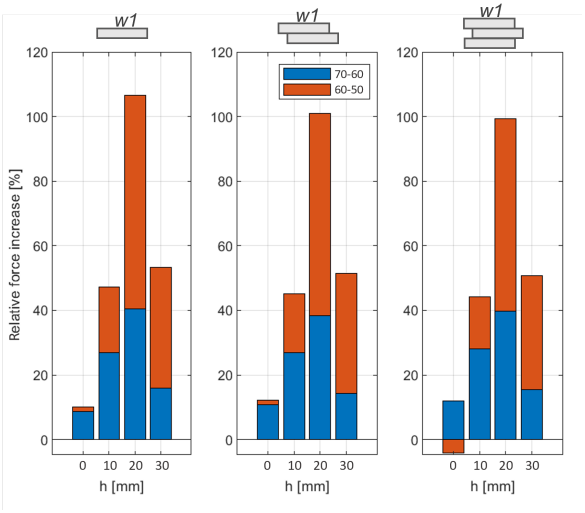

Figure 6.11: *Bar graph for the relative force increase between decreasing fold distance at the same height. Blue indicate the relative increase from d70 to d60. Red indicates the relative increase from d60 to d50.*

force was not constant. The FDR for d50 first showed an increase in elevation force, peaking at $h = 20mm$, followed by a decrease. Similar behavior was found for spring w2.

Identical behavior was found when comparing the three FDRs of Figure 6.10a with Figure 6.10b & 6.10c. The only difference between these three graphs is the number of free stacked layers ($n = 1, 2$ and 3, from top to bottom). Furthermore, the FDRs of spring w1 and w2 are also similar. Therefore, the FDR for each fold distance has a unique pattern, independent of the number of spring layers or spring size.

That the FDR is independent of the number or is confirmed by Figure 6.11. The bar graphs visualize the relative force increase between adjacent fold distances. Although n did not change the shape of the FDR, it did influence the magnitude of the force, conform to the superposition principle found in Section 6.2.3.

Overall, for smaller fold distances the measured F_e increased. But, the increase was not constant for every value of h.This is illustrated in Figure 6.11, by the inconsistent ratio between the length of the red and blue bars, for different values of h. In the right graph of Figure 6.11, a decrease was observed at $h = 0$. At this point, the measured F_e was larger in d60, than compared to d50. But, the difference was marginal and within the standard deviation. The decrease can be considered as a measurement error. The increase in F_e is both dependent on h and d

For the fixed tape spring layers, the FDRs showed a different shape, as can be seen in Figure 6.12. The initial elevation force for $h = 0mm$ at the start of the correction is larger, compared to the free tape spring stacks. Spring w1 with fixed layers first showed a relatively constant elevation

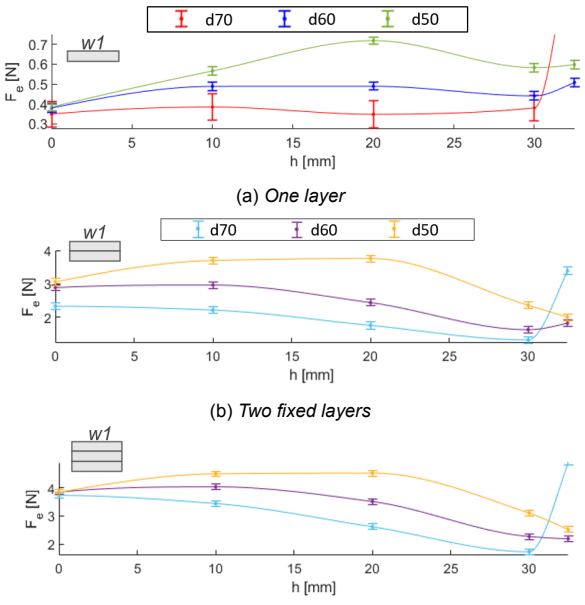

Figure 6.12: *Force-displacement relationship (FDR) for the three different fold distances, in the folded state. Each graph is spring w1 with ascending stacked layers: 1 layer (a); 2 fixed layers (b); and 3 fixed layers (c). The red, blue and green lines indicate the free tape spring layers. The cyan, purple and yellow curve indicate the fixed tape spring layers.*

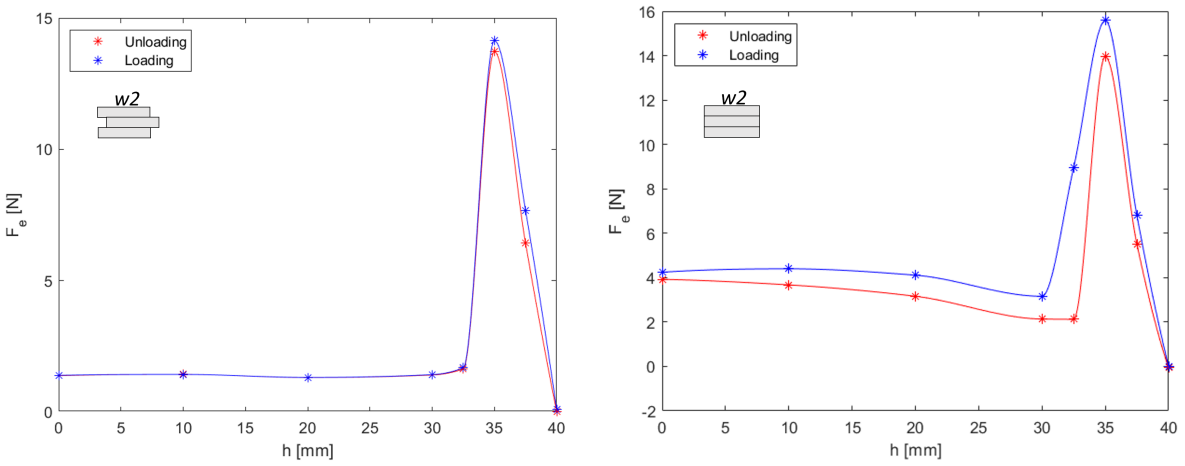

(a) *Free tape spring stack* (b) *Fixed tape spring stack*

Figure 6.13: *The force-displacement relationship (FDR) of spring w2 with three stacked layers in loading and unloading. (a) the FDR of free tape spring stacks, (b) the FDR for fixed tape spring stacks.*

force, followed by a strong decrease. The force decrease started after $h = 20mm$ for d50, after $h = 10mm$ for d60 and after $h = 0mm$ for d70. With spring w2 the fixed layers showed an even larger difference in pattern. For spring w2, d50 did not always supplies the largest value for F_e, as the F_e in d60 increased strongly. Although the FDR for spring w1 clearly showed unique patterns for the different fold distances, the unique patterns are less clearly distinguished for spring w2.

6.2.6. Experiment 5 - Hysteresis

In the final experiment, loading of the tape springs was compared with unloading, to investigate energy losses in the tape spring mechanism in the form of hysteresis. Figure 6.13a shows the loading and unloading cycle of free tape spring stacks. To make a better comparison, the measurement data of loading has been flipped and placed on top of the unloading measurement data. Although the elevation force in loading was slightly larger than in unloading, differences during steady state behavior were minimal. For free tape spring stacks of any number or width, the only observable difference in F_e between loading and unloading, is found in the peak force.

Regarding fixed tape spring stacks, the differences between loading and unloading became more clear (Figure 6.13b). Additional to the difference in peak force, the steady state force in loading was larger than during unloading. The difference in steady state force was largest right before snap back/after buckling and slowly converged when approaching $h = 0mm$.

7 Discussion

7.1. Experimental discussion

7.1.1. Experiment 1 - Spring dimension

When comparing springs w1 and w2, we found a small difference in elevation during steady state behavior and a large difference in peak force. Spring w2 yielded the largest force for all tape spring configurations. The differences between the peak force increase and the steady state force increase, is caused by the stiffness of the tape spring. The stiffness of tape springs is largely influenced by two parameters; thickness t and radius of transverse radius R_t. The stiffness of a tape spring is positively correlated with t and inversely correlated with R_t. For spring w2 t is larger and R_t is smaller than compared to spring w1. Hence spring w2 is more stiff. After snap back, both t and R_t influence the stiffness and thus we would find a large difference in peak force. During steady state, however, the fold has zero transverse radius. Therefore, the small increase of F_e in the fold state between spring w1 and w2 could only be explained by the increase in t.

In design of tape springs for the SCARPE implant, the parameter t is the most important parameter to optimize. The SCARPE implant spends most time in the folded configuration, so increasing the steady state force has most impact on the correction rate. The large peak force can increase the correction rate after snap back. Therefore, R_t should be used as the second most important parameter to optimize.

The snap back could be considered dangerous for the patient, because the implant suddenly applies a large force on the sternum. However, the patient will not experience the snap as an instantaneous correction. Due to the visco-elasticity of the costal cartilage, the thoracic wall will distract slowly in reaction to the large peak force. The sternum settles once it reaches an equilibrium height. The equilibrium height is reached over the course of one hour after snap back. The patient may temporarily experience raised pressure on the thorax. As long as the peak force remains beneath the upper force boundary of 20N, the patient will only experience a minor discomfort and no pain. Therefore, R_t should be chosen in combination with t, such that the peak force is maximized within the force bandwidth.

7.1.2. Experiment 2 - Number of free layers

From Experiment 2 we found a number of advantages and disadvantages for choosing free tape spring stacks as strategy to increase the elevation force. By stacking free layers, each added layer increased the elevation force by 100%, conform to the superposition principle. No plastic deformation was found in the experiment so the number of springs could be increased until meeting the size requirements. Also the elevation force remains constant throughout steady state behavior, which makes control and treatment planning more simple.

Nevertheless, the elevation force of all free tape spring stacks, considered in this study, do not meet the force requirements. A free tape spring stack of 7 layers would be required in order to meet the lower force boundary, for both spring w1 and w2. This is not possible because then the stack will exceed the size requirements. A custom tape spring should be developed to increase the elevation force per tape spring.

7.1.3. Experiment 3 - Number of fixed layers

Increasing the thickness of a tape spring is a more effective method of increasing F_e, than stacking individual layers. The fixed tape spring stacks caused a larger increase in F_e. Nevertheless, two issues arise with using fixed tape spring stacks. First, the elevation force is not constant. This can be a problem for control of the correction rate. An additional control strategy should be developed

when choosing fixed tape spring stacks as method for increasing the elevation force in the SCARPE implant.

Second, if the thickness becomes too large, bending may lead to plastic deformation. Plastic deformation could prevent the tape springs from achieving full correction. In this study, no plastic deformation was observed after the experiments. But after multiple loading cycles, the three layered stack showed signs of delamination. The delamination is not expected to have had a negative influence on the experiments because it only became noticeable after being subjected to multiple cycles once the experiments were completed. Delamination limits the number of fixed tape spring layers that can be used.

7.1.4. Experiment 4 - Fold distance

The FDR of the tape springs showed a unique pattern for each fold distance, independent of the number of free spring layers and spring size. The fold distance and height are the only other variables that changed during the measurements of the the FDRs. Hence, the FDR is determined by two distances, making the behavior and control of a tape spring mechanism very predictable. Also, the behavior of the springs does not change when adding more layers or changing its size.

Furthermore, the smallest fold distance always results in the largest elevation force for all free tape spring stacks. For the SCARPE implant that means the largest force is attained by keeping the tape spring mechanism virtually close to the thoracic wall. Remaining close to the thoracic wall also is one of the clinical requirements. A disadvantage for using a small fold distance is that the FDR at d50 does not remain constant. The correction rate will thus change during correction. The fixed tape spring stacks does yield a more constant force for smaller fold distances.

After snap back, changing the fold distance becomes less important. The peak force remains approximately equal in each fold distance. It should be noted, however, that for large fold distances snap back occurs at a smaller height. Early snap back means the sternum is longer subjected to a large force, which may result in a faster correction, even though the elevation force in steady state might be lower. The snap back height should be taken into account when selecting the suitable fold distance.

7.1.5. Experiment 5 - Hysteresis

Hysteresis was found by evaluating the difference in mechanical work during loading and unloading. Graphically it can be illustrated by the area under the FDR in loading, minus the area under the curve in unloading. For the free tape spring stacks, during loading and unloading were approximately equal. Solely based on this result we could argue there was little to no hysteresis present in the system. That, however, would be very improbable, because self-locking of a tape spring is a hysteresis phenomenon [48]. The self-locking properties of a tape spring are the result of difference in buckling height and snap back height. The measured difference in peak force indicates that in reality the hysteresis losses were larger than was illustrated in the hysteresis plots in Section 6.2.6 and Appendix E.5.1.

Continuous measurements have been performed to verify if the measured data was correct. The leadscrew in the experimental setup was connected to a cordless drill. While applying

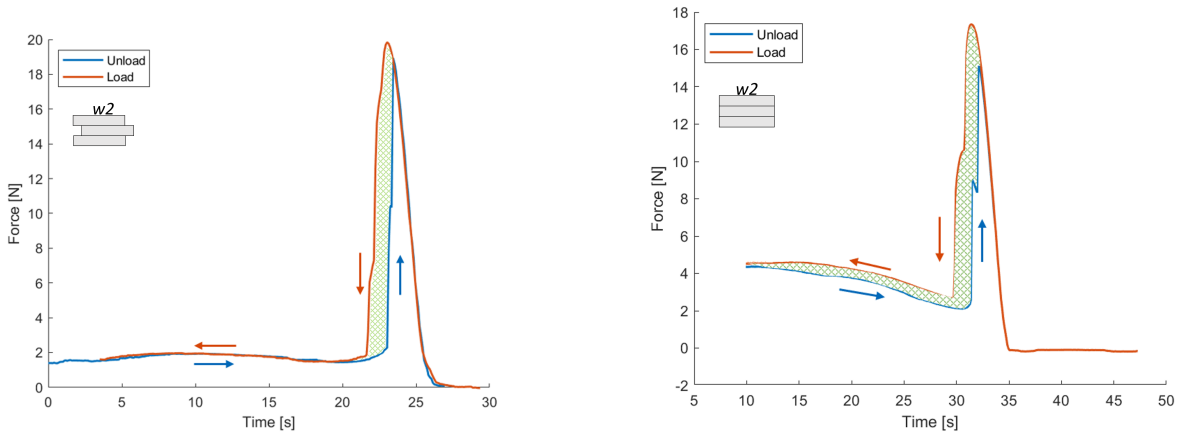

(a) *Free tape spring stack*

(b) *Fixed tape spring stack*

Figure 7.1: *Force response of spring w2 with three layers during continuous unloading (blue) and continuous loading (red). The shaded area in between the curves represents the hysteresis.*

constant power, the elevation force was measured during continuous loading and unloading. The continuous measurements show there is indeed hysteresis present in the tape spring mechanism (Figure 7.1). For all free tape spring stacks, the hysteresis was only found between peaks as already described in literature [48] (Figure 7.1a). Moreover, in the fixed tape spring stacks there is hysteresis present both between peaks and in the folded state (Figure 7.1b).

The hysteresis between peaks is expected and is unavoidable with the use of tape springs. When using fixed tape spring stacks, however, the hysteresis was also present in the folded state. This is likely caused by internal friction inside the glue layers. In the design of future tape spring mechanisms for the SCARPE implant, it is therefore desirable to produce every tape spring configuration as a single piece of material. Nevertheless, hysteresis should not be a limiting factor in the SCARPE implant, because it is designed to only fulfill one cycle.

7.2. Bending moment

In Section 4.2 the assumption was made that tape springs apply a constant bending moment. Based on the measured elevation forces from the experimental data, we could calculate the constant bending moment to verify if this assumption was valid. As illustrated in Figure 7.2a the bending moment remains relatively constant in the folded state for all free tape spring stacks. There was a decrease found of approximately 30% before snap back. Nevertheless, Equation 4.4, for calculating the constant bending moment, is still valid because the equation was derived from the average value over bending stiffness [49].

In Section 4.2 it was also argued that the bending moment is independent of the fold location. In Figure 7.2a the bending moment for each fold distance follows the same line. Thus, for free layers, the bending moment is indeed independent of the fold distance.

In contrast to the free tape spring stacks, the bending moment of fixed tape spring stacks was not independent of fold location. Figure 7.2b clearly illustrates that the bending stiffness during steady state behavior is larger for large fold distances. Moreover, the overall decrease in bending moment during unloading is stronger than compared to the free tape spring stacks. The assumption that the bending moment remains constant in the folded state is therefore only valid for free tape spring stacks. So if the layers of a tape spring stack are fixed, the equation

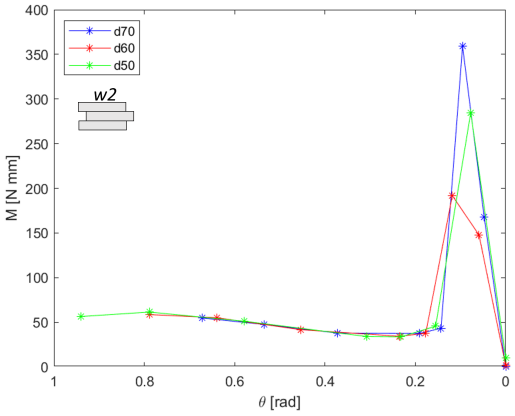

(a) *Free layers*

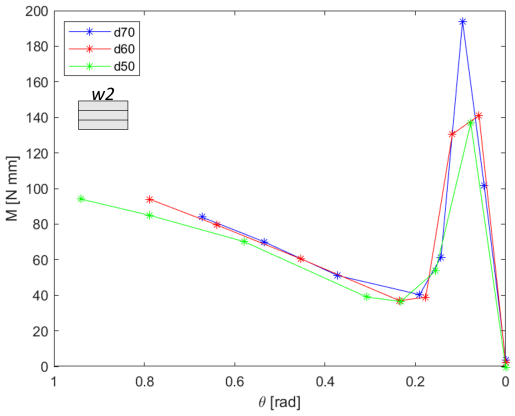

(b) *Fixed layers*

Figure 7.2: *Bending moment (M) versus bending angle (θ) of spring w2 with three layers*

for calculating the steady state bending moment (Equation 4.4), may be not be used.

7.3. Assessment of functional requirements

7.3.1. Force bandwidth

Now that all results are discussed, the findings can be evaluated by the functional requirements.We can draw the general conclusion that the most favorable tape spring configuration should be the tape spring with the largest dimensions, three fixed layers (more would conflict with the size requirements) and the smallest fold distance (allowed by the deformity). Based on the average elevation force in the folded state, the force boundary was only met by spring w2 with three fixed layers, at d60 and d50.

If the peak force is included in the correction, one more tape spring configuration is applicable. When the lower force boundary was determined in Section 2.5, it was assumed that the force would

remain constant throughout the correction. As long as the peak force remains lower than the upper force boundary, the peak force can aid in increasing the correction rate after snap back. See Appendix G for the calculation including the peak force in the force boundary requirement. Spring w1, with three fixed layers, at d50, also passes the lower force boundary, when the peak force is included.

Although two tape spring configurations meet the force requirements, the margin towards the lower force boundary is small. Little deviations in the boundary conditions could cause the SCARPE implant to surpass the total treatment time. In designing a suitable tape spring for use in the SCARPE procedure, increasing the elevation force should be the first concern.

Other factors influencing the elevation force, such as the middle flexure and the coil springs attached at the lateral ends of the tape spring, were not considered in this study. Although these factors would increase the elevation force, the contributions were expected to be small and are considered negligible.

Note that all calculations are based on the selected load case of a 16-year-old male PE patient. For other patients, another spring configuration could be more favorable. For instance, in younger patients the thorax is more compliant and a tape spring configuration with a smaller average elevation force could be better suited. It is, therefore, recommended to make an estimation of the required elevation force before the SCARPE procedure, based on: age, gender, PE severity and muscle mass. Then, the estimation of the required elevation force can aid surgeons in selecting the best suitable tape spring configuration.

7.3.2. Adjustable correction rate

Purely looking at the force bandwidth requirement, only spring w1 and w2 with three fixed layer seem suited for use in the SCARPE implant. Nevertheless, the force requirement was only met at fold distances d60 and d50. By changing the fold distance anywhere between d60 and d50, the mean elevation force could be changed by 0.65N (range, 0.15 - 0.88N). This implies a change in correction rate of 0.5 days/mm (range, 0.2 - 0.65days/mm). For spring w1 it was not possible to meet both the force requirements and an adjustable correction rate simultaneously. Although spring w2 was able to adjust the elevation to some extent, the impact on the correction rate is low.

Changing the fold distance can also be unsafe, potentially causing damage to the soft tissue.Decreasing the fold distance may entangle lung tissue between the tape spring and the thoracic wall. Entangled lung tissue is incredibly painful and could lead to necrosis. Inversely, increasing the fold distance may pressure the soft tissue behind the spring. The pressure could again cause necrosis of the lung tissue or pericardium.

Besides, it may not always be possible to freely determine the position of the fold. For example, correction of wider types of PE may only be achievable with a fold distance of d70. In that instance, both the force requirement and the adjustable correction rate requirement are not met. Moreover, the fold of the tape spring is located at the entrance location to the thoracic cavity of the fold. Moving the fold lever may not even be possible altogether being constrained by the thoracic wall.

It is arguable if changing the fold distance is the optimal way of controlling the elevation force. Movement of the fold lever is often prevented due to anatomical constraints. And even if movement is possible, it could be dangerous for the patient. A different entrance location should be considered to facilitate free control of the fold position.

7.3.3. Achieve & maintain full correction

In order to achieve full correction, the SCARPE implant should be oriented correctly during implantation. After surgical implantation it is not possible to make changes to the final appearance. It is important to place the lateral side of the tape spring horizontally for full correction when the spring reaches the straight state.

The properties of tape springs seem very suitable to maintain full correction. One of the benefits of using tape springs is the self-locking behavior towards the end of the correction. After snap back, the tape springs in the SCARPE implant locks in the straight state. The stiffness automatically increases before full correction is achieved, to support and maintain the posture of the thoracic wall. The self-locking behavior is also an automatic process to cease the correction and prevent overcorrection.

A problem that may arise during the SCARPE procedure is dislocation of the implant. Because of the relatively low elevation forces the SCARPE implant is not clamped at its place, as happens during MIRPE. This might result in out-of-plane sliding or even rotation of the bar. It may be necessary to fix the SCARPE implant at the fold location to prevent dislocation.

7.3.4. Failure safety

The use of tape springs is assumed to be safe. If correction or actuation fails, the implant simply stops. There are no large internal stresses present in the SCARPE implant. The vast majority of stress is located inside the fold, so this would be the most critical are to investigate in the future. As an extra failsafe mechanism, a thin silicon sleeve can be wrapped around the implant to keep the pieces together after breakage.

7.4. Assesment of size & manufacturing requirements

7.4.1. Maximum bar dimensions

In order to remain within the requirement of 3mm cross-sectional height, the investigated number of layers was limited to three. All tape spring configuration with spring w1 (12.7mm) also adhered to the maximum required width of 13mm, whereas spring w2 (15.5mm) exceeded the width. Although spring w2 did not fit within the size requirements, its elevation force was substantially larger than for spring w1. In future design of tape springs for use in the SCARPE implant, a custom tape spring should be designed that optimises the elevation force within the size requirements.

The thickness of the tape spring was not constrained by requirements. Yet, the delamination between three fixed layers imply that the thickness of the stack (0.5mm for w1 and 0.6mm for w2) was too large. The adhesive layer failed because it was not strong enough to resist the bending strain of the increased thickness. The custom spring should consist of a single layer with the largest possible thickness before plastic deformation occurs.

7.4.2. Maximum box dimensions

The actuation box does not travel through the intercostal space, so the box has different dimensional requirements. The outside diameter of the box should not exceed 25x15x40mm (WxTxL) of which the thickness is most critical. In its current form, the box is 25x15x33.5mm, excluding the flaps for rib fixation. Because of their low thickness the flaps are not considered to be an issue. The main reason for the outside dimensions is the size of the gears. If smaller gears are used or the position of the gears is reorganised (by using bevel gears for example) the size of the box can be further reduced.

7.4.3. Simplicity & producibility

Tape springs seem very suitable for continuous correction of PE. Using tape springs as force generator removes the need for joints, small parts and lubrication. The smallest parts are used inside the actuated box. Many of the parts are off-the-shelf or use common materials and dimensions. Parts that were not present in the experimental set-up and that require attention during manufacturing are: the fold lever, connection block, driving plate and the casing of the box. The connection block and driving plate can be manufactured using CNC milling. The fold lever and the casing are recommended to be manufactured by 3D printing or polymer casting.

7.5. Assessment of clinical requirements

In the conceptual design, the clinical requirements are largely met by the SCARPE implant. Adjustments of the SCARPE implant could be performed non-invasively, by transcutaneously transferring magnetic energy. Furthermore, the curvature of the bar-ends can be determined, to fit a variety of thorax sizes. The transmission along the bar-ends is compliant so it does not limit the bar curvature. The middle segment is also compliant to adhere to the shape of the sternum and maximize the contact surface between the SCARPE implant and the sternum. Conversely, the straight region of the tape spring is not closely following the shape of the thorax as the fold distance changes. A challenge still lies in the straight regions of the tape spring, inside the thorax.

All materials in the static and dynamic section are suited for surgical implantation. The materials are non-toxic and can be sterilized before use. However, there are some areas in the SCARPE implant that are prone for the settling of bacteria. Tight areas where bacteria could grow are, for example, in the connection blocks or between the tape spring layers. To protect the areas prone to cause infection, the SCARPE implant should be covered with a thin silicone sleeve. The silicone layer also protects the soft tissue inside the thorax. The edges of the tape spring are relatively sharp and could cause cuts during implantation.

The most vulnerable area for bacterial growth is inside the box. To minimize the hazard of infection, precautions should be taken. The areas where the rotating magnet and the gearbox are located should be sealed from the driving plate. The area of the driving plate should remove all corners and limit tight spaces.

8

Recommendations for future work

8.1. Methods for increasing the elevation force

8.1.1. Tape spring dimensions

To improve the SCARPE procedure in the future, a single layer tape spring should be developed that meets both the force and size requirements. We propose to optimize the tape spring based on two principles: 1) optimize the cross-sectional dimensions within the size requirements; 2) use different materials to increase the strain energy in the fold. When optimizing the cross-sectional dimensions, three variables should be considered: thickness t, transverse radius R and subtended angle α. Dewalque et al. defined the upper and lower boundaries for these three variables [48]. The boundary values are presented in Table 8.1.

Table 8.1: *Boundaries of the thickness, radius and subtended angle for design of a tape spring [48].*

	t [mm]	R [mm]	α [°]
Lower bound	0.08	10	60
Upper bound	0.25	32.5	130

First of all, t should be as close to the upper bound as possible. A larger t causes an increase in both peak force and steady state force. The steady state bending moment scales with t to the power of three. Secondly, α should be maximized, because the effect of α on the steady state bending moment is larger than the effect of R [64]. Next, A circle segment with a thickness $t = 0.25mm$ and uniform radius is drawn. The width is constrained to a maximum of 12mm, to allow for a coating or cover around the spring. Optimizing the circle segment for α, resulted $\alpha = 72.7°$ untill reaching the lower bound for R. The resulting cross section of the optimized tape spring can be found in Figure 8.1.

Using Equation 4.4, the bending moment of the optimized tape spring (495.6Nmm) is about five times larger than the bending moment of spring w2 (103.3Nmm). The bending moment is directly related to the perpendicular force, therefore, $F_\perp$ also increases by a factor five. The bending moment can be increased even further, by stacking smaller tape springs (without fixation) on top of the optimized tape spring. The concave side of a tape spring essentially houses empty space. Stacking smaller tape springs utilizes the empty space without compromising on outside dimensions or risking plastic deformation. Future research should investigate if this tape spring can supply sufficient elevation force for continuous correction of PE.

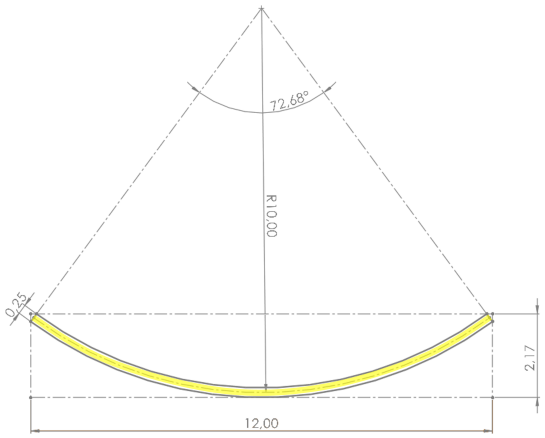

Figure 8.1: *Cross sectional dimensions of a tape spring (yellow) optimized to yield the largest elevation force within in the size requirements without plastic deformation.*

8.1.2. Alternative materials

If a steel tape spring with optimized dimensions still does not supply the appropriate elevation force, it is recommended to explore the use of different materials. A lot of research has been done on the use of composite tape springs in deployable structures. Manufacturing a tape spring from composite materials could reach same stiffness properties as a steel tape spring, for a smaller thickness. Composite materials for tape springs that are frequently described in

literature are carbon fiber reinforced polymers [53, 65, 66] and glass fiber reinforced polymers [61, 67]. A variety of composite materials has been tested for use in orthopedics. Both carbon and glass fiber reinforced polymers have been successfully adopted in hip implants and usage of these materials is considered safe [68]. In future research, the design of the SCARPE implant utilizing composite tape springs could achieve higher elevation forces within the same dimensions, as compared to steel.

It is worth mentioning that fiber reinforced materials have different mechanical properties in the fiber direction, opposed to perpendicular on the fiber. The analysis of composite tape springs is, therefore, not as straight forward as for steel. The equations stated in Section 4.2 are based on tape springs consisting of isotropic materials and are not applicable on tape springs constructed from orthotropic composite materials [53, 61].

Furthermore, composites materials using a polymer matrix show visco-elastic behavior. Being subjected to bending for a long period results in creep of the polymer. Creep decreases the strain energy stored in the fold over time. This could lead to a decrease in the elevation force during correction for a composite tape spring [69]. Creep should be the leading factor in selecting an appropriate matrix material for composite tape springs.

8.2. Asymmetrical PE correction

This study only considers symmetric types of PE. In reality, asymmetric types of PE are rather common [3, 38]. In asymmetric types of PE, the deepest point is located at an offset from the vertical middle line of the thorax. Moreover the sternum can be situated at an angle with respect to the horizontal line (Figure 8.2). The deepest point being asymmetrically located suggests that the distance between the highest and lowest point on the left side of the deformity, is different than the distance between the highest and lowest point on the right side. The SCARPE procedure may also be beneficial for correction of asymmetric types of PE, by applying a different perpendicular force from each tape spring.

If the perpendicular force of one tape spring is larger than the other, the elevation force is not purely vertical. The fold distance is shorter on the side where the deepest point is located, hence the arm on that side of the tape spring is shorter. The perpendicular force is larger on the short side. To maintain horizontal force equilibrium, the elevation force contains a horizontal component. The horizontal force component could be used to repair asymmetry. Future research should study the effects of the SCARPE procedure on asymmetric types of PE and investigate if the horizontal force component is large enough to correct asymmetric types of PE.

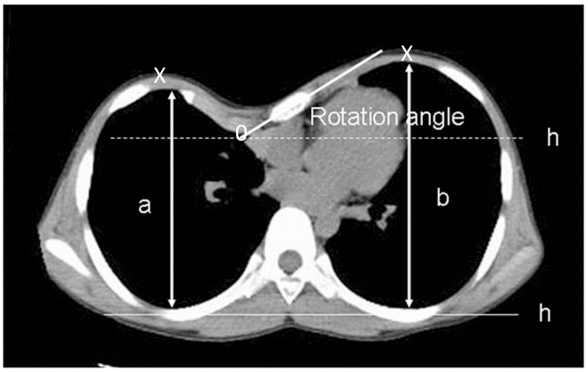

Figure 8.2: *CT scan of a patient with asymmetric type of PE [70]. Here, X mark the highest points of the deformity, O marks the lowest point of the deformity, a and b indicates the maximum free space in the left and right side of the thoracic cavity respectively and h is the horizontal line.*

8.3. Alternative force control mechanisms

In this section, two alternative design proposals are presented to overcome the challenges in the SCARPE implant related to the changing fold location. The first alternative design proposes to change the entry location, in order to create more freedom in choosing the fold location. The second alternative design proposal uses an alternative control mechanism altogether, in which the fold lever is fixed and the tape spring is moved actively.

In the first alternative design proposal, the entire tape spring is outside of the thoracic cavity. The entry location is relocated towards the far medial end of the tape spring (Figure 8.3). Only the middle segment enters the thoracic cavity just before the sternum. The middle segment of the SCARPE implant is changed to a ”cup-shaped” flexure, able to wrap around the sternum. In this manner, the entire mechanism determining the fold distance is in between the superficial fascia and the costal muscles. Between these layers is more free space to change the fold location. The tape spring mechanism is still subdermal, but prevents damage to the lungs or pericardium and is not constrained by the thoracic wall.

Changing the entry location should be carefully evaluated, as it could compromise the aesthetic outcome of the procedure. The straight region

of the tape spring lateral to the fold should be horizontal (or slightly towards overcorrection). If the lateral side of the tape spring is tilted insufficiently, the tape spring is not able to achieve complete elevation. If the tape spring is tilted too far, overcorrection could occur. In the alternative design proposal of Figure 8.3, the curvature of the gray bar-end determines the final position of the sternum.

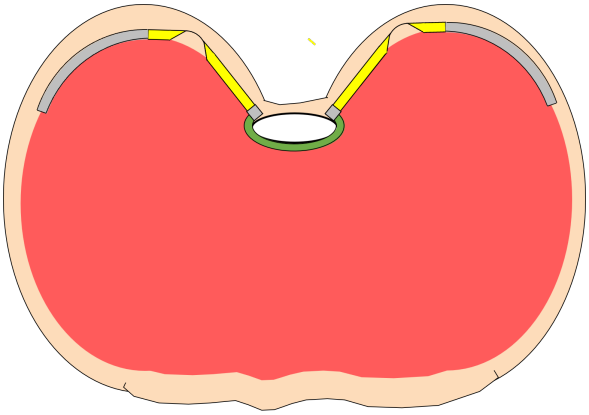

Figure 8.3: *Schematic drawing of the first alternative design proposal in which the entire tape springs (yellow) and bar-ends (gray) are outside thoracic cavity. The "cup-shaped" middle segment (green) only enters the thoracic cavity right before the sternum (white).*

The second alternative design proposal presents a different control mechanism, with a fixed fold lever. In the SCARPE implant, the purpose of changing the fold distance is to change the effective length of the tape springs. Alternatively, if the fold distance is fixed, the effective length can be changed by moving the tape spring itself. An example of such a device is illustrated in Figure 8.4. The fold lever has a fixed position and is rigidly connected to the bar-end. The tape spring is directly actuated in the box to change the arm length.

The tape spring itself can be manufactured such that the actuator can drive the tape spring directly. The use of a transmission then becomes redundant. It is not possible to make a tape spring follow the shape of the curved bar-ends, because of the stiffness and buckling behavior. Therefore a custom spring was designed. The custom spring is shaped like a tape spring on the medial side (with an constant transverse radius) and transitions into an straight flexure (with zero transverse curvature) as we move laterally. The tape spring side of the custom spring can be used for continuous correction. The flexure side is compliant and can be placed along the bar-end and is actuated in the box. A custom tape spring also makes the use of coil springs for passive displacement superfluous. The custom spring is driven to actively change the tape spring length.

The actuator retract the flexure side around a spool in the box. When the custom spring is retracted, the effective length between the fold and the middle segment reduces. Thereby increasing the perpendicular force and decreasing the bending angle. So both the perpendicular force and the length of its projection positively influence the total elevation force. In addition, shortening the custom spring raises the sternum. Therefore, the second alternative design effectively uses a combination of a gradual correction and continuous correction.

The tape spring section corrects the deformity autonomously, however, if an increase in correction rate is required, the sternum can be raised. In order to raise the sternum the custom tape spring is subjected to tension by the actuator.Friction between the tape spring and the fold lever is low. The fold, being considered a zero-stiffness joint, acts as a pulley to prevent large internal stresses in the custom spring. The gradual correction of the sternum is most effective at the start of the correction, when bending angles are large.

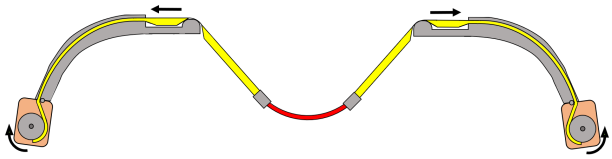

Figure 8.4: *Alternative concept for changing the effective length of the tape spring by actuating the spring ends at the extremities of the implant device.*

As the bending angle approaches zero, the required tension to lift the sternum increases asymptotically. At some point, the required tension grows too large for an actuator to achieve another gradual correction step. In contrast, the continuous correction becomes more effective towards the end of the correction. The continuous elevation force can be used for correction of the remaining deformity. Appendix H provides a more elaborate analysis of this alternative concept. The combination between the gradual and continuous correction is seen as a favorable solution to accelerate the correction rate and increase control in PE repair. We recommend to investigate this alternative concept in future research.

9 Conclusion

The SCARPE procedure presents a conceptual design to use tape springs for correction of PE continuously over time. The design showed promising results, but some optimizations should be done to make the SCARPE implant clinically applicable.

First of all, the elevation force should be increased. The cross-sectional dimensions should be maximized within the size requirements. Therefor the tape spring thickness is the most important parameter. Simultaneously, the dimensional properties should be limited to prevent plastic deformation and to keep the peak force below 20N. When increasing the elevation force by stacking layers on top of each other, the individual layers should not be fixed together. Free tape spring stacks have no risk of delamination and make control more straightforward.

Secondly, the method of adjusting the correction rate should be modified. Changing the fold distance inside of the thoracic cavity could be unsafe and may not be feasible due to anatomical constraints. Either, the entrance location to the thoracic cavity should be changed, or the adjustment method should be changed altogether. The preferred alternative embodiment is an implant that facilitates both gradual and continuous correction simultaneously.

The SCARPE implant provides an alternative way of approaching PE repair. Implementing these optimizations, SCARPE has great potential for future repair of PE. The SCARPE procedure should be used as a source of inspiration to improve treatment of PE in the future.

Acknowledgements

Arriving at the end of this thesis, I would like to use this last chapter to express my gratitude towards some people who helped me in the process of this thesis.

First of all, I want to thank PJ. van Huijstee for teaching me in depth about the anatomy of PE patients. I enjoyed our discussions about the human body and about what is (and definitely what is not) possible during surgery. It was very refreshing to receive advice from someone who has a completely different perspective on engineering. It was a pleasure doing my thesis together with the Haga hospital.

Secondly, I would like to thank my supervisor P. Breedveld. The route to my graduation was a long one. The spare time you had was often limited, but still I am grateful for the elaborate advice, recommendations and feedback you gave me. Things I have learned from you (outside of the technical stuff) is to say ”no”, so now and then, and to set boundaries around what is really important. A lesson I am going to take with me, through the rest of my career.

Lastly, a honorable mention to A.W. van Beurden. Someone who really stood by me during the whole process. Someone who had to listen to all my absurd ideas. But really someone who could put it all into perspective, giving me renewed energy to keep pushing on.

Bibliography

1. Croitoru D and Nuss D. Chest wall anomalies: pectus excavatum and pectus carinatum. Adolesc Med 2004;15:455–71.
2. Okawada M, Lane GJ, and Yamataka A. Bone Mineral Density as a Marker for Pectus Correction. In: *Chest Wall Deformities*. Springer, 2017:75–9.
3. Willital GH, Saxena AK, Schütze U, et al. Chest-deformities: a proposal for a classification. World Journal of Pediatrics 2011;7:118–23.
4. Hebra A, Calder BW, and Lesher A. Minimally invasive repair of pectus excavatum. Journal of visualized surgery 2016;73.
5. Amerstorfer EE and Saxena AK. Syndromes Associated with Pectus Deformities. In: *Chest Wall Deformities*. Springer, 2017:101–40.
6. Liu C and Wen Y. Research progress in the effects of pectus excavatum on cardiac functions. World Journal of Pediatric Surgery 2020;3.
7. Lawson ML, Mellins RB, Paulson JF, et al. Increasing Severity of Pectus Excavatum is Associated with Reduced Pulmonary Function. The Journal of Pediatrics 2011;159:256–261.e2.
8. Morshuis W, Folgering H, Barentsz J, et al. Pulmonary Function Before Surgery for Pectus Excavatum and at Long-term Follow-up. Chest 1994;105:1646–52.
9. Feng J, Hu T, Liu W, et al. The biomechanical, morphologic, and histochemical properties of the costal cartilages in children with pectus excavatum. Journal of Pediatric Surgery 2001;36:1770–6.
10. Stearns JD, Twaibu J, Kwaku D, et al. Efficacy of standard chest compressions in patients with Nuss bars. Journal of Thoracic Disease 2020;12:4299.
11. Nuss D and Kelly RE. The Minimally Invasive Repair of Pectus Excavatum. Operative Techniques in Thoracic and Cardiovascular Surgery 2014;19:324–47.
12. Schier F, Bahr M, and Klobe E. The vacuum chest wall lifter: an innovative, nonsurgical addition to the management of pectus excavatum. J Pediatr Surg 2005;40:496–500.
13. Haecker FM and Sesia S. Vacuum bell therapy. Annals of cardiothoracic surgery 2016;5:440.
14. Patel AJ and Hunt I. Is vacuum bell therapy effective in the correction of pectus excavatum? Interactive CardioVascular and Thoracic Surgery 2019;29:287–90.
15. Haller JA, Colombani PM, Humphries CT, et al. Chest wall constriction after too extensive and too early operations for pectus excavatum. The Annals of Thoracic Surgery 1996;61:1618–25.
16. Nuss D, Kelly RE, Croitoru DP, et al. A 10-year review of a minimally invasive technique for the correction of pectus excavatum. Journal of Pediatric Surgery 1998;33:545–52.
17. Harrison MR, Estefan-Ventura D, Fechter R, et al. Magnetic Mini-Mover Procedure for pectus excavatum: I. Development, design, and simulations for feasibility and safety. Journal of Pediatric Surgery 2007;42:81–6.
18. Ravitch MM. The Operative Treatment of Pectus Excavatum. Annals of surgery 1949;129:429–44.
19. Funk J and Gross C. Surgical Techniques-Pectus Excavatum: The Modified Ravitch Procedure. In: *Chest Wall Deformities*. Springer, 2017:431–6.
20. Pilegaard HK. Minimal Access Repair of Pectus Excavatum (MARPE)-Pilegaard Modification. In: *Chest Wall Deformities*. Springer, 2017:457–65.
21. Schwabegger AH. Special instruments, technical refinements. In: *Congenital Thoracic Wall Deformities: Diagnosis, Therapy and Current Developments*. Springer, 2011:318–25.
22. Nagasao T, Miyamoto J, Tamaki T, et al. Stress distribution on the thorax after the Nuss procedure for pectus excavatum results in different patterns between adult and child patients. Journal of Thoracic and Cardiovascular Surgery 2007;134:1502–7.

23. Schwabegger AH and Fonkalsrud EW. Special considerations in adults with MIRPE and MOVARPE techniques. In: *Congenital Thoracic Wall Deformities: Diagnosis, Therapy and Current Developments*. Springer, 2011:127–42.
24. Del Frari B and Schwabegger AH. Clinical results and patient satisfaction after pectus excavatum repair using the MIRPE and MOVARPE technique in adults: 10-year experience. Plastic and Reconstructive Surgery 2013;132:1591–602.
25. Chang PY, Hsu ZY, Chen DP, et al. Preliminary analysis of the forces on the thoracic cage of patients with pectus excavatum after the Nuss procedure. Clinical Biomechanics 2008;23:881–5.
26. Frantz F and Goretsky MJ. Complications of Minimally Access Pectus Excavatum Repair. In: *Chest Wall Deformities*. Ed. by Saxena AK. Berlin, Heidelberg: Springer Berlin Heidelberg, 2017:373–81.
27. Park HJ, Lee SY, Lee CS, et al. The Nuss procedure for pectus excavatum: evolution of techniques and early results on 322 patients. The Annals of Thoracic Surgery 2004;77:289–95.
28. Nuss D. Minimally invasive surgical repair of pectus excavatum. Seminars in Pediatric Surgery 2008;17. Chest Wall Deformities:209–17.
29. Höllwarth M and Saxena AK. Minimal Access Repair of Pectus Excavatum. In: *Chest Wall Deformities*. Ed. by Saxena AK. Berlin, Heidelberg: Springer Berlin Heidelberg, 2017:417–29.
30. Kim DH, Hwang JJ, Lee MK, et al. Analysis of the Nuss Procedure for Pectus Excavatum in Different Age Groups. The Annals of Thoracic Surgery 2005;80:1073–7.
31. Jamshidi R and Harrison M. Magnet-mediated thoracic remodeling: a new approach to the sunken chest. Expert Review of Medical Devices 2007;4:283–6.
32. Harbaugh CM, Johnson KN, Kein CE, et al. Comparing outcomes with thoracic epidural and intercostal nerve cryoablation after Nuss procedure. Journal of Surgical Research 2018;231:217–23.
33. Schwabegger AH, Del Frari B, and Metzler J. Technical consideration of the MOVARPE technique in intricate pectus excavatum deformity. Wiener klinische Wochenschrift 2017;129:702–8.
34. Graves CE, Hirose S, Raff GW, et al. Magnetic Mini-Mover Procedure for pectus excavatum IV: FDA sponsored multicenter trial. Journal of Pediatric Surgery 2017;52:913–9.
35. Harrison MR, Gonzales KD, Bratton BJ, et al. Magnetic mini-mover procedure for pectus excavatum III: safety and efficacy in a Food and Drug Administration-sponsored clinical trial. Journal of Pediatric Surgery 2012;47:154–9.
36. Engelkemier D, Kruk P, Naheedy J, et al. Chest wall. 2018.
37. Forman JL and Kent RW. The effect of calcification on the structural mechanics of the costal cartilage. Computer Methods in Biomechanics and Biomedical Engineering 2014;17:94–107.
38. Coorens NA, Daemen JH, Slump CH, et al. The Automatic Quantification of Morphological Features of Pectus Excavatum Based on Three-Dimensional Images. Seminars in Thoracic and Cardiovascular Surgery 2021.
39. Fonkalsrud EW and Reemtsen B. Force required to elevate the sternum of pectus excavatum patients. Journal of the American College of Surgeons 2002;195:575–7.
40. Weber PG, Huemmer HP, and Reingruber B. Forces to be overcome in correction of pectus excavatum. The Journal of Thoracic and Cardiovascular Surgery 2006;132:1369–73.
41. Boia ES, Susan-Resiga R, Raicov PC, et al. Determination of the Mechanical Requirements for a Progressive Correction System of Pectus Excavatum in Children. Journal of Laparoendoscopic & Advanced Surgical Techniques 2005;15:478–81.
42. Sesia SB, Hradetzky D, and Haecker FM. Monitoring the effectiveness of the vacuum bell during pectus excavatum treatment: Technical innovation. Journal of Pediatric Surgery 2018;53:411–7.
43. Oyen ML. Spherical Indentation Creep Following Ramp Loading. Journal of Materials Research 2005;20:2094–100.
44. Oyen M, Murakami D, and Kent R. Mechanical characterization of costal cartilage. In: *33rd Proceedings of the International Workshop on Human Subjects for Biomechanical Research*. 2005.

45. Saxena AK. Overview of Repair of Pectus Excavatum Type of Deformities. In: *Chest Wall Deformities*. Ed. by Saxena AK. Berlin, Heidelberg: Springer Berlin Heidelberg, 2017:329–49.
46. Breedveld P, Herder J, and Tomiyama T. Teaching creativity in mechanical design. In: *Diversity and Unity. Proceedings of IASDR2011*. 2011:1–10.
47. Works. S. Carpenter uses a construction tape to measure the length of a piece of wood. `https : / / www . stanleyworks.nl/products/detail/ Producten / HANDGEREEDSCHAP / Meetinstrumenten / Rolbandmaten / STANLEY % C2 % AE + FATMAX % C2 % AE + NGT + ROLBANDMAAT + 8Mfwdslash32MM`. Accessed: 2022-11-24.
48. Dewalque F, Collette JP, and Brüls O. Mechanical behaviour of tape springs used in the deployment of reflectors around a solar panel. Acta Astronautica 2016;123:271–82.
49. Seffen K and Pellegrino S. Deployment dynamics of tape springs. Proceedings of the Royal Society of London. Series A: Mathematical, Physical and Engineering Sciences 1999;455:1003–48.
50. Seffen KA. On the Behavior of Folded Tape-Springs. Journal of Applied Mechanics 2000;68:369–75.
51. Wüst W. Some applications of the theory of the cylinder shell. Z. Angew. Math. Mech. 1954;34:444–54.
52. Walker S and Aglietti G. A study of tape spring fold curvature for space deployable structures. Proceedings of the Institution of Mechanical Engineers, Part G: Journal of Aerospace Engineering 2007;221:313–25.
53. Piovesan D, Zaccariotto M, Bettanini C, et al. Design and validation of a carbon-fiber collapsible hinge for space applications: a deployable boom. Journal of Mechanisms and Robotics 2016;8:031007.
54. Watt AM and Pellegrino S. Tape-spring rolling hinges. In: *Proceedings of the 36th Aerospace Mechanisms Symposium*. Citeseer. 2002:15–7.
55. Croitoru DP, Kelly RE, Goretsky MJ, et al. Experience and modification update for the minimally invasive Nuss technique for pectus excavatum repair in 303 patients. Journal of Pediatric Surgery 2002;37:437–45.
56. Park HJ, Chung WJ, Lee IS, et al. Mechanism of bar displacement and corresponding bar fixation techniques in minimally invasive repair of pectus excavatum. Journal of Pediatric Surgery 2008;43:74–8.
57. Jenks M, Craig J, Higgins J, et al. The MAGEC system for spinal lengthening in children with scoliosis: A NICE Medical Technology Guidance. Applied health economics and health policy 2014;12:587–99.
58. Paley D. PRECICE intramedullary limb lengthening system. Expert Review of Medical Devices 2015;12.
59. Pool S, Walker B, and Chang A. External adjustment device for distraction device. United States patent US 2010121323A1. 2010 May 13.
60. Walker B, Pool S, Mccoy J, et al. Skeletal manipulation method. United States patent US 20160030089A1. 2016 Feb 4.
61. Wang B, Seffen K, and Guest S. Folding of bistable composite tape-springs. 2019.
62. Verzendaal J. Increasing energy storage in compliant tape-spring mechanisms. Master thesis, TU Delft Repository 2020.
63. Walker SJ and Aglietti GS. Modeling the Hinge Moment of Skew-Mounted Tape Spring Folds. Journal of Aerospace Engineering 2007;20:102–15.
64. Ye H, Zhao C, Zhang Y, et al. Analysis of mechanical properties in bending processes and optimal design of simple tape spring. Journal of Modeling in Mechanics and Materials 2017;1.
65. Yee J, Soykasap O, and Pellegrino S. Carbon fibre reinforced plastic tape springs. In: *45th AIAA/ASME/ASCE/AHS/ASC Structures, Structural Dynamics & Materials Conference*. 2004:18–9.
66. Mallikarachchi H and Pellegrino S. Simulation of quasi-static folding and deployment of ultra-thin composite structures. In: *49th AIAA/ASME/ASCE/AHS/ASC Structures, Structural Dynamics, and Materials Conference*. 2008:2053.
67. Mierheim O, Glaser T, Hobbie CF, et al. The Tape Spring Hinge Deployment System of the EU: CROPIS Solar Panels. European conference on spacecraft structures, materials and mechaniscal testing, proceedings 2018.

68. Salernitano E and Migliaresi C. Composite materials for biomedical applications: a review. Journal of applied biomaterials and biomechanics 2003;1:3–18.

69. Kwok K and Pellegrino S. Micromechanics Models for Viscoelastic Plain-Weave Composite Tape Springs. AIAA Journal 2017;55:309–21.

70. Yoshida A, Uemura S, Yamamoto M, et al. Correlation of asymmetric chest wall deformity and growth in patients with pectus excavatum. Journal of pediatric surgery 2013;48 4:771–5.

71. Park HJ, Chung WJ, Lee IS, et al. Mechanism of bar displacement and corresponding bar fixation techniques in minimally invasive repair of pectus excavatum. Journal of Pediatric Surgery 2008;43:74–8.

A

Usage of the SCARPE procedure

A.1. Usage

During the SCARPE procedure, the SCARPE implant is minimally invasive inserted in the thorax of a PE patient. The surgical technique is a vital part to advance the SCARPE procedure from a conceptual design to a clinically applicable procedure. The surgical technique for implantation is described in this section and is illustrated in Figure A.1. The start of the procedure is similar to the surgical technique of MIRPE (see Section 2.1). After the patient is prepared and under general anaesthesia, the surgeon uses a marker to identify the highest and lowest point of the deformation (Figure A.1a). By pressing on the thorax the intercostal spaces are identified and marked. A pectus bar template is curved along the desired circumference of the thorax. The template will be used later to accurately determine the curvature of the bar-ends. Two small skin incisions are made on both sides of the thorax, on the transverse line from the deepest point (Figure A.1a). A third incision is made lower on the right side to allow the use of a thoracoscope for visual guidance during implantation. The right lung is deflated to improve the sight of the thoracoscope. An introducer is used to make a substernal tunnel, similar to MIRPE. The introducer enters the thoracic cavity slightly medial of the highest point of the deformity (Figure A.1b). Through the thoracic cavity, the introducer travels while keeping constant contact with the sternum and the thoracic wall (Figure A.1c). The introducer is then used to lift the sternum up to ”loosen” the cartilage (Figure A.1d). Lifting the sternum before implantation, simplifies correction in a later stage.

Next, a thorax drain is connected to the tip of the introducer and pulled through the tunnel (Figure A.1e). Once the thorax drain is in place, two tape springs are combined with a middle segment of appropriate length. The tape spring connection is fixed to the thorax drain on the right side of patient and pulled in, through the substernal tunnel (Figure A.1f). It is recommended to wrap a plastic or silicon sleeve around the tape spring, as the edges of a tape spring are relatively sharp and may be a safety hazard due to cutting. The straight bar-ends are curved using a table top bender (Figure A.2), until the curvature of the bar-ends match the curvature of the template. The fold lever is set in the right place and the bar-ends are placed on the thorax to measure the desired length of the tape spring. The tape springs are cut and the excess material is removed (Figure A.1g). The cut tape spring ends are fastened to the bar-ends by one small bolt on each side (Figure A.1h). To fix the tape spring mechanism to the ribs, the surgeon selects a suiting fixation method. Fixation can be done by using surgical steel wire or by selecting the best suiting rib clamps. The box is fixed to the ribs by using that specific method (Figure A.1i). Finally the thoracoscope is removed and all the incisions are sutured (Figure A.1j). A thorax drain is left in the thorax to remove all excessive air in the thorax using an air lock.

Some surgeons prefer to observe the thorax in the fully corrected position before making the definitive decision to use one specific correction procedure. To visualize full correction in the SCARPE procedure, a sternal crane can be used as proposed by Park et al. [71]. A rigid crane structure is assembeled and placed over the patient. A wire suture is passed though the sternum percutaneously and connected as a loop to the crane structure. As the crane raises, it elevates the sternum and thoracic wall. Elevating the sternum high enough for snap back to occur, provides an excellent view of the thorax after correction. If full correction of the sternum is not sufficient, the decision can always be

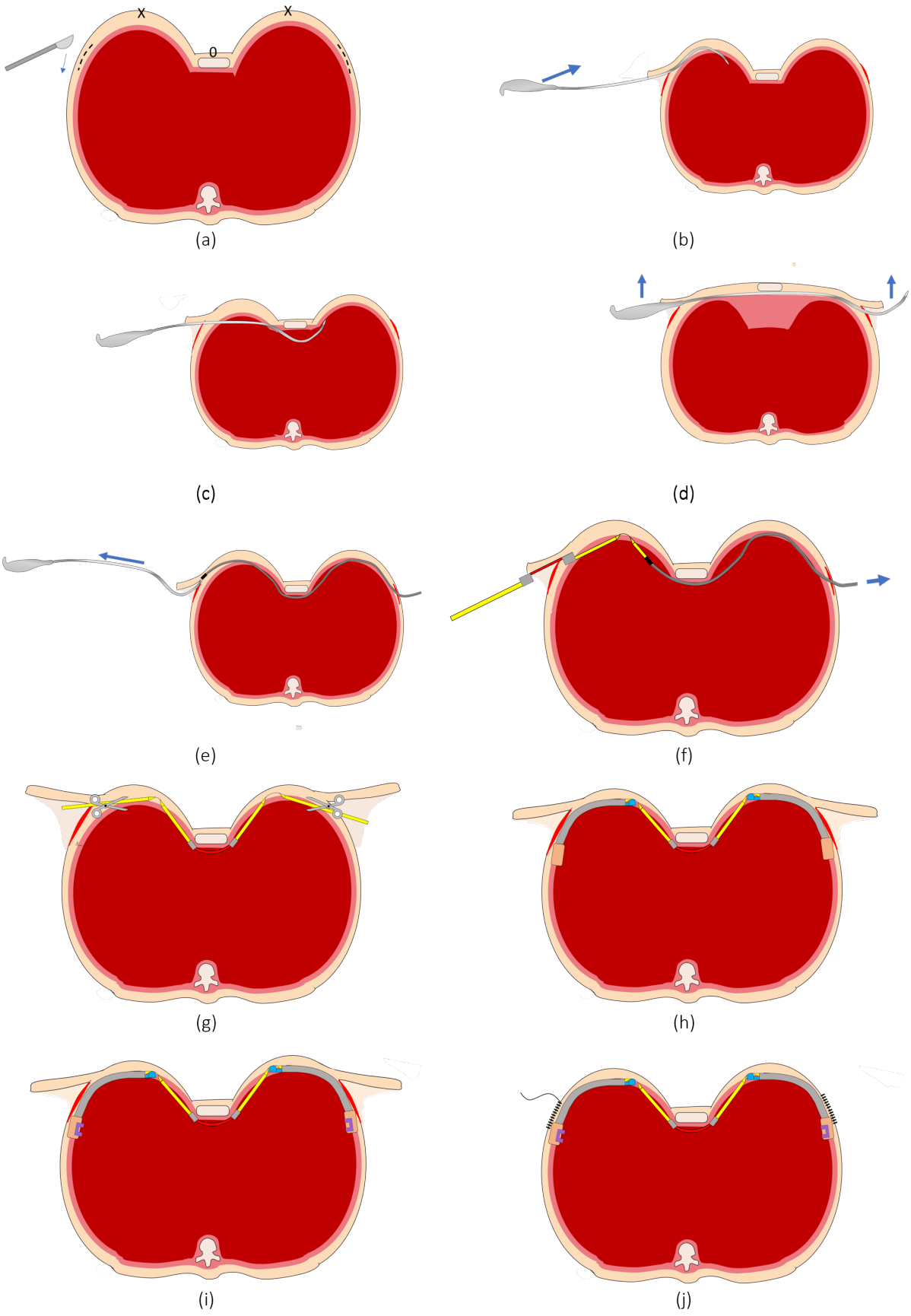

Figure A.1: *Surgical method of implantation in the SCARPE procedure in steps. (a) Mark landmarks on the patient body. X indicates the highest point of the deformation, 0 indicates the lowest point. Incisions are made on both sides of the thorax. (b) The introducer enters the chest cavity slightly medial from the highest point. (c) The introducer travels from left to right to make a substernal tunnel. (d) The introducer is lifted to raise the sternum and "loosen" the costal cartilage. (e) A thorax drain is pulled though the substernal tunnel. (f) The tape springs and middle segment are pulled in place with the thorax drain. (g) The required tape spring length is measured and excessive material is removed. (h) Bar-ends are implanted and connected to the tape springs. (i) The bar-ends are connected to the ribs. (j) Incisions are closed with a suture.*

Figure A.2: *Surgeons bending a pectus bar using a table top bender [4]*

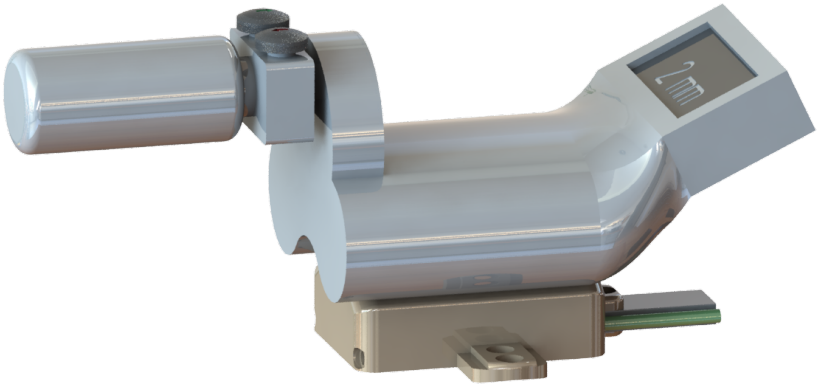

Figure A.3: *The external drive mechanism on the box.*

made to remove the SCARPE implant and resort back to MIRPE.

A.1.1. Post-operative adjustments

After surgical implantation, the SCARPE implant slowly corrects the sternum. This is an automatic process and does not require adjustments to be made. However, if a change in correction rate is required, the fold distance can be adjusted. Inside the box is an actuation mechanism which can be operated by the external drive mechanism. The external drive mechanism is placed on the skin of the thorax at the location of the box. The cylindrical magnets should be parallel to the box (Figure A.3). The direction does not matter as long as the same direction is consistently applied throughout treatment. Turning on the external drive mechanism creates a rotating magnetic field, rotating the permanent magnet in the box. The direction of the rotating magnetic field determines the translation direction of the fold lever. The travelled distance of the fold lever is displayed on a screen. The external drive mechanism should be turned off and removed once the fold lever is located at the required position.

Use of the external drive mechanism is non-invasive and easy to perform. Therefore, adjustments can be operated in a non-clinical setting. A physician may control the SCARPE implant on out-patient basis. In an ideal situation the patient may do the adjustment themselves at home. Nonetheless, caution should be taken when moving the fold lever, as it does present some additional risk. THis is discussed in Section 7.3.2.

A.1.2. Removal procedure

The SCARPE implant should facilitate correction of the deformity over the course of two years. After the two years, the bar should lock itself in the straight configuration. In this configuration the SCARPE implant is left in place for at least one year to prevent relapse of the deformity.

As a total of three years have passed, the SCARPE implant is surgically removed. The removal of the SCARPE implant follows a similar procedure as described above but in reversed fashion. Three incisions are made at the scars from the implantation procedure. The box is detached from the ribs and the bar-ends are removed on each side. The tape springs and middle segments are removed by retraction to the right side. A sleeve of connective tissue may have formed around the SCARPE implant during the procedure. In that case, the connective tissue should be resected before retraction of the tape springs. Once the implant is removed, the incisions are sutured. The patient should remain with a aesthetically satisfactory shape of the chest, improving cardio-pulmonary capacity and overall self-image.

B

Iterations of the middle flexure

During the design of the SCARPE implant, a concept was developed where two tape springs were connected via a rigid segment. A rough prototype was developed to test the feasibility of this concept. However, it appeared that this configuration is highly unstable. A rigid segment connection two tape springs essentially makes a trapezoidal four-bar linkage. The fourth ”bar” is not actually present, but because the distance between the top joints of the tape springs are fixed, the system acts like there is a physical bar present. The fourth ”bar” is schematically depicted by the dashed line in Figure B.1. The springs (yellow), both apply a moment on the rigid segment (red), equal in magnitude, opposite in sign. The folds in the tape spring are indicated as node joints (blue). In perfect symmetry the two moments would cancel out, however, this is nearly impossible to achieve. Even a slight deviation would rotate the rigid segment towards one of two stable positions where one tape spring and the middle segment are co-linear.

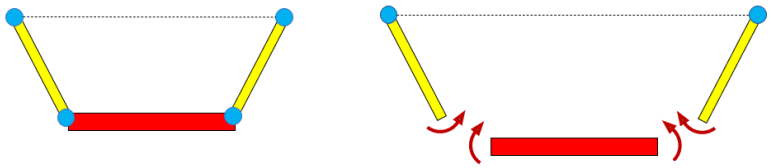

Figure B.1: *Trapezoidal four bar linkage configuration with: straight section of the tape springs (yellow), rigid segment (red) and folds of the tape spring (blue). The dotted line is the hypothetical fourth bar caused by the fixed distance between the top-left and top-right nodes. The red arrows illustrate the bending moment of the tape spring, acting on the rigid segment and vise versa.*

The trapezoidal configuration therefore, has no unique configuration. Rather, the trapezoidal configuration bi-stable. This principle is often used in compliant switches. Instability in the system was found after fabrication of a rough prototype and doing some preliminary experiments. This can be seen in Figure B.2 below. The tape springs in this configuration were not applicable in SCAPE, because of the bistable behavior.

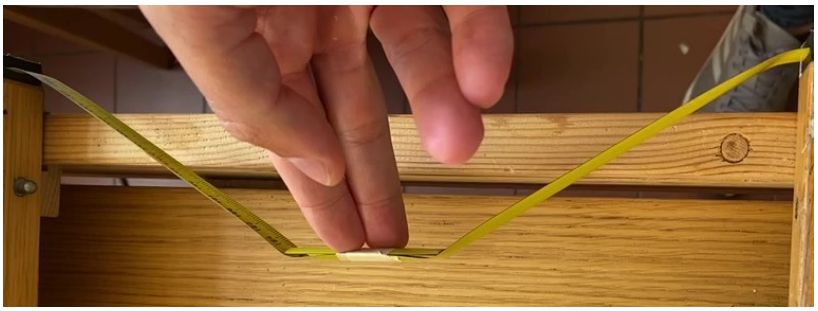

(a) *Unstable state*

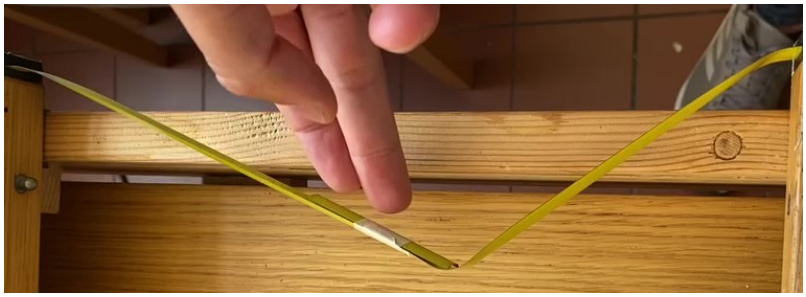

(b) *stable state 1*

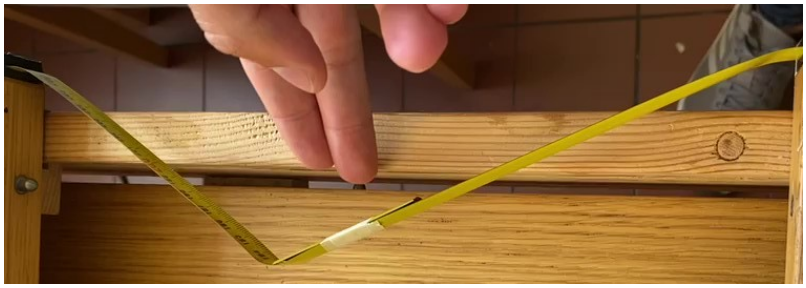

(c) *Stable state 2*

Figure B.2: *Tape springs connected to a rigid segment in three states*

multiple iterations were performed to find the optimal configuration of the middle segment (Figure B.3) To improve stability, V-shaped configurations we considered only have one bending point in the center of the middle segment. One bending point means there is only one stable configuration possible. The first v-shaped middle segment was designed as two rigid segments with a pivot point in between (Figure B.3c). Although the system remains stable, the contact surface is reduced . The pivot point and the sternum are not always in contact. Moreover, the pivot point may exert a large point load on the soft tissue behind the sternum. This poses a problem, especially at the start of the correction.

Other pivoting middle segments were designed to minimize the distance between the sternum and pivot point at the start of the correction (Figure B.3d). Yet, the increased contact surface at the start, came at the expanse of a reduced contact surface towards the end of the correction. Prolonged pressure on a small surface of the sternum causes bone remodeling to alter the shape of the sternum. Through an iterative process, the optimal balance between pivot distance and contact pressure was tried to be found. Nevertheless, the v-shaped configurations were deemed as not feasible. As a logical step next step, we opted to reduce the number of joints even further, to zero. The resulting design was a flexure with a certain stiffness that supports the sternum.

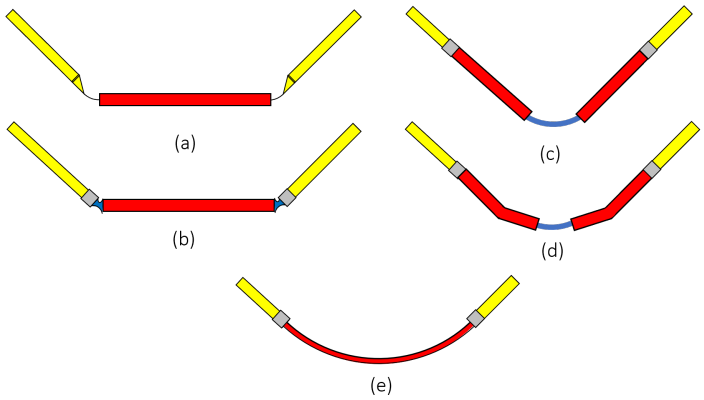

Figure B.3: *Iterations of design of the middle segment with: tape springs (yellow), middle segment (red), connection block (gray) and compliant joint (blue). (a) Rigid middle segment with tape spring folds as joints. (b) Rigid middle segment with additional compliant joints. (c) V-shaped joint with straight rigid segments. (d) V-shaped joint with angled rigid segments. (e) Middle segment as a flexure.*

C

Validation of sample size

The load cell used in the experiment has a finite accuracy. The measured force tends to fluctuate within a certain bandwidth (Figure C.1). The bandwidth seems to be worse for small forces (below 1N). In order to retrieve a representative mean value from the measurements, the sample size should be carefully evaluated. In establishing the sample size, there is a trade-off between accuracy and measurement time.The measured mean of a large number of data points is more precise and lies closer to the true mean. However, increasing the sample size also increases the measurement time, as the sampling frequency is fixed by NI Labview at 10 Hz.

Two long measurements were performed of 150 seconds (1500 data points), in order to determine the sample size. The long measurement is believed to have a mean closest to the true value. The large resulting data set, is split into matrices with a different number of rows. For example, investigating a sample size of 100, yields a matrix of 15 columns of 100 rows. Each column in the matrix represents a measurement, where the value in every row contains a measured data point. The mean and standard deviation of each column are calculated, as well as the error between the means a column and the large data. We evaluated sample sizes of 50, 100, 150, 250, 300, 400 and 500 data points. We found that around 200-300 data points is a suitable choice. For 200 and 250 data points, the absolute error between the column mean and the mean of the large data set, first fell below 0.001. If we increase sample size beyond 300 data points, the error between means will reduce slightly. Nevertheless the gain is too little for increasing the measurement time. The sample size was eventually chosen at 250 data points.

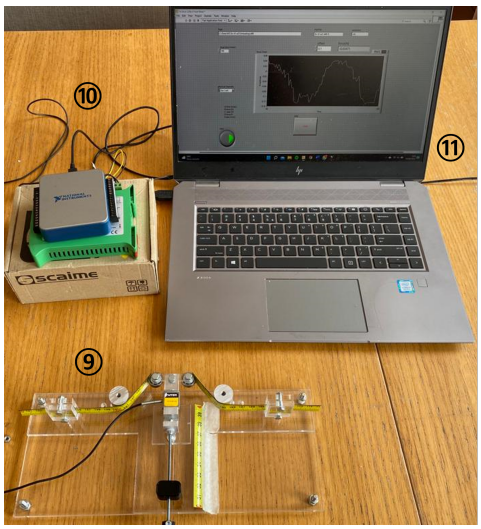

Figure C.1: *Complete experimental setup, showing the fluctuating behavior of the load cell on the screen. With 1) experimental setup, 2) DAQmx terminal and 3) laptop running NI labview*

D Matlab files

D.1. Usage

The Matlab scripts used for processing all the measurement data and plotting the results in a figure are presented below. After each measurement, the data was saved to an Excel-file (Microsoft, Redmond WA, USA). The Matlab file *Import.m* was used to extract the right data from Excel sheets and import the data into Matlab. The data form eight measurements was saved as one data set in an 8x4 matrix. Each column included: h, mean of F_e, standard deviation of F_e and the bending moment M, respectively. The Matlab file *CentralFile.m* was used to compare data sets and plot figures. Dependent on the experiment, a different function file called to compare the right data sets. The dependant variables need to be filled in as a cell in the *CentralFile.m* to plot a figure.

D.2. Import.m

```
%% Import data from Experiments
% Bas Ackermans
% 04-08-2022

 clear all
 close all

%%  Import Data
myFolder = uigetdir('C:\Data', 'Choose file location');          % Manually select folder
filePatern = fullfile(myFolder,'*.xls');                         % Add xls for all file names
xlsFiles = dir(filePatern);                                      % Make struct containing info
     of each file in the folder
n=length(xlsFiles);

for ii=1:n
     baseFileName = xlsFiles(ii).name;                           % Extract filename from
    struct
     fullFileName = fullfile(myFolder, baseFileName);            % filename + path
     sprintf('%s\n', fullFileName);                              % Print filename as text-
    string

     Fraw(:,ii) = readmatrix(fullFileName,'FileType','text','Range','C1:C250');
                                                                 % Forces raw data in each
    column
     nameCell = strsplit(baseFileName,{' ','-'});                          % Split name
    components in separate cells

end

%% Data Analysis

offset = 0;
Mean = mean(Fraw)-offset;                                % calculate mean [N]
StanDiv = std(Fraw);                                  % calculate standard deviation
```

```
m_loading = [0, 2.5, 5, 7.5, 10, 20, 30, 40]';       % distance to correction [m]
m_unloading = [40, 30, 20, 10, 7.5, 5, 2.5, 0]';

if Mean(1)<=Mean(n)
    disp('Loading')
    Data = [m_loading , Mean', StanDiv'];
elseif Mean(n)<=Mean(1)
    disp('Unloading')
    Data = [m_unloading , Mean', StanDiv'];
end

Info = [{'number of layers'},nameCell(7); {'thickness independend layers'}, nameCell(8); {'
    Width'}, nameCell(9); {'Distance to center'}, nameCell(10)];

%% Save to File

if nameCell(10) == "ul"                                    % saves d50 to file name iso ul
    nameCell(10) = {'d50'};
else
    nameCell(10) = nameCell(10);
end

if nameCell(9) == "w2"                                    % saves w15 to file name iso w2
    nameCell(9) = {'w15'};
else
    nameCell(9) = nameCell(9);
end

saveFileNameCell = nameCell(7:10);                         % retrieve data from file name as {
    cell}
saveFileNameString = strjoin(saveFileNameCell,'.');       % Join data-cells as text "string"
Ext = "3.mat";                                             % Define Extention of file type "
    string"
saveFileName = append(saveFileNameString,Ext);             % Combine file name with extention

% save to file in this folder
save(saveFileName,'Data')

disp('Data saved succesfully to')
disp(saveFileName)
 %% Constant moment?
 % check if 2 is necessary
 distance = nameCell(10);
d=0;
 if     distance == "d50"
     d = 50;
 elseif distance == "d40"
     d = 40;
 elseif distance == "d30"
     d = 30;
 end
 %%
  rl = 13/2;

 for ii=1:8
     theta(ii) = atan((Data(ii,1))/(d - 17.5));                                %calculate
    angle at bottom of the bearing
    xbear(ii) = rl*sin(theta(ii));                                             % xcorrection
    for bearing
    ybear(ii) = ( rl- rl*cos(theta(ii)));                                      % ycorrection
    for bearing
     theta2(ii) = atan( (Data(ii,1) - ybear(ii))/(d-17.5 - xbear(ii)) );       % new angle
     r(ii) = sqrt( (d-17.5 - xbear(ii))^2 + (Data(ii,1)- ybear(ii))^2 );       % length of
    spring
     F(ii) =    (Data(ii,2)/2)/cos(theta2(ii));                                %calculate perp
    . force from elevation force
     M(ii) =    F(ii)*r(ii);                                                   % moment of one
     spring [Nmm]
 end

 %%
```

```
Data = [Data, M'];
disp('Data = ')
disp(Data)

%% Save Moment

save(saveFileName,'Data')
if size(Data) == [8 4]
 disp('Successfully stored to ')
disp(saveFileName)
else
    disp('---- ERROR ---- ')
    disp('Data matrix has the wrong size. Run script again.')
    Data = Data(:,(1:3));
    save(strName,'Data')
end
```

D.3. CentralFile.m

```
%% Central script for comparing data
% shows and/or stores comparisson plot
  % Bas Ackermans
  % 09-08-2022


clear
close all

%% Input variables

% short list of values to make loading easy
% To compare certain values add them in a cell

layer =          '1x';
thickness =      't1';
width =          'w15';
distance =       {'d503','d403','d303'};
store  =         1;                      % 1 is yes, 0 is no
n =              (1:8);                  % values that should be displayed, h40=1
out =            0;                      % outliers [d,value]


% Load data in correct function

if length(layer) == 3 && length(thickness) == 3
    [thickData] = ThickComp(layer,thickness,width,distance,store,n,out);

elseif length(layer) == 3
    [layerData] = LayerComp(layer,thickness,width,distance,store,n);

elseif length(width) == 2
    [widthData] = WidthComp(layer,thickness,width,distance,store,n);

elseif length(distance) == 3
    [distData] = DistanceComp(layer,thickness,width,distance,store,n);

elseif length(distance) == 2
    [loadData] = LoadComp(layer,thickness,width,distance,store,n);

end
```

D.4. Function Files

D.4.1. ThickComp.m

```
%% Plot data
% Bas Ackermans
% 09-08-2022

% Input
```

```
   % layer:      1x3 cell
   % thickness:  1x3 cell
   %  width:     1x1 struct
   %  distance:  1x1 struct
% Output
   % data: 1x3 cell each containing a 8x3 matrix with
            % 8,1 distance in mm
            % 8,2 mean
            % 8,3 standard deviation

function[data] = ThickComp(layer,thickness,width,distance,store,n,out)

disp('Now loading: ThickComp')

%% Input variables

% make a short list of values to make loading easy

layerName =    {'x1t1','x2t2','x3t3'} ;
fileExt =       'mat'   ;

 %% Load data

   for ii=1:length(layer)
    strLayer = char(layer(ii));
    strThick = char(thickness(ii));
    inputStr = {strLayer,strThick,width,distance,fileExt};      % make string from all input
    strName = strjoin(inputStr,'.');                            % Add string to one name

    Data = load(strName);                                       % load data
    data.(layerName{ii}) = cell2mat(struct2cell(Data));         % save data to data.distance
    struct
   end

   %% Analyse Data
   for jj=1:7
absDiff3_1(jj) = data.x3t3(jj,2) - data.x1t1(jj,2);                             % absolute
    change
relDiff3_1(jj) = ((data.x3t3(jj,2) - data.x1t1(jj,2))/data.x1t1(jj,2))'*100;    % relative
    change


absDiff3_2(jj) = data.x3t3(jj,2) - data.x2t2(jj,2);                             % absolute
    change
relDiff3_2(jj) = ((data.x3t3(jj,2) - data.x2t2(jj,2))/data.x2t2(jj,2))'*100;    % relative
    change

absDiff2_1(jj) = data.x2t2(jj,2) - data.x1t1(jj,2);                             % absolute
    change
relDiff2_1(jj) = ((data.x2t2(jj,2) - data.x1t1(jj,2))/data.x1t1(jj,2))'*100;    % relative
    change
   end

    X = [absDiff2_1(1:4)',absDiff3_2(1:4)', absDiff3_1(1:4)'];  %fit changes to matrix
 xrel = [relDiff2_1',relDiff3_2', relDiff3_1'];

 if (out > 0 )
 xrel(out,:) = []; %  Remove outliers from values
 elseif (out == 0)
 end

 meanRel = mean(xrel)';     % mean relative change
 disp(xrel)
 meanAbs = mean(X)';        % mean absoltue change
 disp(X)

 %% Plot data

 purple = [0.4940, 0.1840, 0.5560];
 green =  [1, 0.6940, 0.1250];
 h = [0 10 20 30 32.5 35 37.5 40]';
```

```
h = h(n);

f1 = fit(h,data.x1t1(n,2),"pchipinterp");  %fit model through datapoints
f2 = fit(h,data.x2t2(n,2),"pchipinterp");
f3 = fit(h,data.x3t3(n,2),"pchipinterp");

figure
% plot datapoints with error bars
e1 = errorbar(h,data.x1t1(n,2),data.x1t1(n,3),'.r','LineStyle','None','LineWidth',0.8);
hold on
e2 = errorbar(h,data.x2t2(n,2),data.x2t2(n,3),'.','LineStyle','None','LineWidth',0.8,'Color'
    ,purple);
e3 = errorbar(h,data.x3t3(n,2),data.x3t3(n,3),'.','LineWidth',0.8,'Color',green);


p1 =  plot(f1,'-r');  %plot model
p2 =  plot(f2,'-b');
p3 =  plot(f3,'-');
legend([e1 e2 e3], '1 layer','2 layers fixed','3 layers fixed','Location','northwest')
xlabel('h [mm]')
ylabel('F_e [N]')
ylim([-1 20])
set(p2, 'Color',purple)
set(p3, 'Color',green)

%% Save plot

myFolder = 'C:\Users\Bas10\OneDrive\Documents\BMD\Afstuderen\Documenten\Matlab\Data\
    Comparison plot\Thickness';
fileName = strjoin({width,distance,'png'},'.');
figName = fullfile(myFolder, fileName);

% SAVE ONLY IF store=1
if store ==1
saveas(figure(1),figName);
disp('Figure succesfully stored as')
disp(fileName)
elseif store == 0
end
end
```

D.4.2. LayerComp.m

```
%% Plot data
% Bas Ackermans
% 09-08-2022

% Input
   % layer: 1x3 cell
   % thickness: 1x1 struct
   %  width: 1x1 struct
   %  distance: 1x1 struct
% Output
   % data: 1x3 cell each containing a 8x3 matrix with
            % 8,1 distance in mm
            % 8,2 mean
            % 8,3 standard deviation

function[data] = LayerComp(layer,thickness,width,distance,store,n,out)

disp('Now loading: LayerComp')

%% Input variables

% make a short list of values to make loading easy

layerName =    {'x1','x2','x3'} ;
fileExt =       'mat'    ;

 %% Load data

```

```
   for ii=1:length(layer)
    strLayer = char(layer(ii));
    inputStr = {strLayer,thickness,width,distance,fileExt};      % make string from all input
    strName = strjoin(inputStr,'.');                             % Add string to one name

    Data = load(strName);                                        % load data
    data.(layerName{ii}) = cell2mat(struct2cell(Data));          % save data to data.distance
     struct
   end

%% Data analysis
% change in force value
for jj = 1:7
absDiff3_1(jj) = data.x3(jj,2) - data.x1(jj,2);                              % absolute change
relDiff3_1(jj) = ((data.x3(jj,2) - data.x1(jj,2))/data.x1(jj,2))'*100;       % relative change


absDiff3_2(jj) = data.x3(jj,2) - data.x2(jj,2);                              % absolute change
relDiff3_2(jj) = ((data.x3(jj,2) - data.x2(jj,2))/data.x1(jj,2))'*100;       % relative change

absDiff2_1(jj) = data.x2(jj,2) - data.x1(jj,2);                              % absolute change
relDiff2_1(jj) = ((data.x2(jj,2) - data.x1(jj,2))/data.x1(jj,2))'*100;       % relative change
end
%  disp(max(relDiff3_1))

 X = [absDiff2_1(1:4)',absDiff3_2(1:4)', absDiff3_1(1:4)'];
 xrel = [relDiff2_1',relDiff3_2', relDiff3_1'];

 if (out > 0 )
 xrel(out,:) = [];
 elseif (out == 0)
 end


 meanRel = mean(xrel)'
 disp(xrel)
 meanAbs = mean(X)'
 disp(X)

 %% Plot data

 yellow = [0.4660 0.6740 0.1880];
 h=[0 10 20 30 32.5 35 37.5 40]';
 h = h(n);

 f1 = fit(h,data.x1(n,2),"pchipinterp");            % Fit pchip model through data points
 f2 = fit(h,data.x2(n,2),"pchipinterp");
 f3 = fit(h,data.x3(n,2),"pchipinterp");

  figure
% plot datapoints with error bar
 e1 = errorbar(h,data.x1(:,2),data.x1(:,3),'.r','LineStyle','None','LineWidth',0.8);
 hold on
 e2 = errorbar(h,data.x2(:,2),data.x2(:,3),'.b','LineStyle','None','LineWidth',0.8);
 e3 =  errorbar(h,data.x3(:,2),data.x3(:,3),'.','LineWidth',0.8,'Color',yellow);

% plot model
 p1 =  plot(f1,'-r');
 p2 =  plot(f2,'-b');
 p3 =  plot(f3,'-');


legend([e1 e2 e3],'1 layer','2 layers','3 layers','location','northwest')
xlabel('h [mm]')
ylabel('F_e [N]')
set(p3, 'Color',yellow)

 xlim([0 h(n(end))])
%% Save plot

myFolder = 'C:\Users\Bas10\OneDrive\Documents\BMD\Afstuderen\Documenten\Matlab\Data\
```

```
    Comparison plot\Layers';
fileName = strjoin({thickness,width,distance,'3','png'},'.');
figName = fullfile(myFolder, fileName);

% SAVE ONLY IF store=1
if store == 1
saveas(figure(1),figName);

disp('Figure succesfully stored as')
disp(fileName)
elseif store == 0
end

end
```

D.4.3. WidthComp.m

```
%% Experiment 1 - Width compatison
% Bas Ackermans
% 09-08-2022

% Input
   % layer:      1x3 cell
   % thickness:  1x3 cell
   %  width:     1x1 struct
   %  distance:  1x1 struct
% Output
   % data: 1x3 cell each containing a 8x3 matrix with
            % 8,1 distance in mm
            % 8,2 mean
            % 8,3 standard deviation

function[data] = WidthComp(layer,thickness,width,distance,store,n)

disp('Now loading: WidthComp')

%% Input variables

fileExt = 'mat';
nSize = length(n);

 %% Load data

   for ii=1:length(layer)
    strWidth = char(width(ii));
    inputStr = {layer,thickness,strWidth,distance,fileExt};      % make string from all input
    strName = strjoin(inputStr,'.');                             % Add string to one name

    Data = load(strName);                                        % load data
    data.(width{ii}) = cell2mat(struct2cell(Data));              % save data to data.distance
     struct
   end

 %% Data analysis

 for jj = 1:nSize
absDiff(jj) = data.w15(jj,2)- data.w13(jj,2);           % absolute change
relDiff(jj) = (absDiff(jj)/data.w15(jj,2))'*100;        % relative change

stdDiff(jj) = (data.w15(jj,3)- data.w13(jj,3))/data.w15(jj,3)*100; %standard deviation
 end

 Mean = [mean(absDiff),mean(relDiff)];
 X = [absDiff',relDiff',stdDiff'];
 %disp(stdDiff);
 %disp(mean(data.w15(jj,2)));
 %% Plot data

h = [0 10 20 30 32.5 35 37.5 40]';
h = h(n);

```

```
f1 = fit(h,data.w13(n,2),"pchipinterp");    %fit pchip model through datapoints
f2 = fit(h,data.w15(n,2),"pchipinterp");

 figure
 % plot data points with errorbars
 e1 = errorbar(h,data.w13(n,2),data.w13(n,3),'.r','LineWidth',0.8);
 hold on
 e2 = errorbar(h,data.w15(n,2),data.w15(n,3),'.b','LineWidth',0.8);
 p1 =  plot(f1,'-r');                        % plot model
 p2 =  plot(f2,'-b');

legend([e1 e2], '12.7mm width','15.5mm width','location','northwest')
xlabel('h [mm]')
ylabel('F_e [N]')
 xlim([0 h(n(end))])
%% Save plot

myFolder = 'C:\Users\Bas10\OneDrive\Documents\BMD\Afstuderen\Documenten\Matlab\Data\
    Comparison plot\Width';
fileName = strjoin({layer,thickness,distance,'png'},'.');
figName = fullfile(myFolder, fileName);

% SAVE ONLY IF store=1
if store == 1
saveas(figure(1),figName);

disp('Figure succesfully stored as')
disp(fileName)
elseif store == 0
end

end
```

D.4.4. DistanceComp.m

```
%% Plot data
% Bas Ackermans
% 05-08-2022

% Input
   % layer:      1x3 cell
   % thickness:  1x3 cell
   %  width:     1x1 struct
   %  distance:  1x1 struct
   %  store:     variable --> 0 or 1
   %  n          vector   --> index of data points to be evaluated
% Output
   % data: 1x3 cell each containing a 8x3 matrix with
            % 8,1 distance in mm
            % 8,2 mean
            % 8,3 standard deviation
            % 8,4 Moment


function [data] = DistanceComp(layer,thickness,width,distance,store,n,out)

disp('Now loading: DistanceComp')

%% Load data

 fileExt = 'mat';

     distance2 = {'d50', 'd40','d30'};

   for ii=1:length(distance)
    strDistance = char(distance(ii));
    inputStr = {layer,thickness,width,strDistance,fileExt};      % make string from all input
    strName = strjoin(inputStr,'.');                             % Add string to one name

    Data = load(strName);                                        % load data
    data.(distance2{ii}) = cell2mat(struct2cell(Data));          % save data to data.distance
```

```
    struct

 end
%% Data analysis
% change in force value


for jj = n
absDiff30_50(jj) = data.d30(jj,2) - data.d50(jj,2);                          % absolute
    change
relDiff30_50(jj) = ((data.d30(jj,2) - data.d50(jj,2))/data.d50(jj,2))'*100;  % relative
    change


absDiff30_40(jj) = data.d30(jj,2) - data.d40(jj,2);                          % absolute
    change
relDiff30_40(jj) = ((data.d30(jj,2) - data.d40(jj,2))/data.d50(jj,2))'*100;  % relative
    change

absDiff40_50(jj) = data.d40(jj,2) - data.d50(jj,2);                          % absolute
    change
relDiff40_50(jj) = ((data.d40(jj,2) - data.d50(jj,2))/data.d50(jj,2))'*100;  % relative
    change
end

 for kk=1:3
    [Max(kk), index(kk)] = max(data.(distance2{kk})(n,2));          % find force max value
    maxDist(kk) = data.(distance2{kk})(index(kk),1);                % h for force max value
 end

 disp([Max; maxDist])
 %% Plot data
 red = [0.6350 0.0780 0.1840];          %red& yellow for free layers
 yellow = [0.4660 0.6740 0.1880];
 purple = [0.4940, 0.1840, 0.5560];     %purple, green & blue for fixed layers
 green =  [1, 0.6940, 0.1250];
 blue = [0.3010 0.7450 0.9330];

 h = [0 10 20 30 32.5 35 37.5 40]';
 h = h(n);

 f1 = fit(h,data.d50(n,2),"pchipinterp");  %fit model through data points
 f2 = fit(h,data.d40(n,2),"pchipinterp");
 f3 = fit(h,data.d30(n,2),"pchipinterp");

 figure
%plot datapoints with errorbars
 e1 = errorbar(h,data.d50(n,2),data.d50(n,3),'.','LineWidth',0.8,'Color',blue);
  hold on
 e2 = errorbar(h,data.d40(n,2),data.d40(n,3),'.','LineWidth',0.8,'Color',purple);

 e3 = errorbar(h,data.d30(n,2),data.d30(n,3),'.','LineWidth',0.8,'Color',green);
 p1 =  plot(f1,'-r');
 p2 =  plot(f2,'-b');
 p3 =  plot(f3,'-');

legend([e1 e2 e3],'d50','d40','d30','location','northeast')
xlabel('h [mm]')
ylabel('F_e [N]')
set(p1, 'Color',blue)
set(p2, 'Color',purple)
set(p3, 'Color',green)
 xlim([0 h(n(end))])
 ylim([0 20])

%% Save plot

myFolder = 'C:\Users\Bas10\OneDrive\Documents\BMD\Afstuderen\Documenten\Matlab\Data\
    Comparison plot\Fold_distance\steady state';
fileName = strjoin({layer,thickness,width,'fig'},'.');
figName = fullfile(myFolder, fileName);
```

```
100
101 % SAVE ONLY IF store=1
102 if store == 1
103 saveas(figure(1),figName);
104 disp('Figure succesfully stored as')
105 disp(fileName)
106 elseif store == 0
107     disp('Figure not stored')
108 end
109 end
```

D.4.5. LoadComp.m

```
1  %% Experiment 5 - Hysteresis
2  % Bas Ackermans
3  % 15-08-2022
4
5  % Input
6     % layer:      1x3 cell
7     % thickness:  1x3 cell
8     %  width:     1x1 struct
9     %  distance:  1x1 struct
10    %  store:     variable --> 0 or 1
11    %  n          vector   --> index of data points to be evaluated
12 % Output
13    % data: 1x3 cell each containing a 8x3 matrix with
14              % 8,1 distance in mm
15              % 8,2 mean
16              % 8,3 standard deviation
17              % 8,4 Moment
18
19 function[data] = LoadComp(layer,thickness,width,distance,store,n)
20
21 disp('Now loading: LoadComp')
22
23 %% Input variables
24
25 fileExt = 'mat';
26
27  %% Load data
28
29    for ii=1:length(distance)
30     strDist = char(distance(ii));
31     inputStr = {layer,thickness,width,strDist,fileExt};          % make string from all input
32     strName = strjoin(inputStr,'.');                             % Add string to one name
33
34     Data = load(strName);                                        % load data
35     data.(distance{ii}) = cell2mat(struct2cell(Data));           % save data to data.distance
        struct
36    end
37
38  %% Plot data
39
40   h=[0 10 20 30 32.5 35 37.5 40]';
41   h= h(n);
42
43   f1 = fit(h,data.d50(n,2),"pchipinterp");              % Fit pchip model to data points
44   f2 = fit(flip(h),data.lo(n,2),"pchipinterp");
45
46 figure
47 e1 = plot(h,data.d50(n,2),'*r');                        % plot datapoint
48 hold on
49 e2 = plot(flip(h),data.lo(n,2),'*b');
50  p1 =  plot(f1,'-r');                                    % plot model
51  p2 =  plot(f2,'-b');
52
53 legend([e1 e2],'Unloading','Loading','Location','northwest')
54 xlabel('h [mm]')
55 ylabel('F_e [N]')
56 xlim([0 h(n(end))])
57
```

```
58 %% Save plot
59
60 myFolder = 'C:\Users\Bas10\OneDrive\Documents\BMD\Afstuderen\Documenten\Matlab\Data\
       Comparison plot\Hysteresis';
61 fileName = strjoin({layer,thickness,width,'png'},'.');
62 figName = fullfile(myFolder, fileName);
63
64 % SAVE ONLY IF store=1
65 if store == 1
66 saveas(figure(1),figName);
67
68 disp('Figure succesfully stored as')
69 disp(fileName)
70 elseif store == 0
71 end
72
73 end
```

E

Experimental graphs

E.1. Experiment 1 - Width

Spring $n1, n_t1$

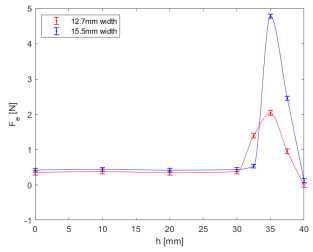

(a) *d70*

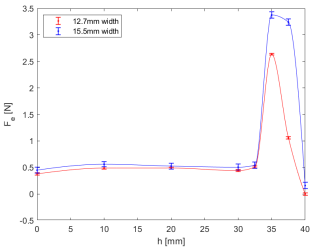

(b) *d60*

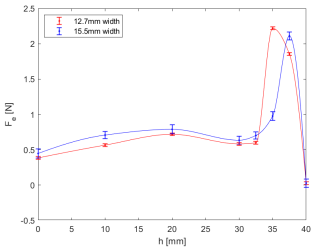

(c) *d50*

Spring $n2, n_t1$

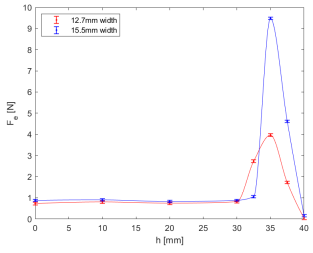

(d) *d70*

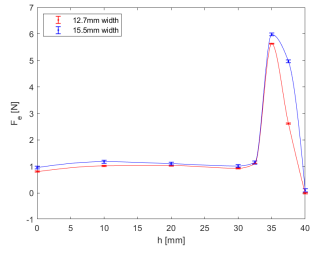

(e) *d60*

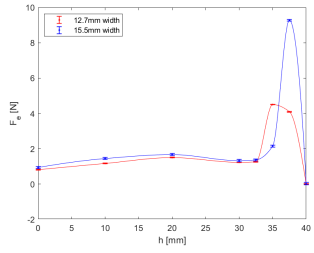

(f) *d50*

Spring $n2, n_t2$

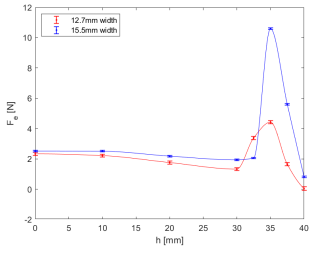

(g) *d70*

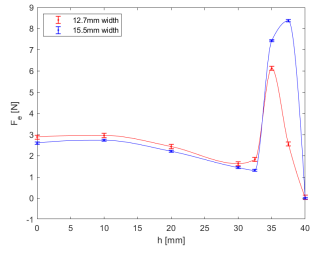

(h) *d60*

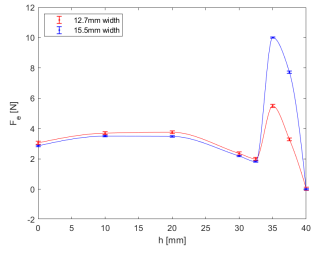

(i) *d50*

Spring $n3, n_t1$

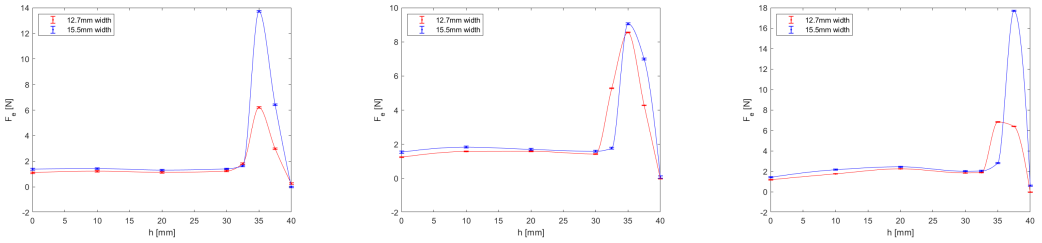

(j) *d70* (k) *d60* (l) *d50*

Spring $n3, n_t3$

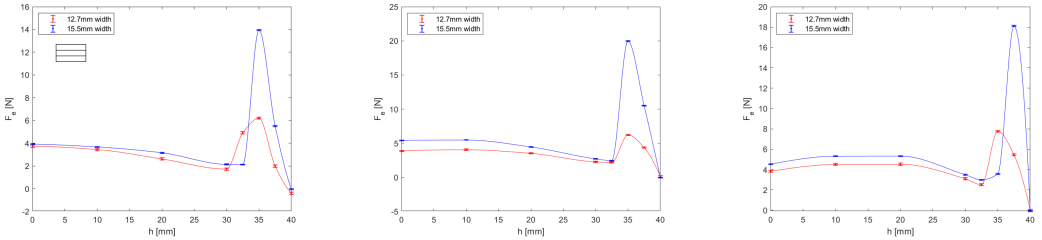

(m) *d70* (n) *d60* (o) *d50*

Figure E.1: *Force-displacement relation of two different sizes of tape springs. Where d_i indicates the fold distance, with $i = 50, 60, 70$. nj indicates the number of layers and $n_t j$ the thickness of one layer. With $j = 1, 2, 3$.*

E.2. Experiment 2 - Number of layers

Spring w1

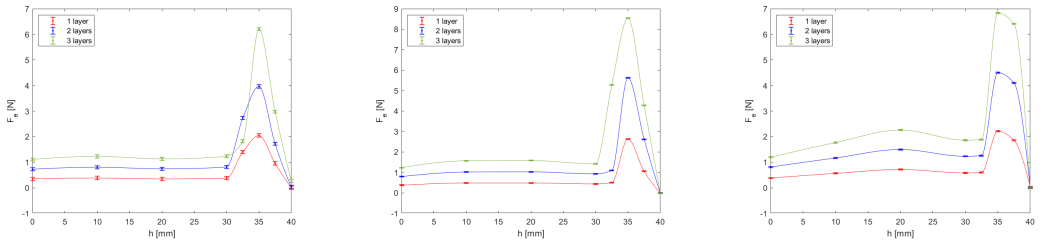

(a) *d70* (b) *d60* (c) *d50*

Spring w2

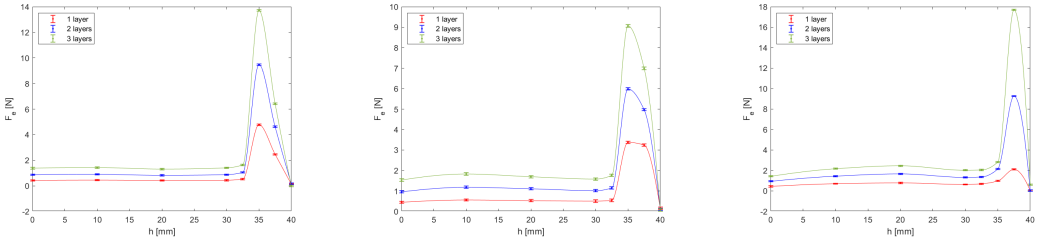

(d) *d70* (e) *d60* (f) *d50*

Figure E.2: *Force-displacement relations comparing an increasing number of free spring layers for each tape spring configuration. Where d_i indicates the fold distance, with $i = 50, 60, 70$. Spring w1 is a tape spring of 12.7mm width, spring w2 is a tape spring of 15.5mm width.*

E.3. Experiment 3 - Number of fixed layers

Spring w1

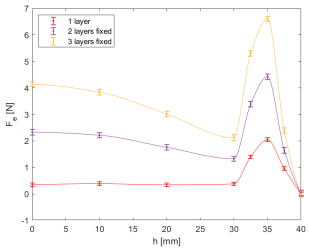

(a) *d70*

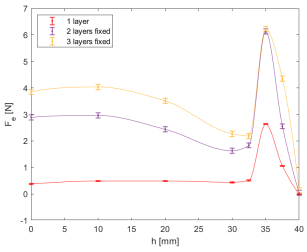

(b) *d60*

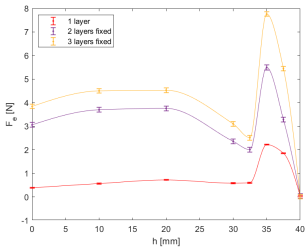

(c) *d50*

Spring w2

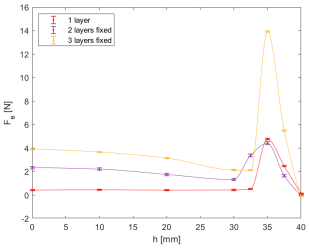

(d) *d70*

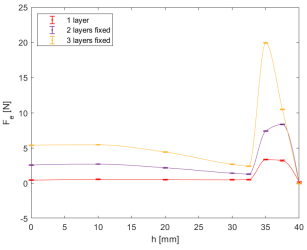

(e) *d60*

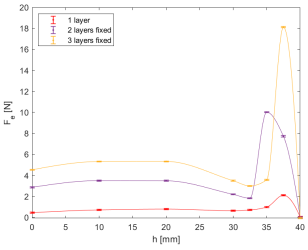

(f) *d50*

Figure E.3: *Force-displacement relations comparing an increasing number of fixed spring layers for each tape spring configuration. Where d_i indicates the fold distance, with $i = 50, 60, 70$. Spring w1 is a tape spring of 12.7mm width, spring w2 is a tape spring of 15.5mm width.*

E.4. Experiment 4 - Fold distance

$n1, n_t1$

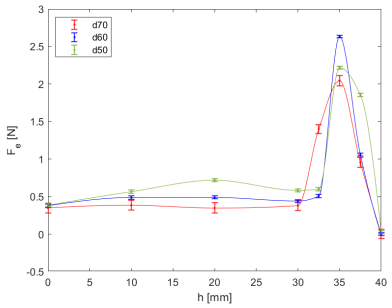

(a) *w1*

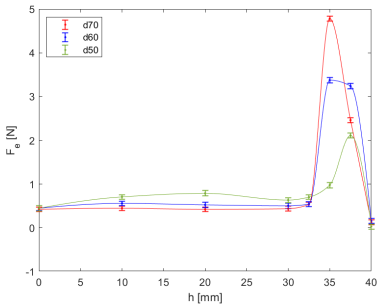

(b) *w2*

$n2, n_t1$

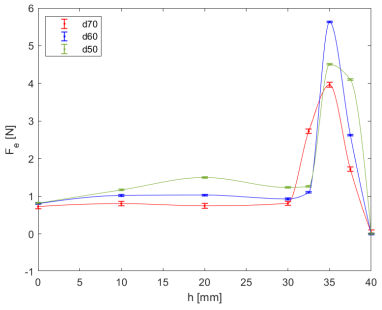

(c) *w1*

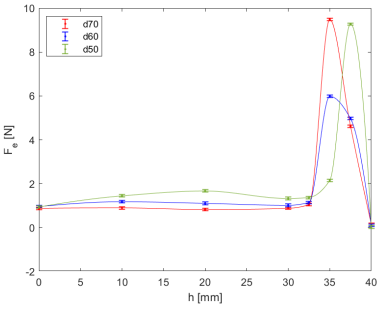

(d) *w2*

$n2, n_t2$

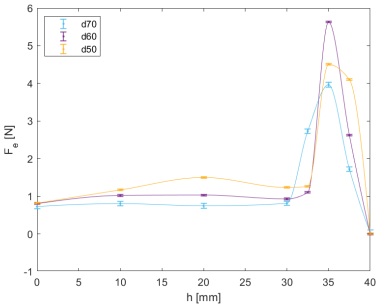

(e) *w1*

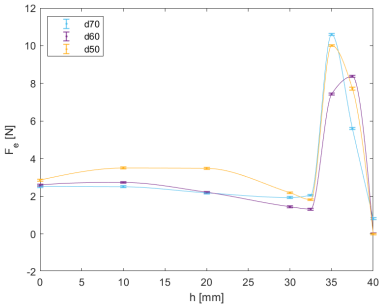

(f) *w2*

$n3, n_t1$

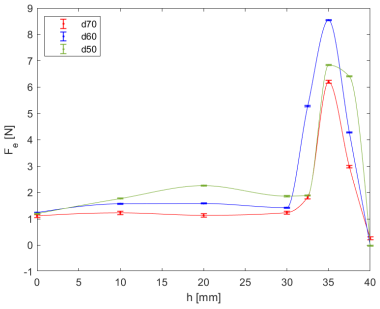

(g) *w1*

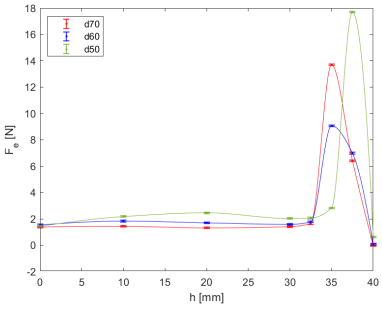

(h) *w2*

$n3, n_t3$

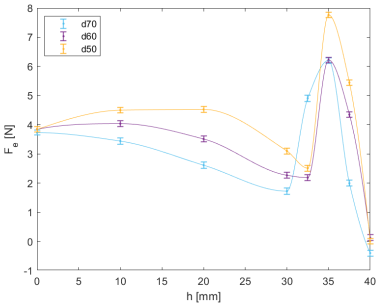

(i) *w1*

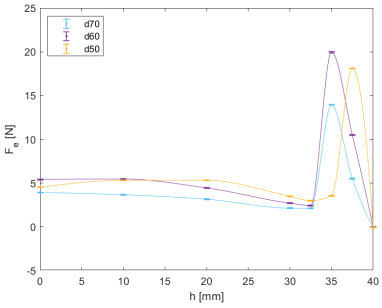

(j) *w2*

Figure E.4: *Force-displacement relationship comparing three different fold distances for each tape spring configuration. Where nj indicates the number of layers and n_tj the thickness of one layer, with $j = 1, 2, 3$. Spring w1 is a tape spring of 12.7mm width, spring w2 is a tape spring of 15.5mm width.*

E.5. Experiment 5 - Hysteresis

E.5.1. Discrete measurements

Spring $n1, n_t1$

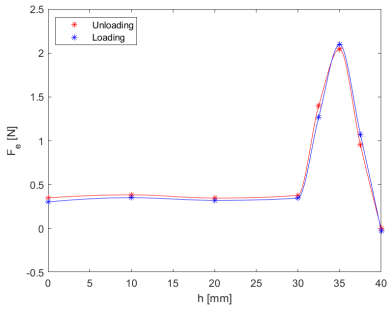

(a) *w1*

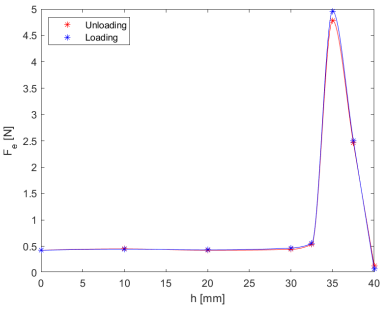

(b) *w2*

Spring $n2, n_t1$

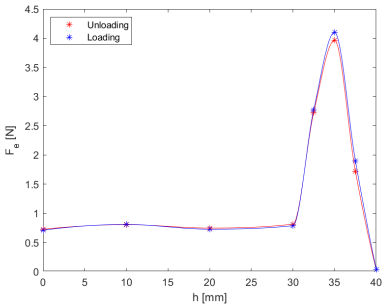

(c) *w1*

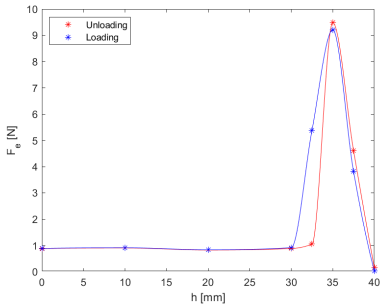

(d) *w2*

Spring $n2, n_t2$

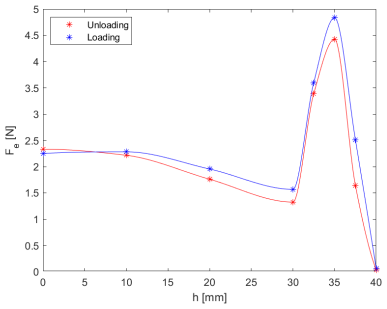

(e) *w1*

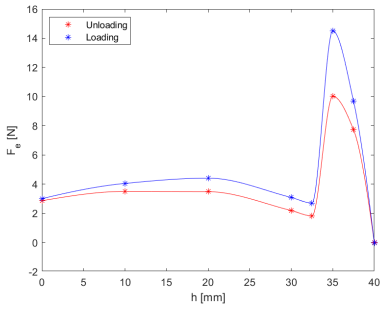

(f) *w2*

Spring $n3, n_t1$

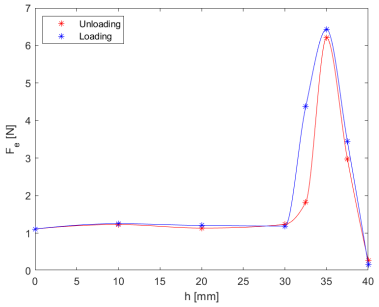

(g) *w1*

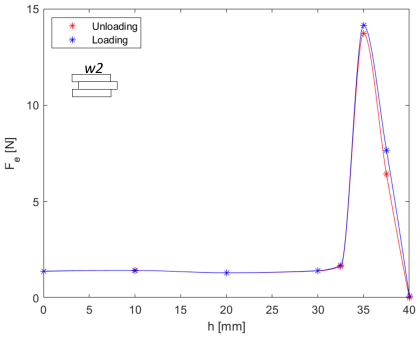

(h) *w2*

Spring $n3, n_t3$

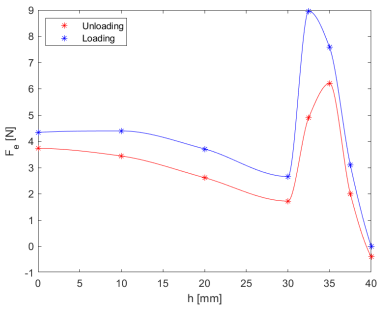

(i) *w1*

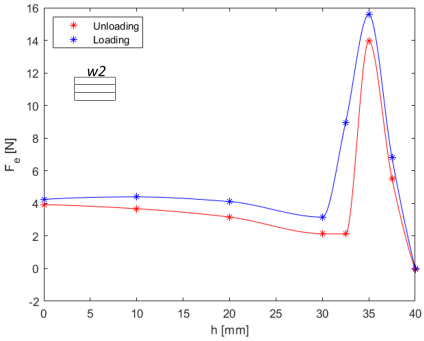

(j) *w2*

Figure E.5: *Force-displacement relationship comparing loading and unloading for each tape spring configuration in d70. Where nj indicates the number of layers and n_tj the thickness of one layer, with $j = 1, 2, 3$. Spring w1 is a tape spring of 12.7mm width, spring w2 is a tape spring of 15.5mm width.*

E.5.2. Continuous measurements

Spring $n1, n_t1$

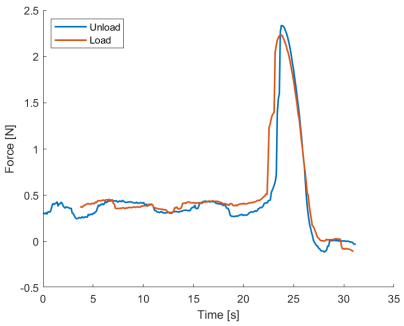

(a) *w1*

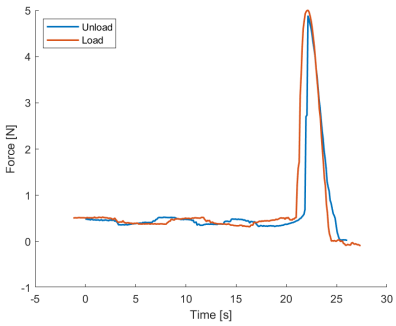

(b) *w2*

Spring $n2, n_t1$

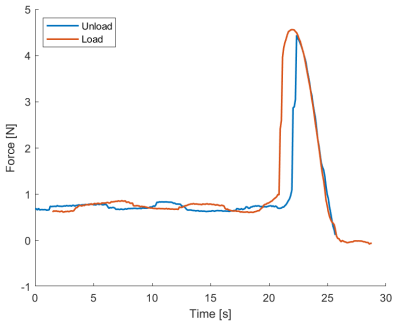

(c) *w1*

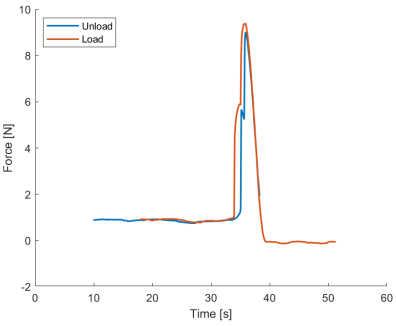

(d) *w2*

Spring $n2, n_t2$

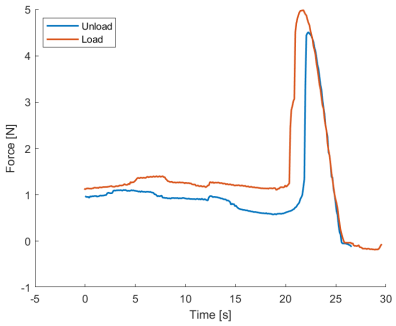

(e) *w1*

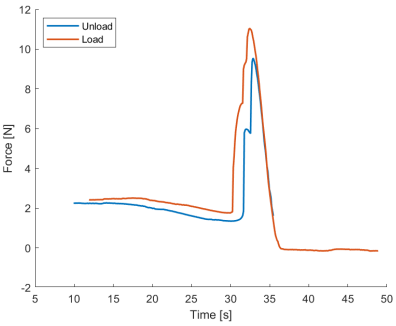

(f) *w2*

Spring $n3, n_t1$

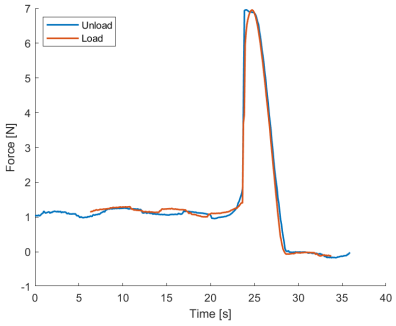

(g) *w1*

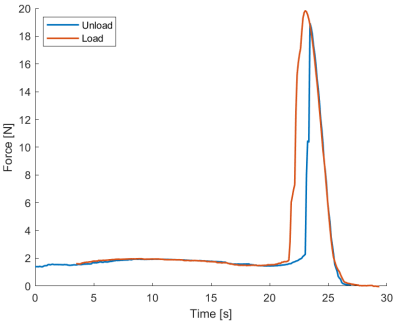

(h) *w2*

Spring $n3, n_t3$

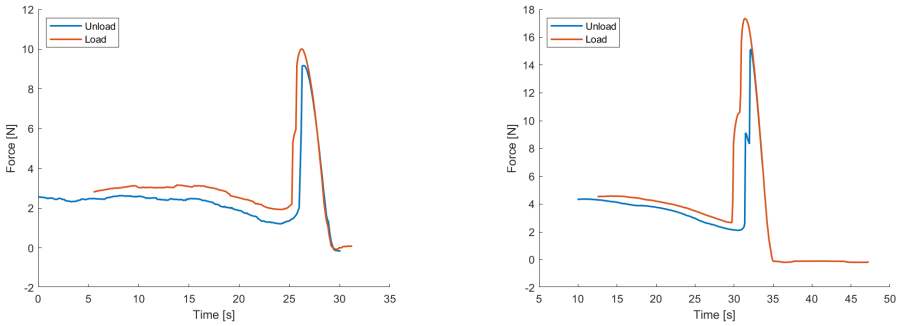

(i) *w1* (j) *w2*

Figure E.6: *Force-displacement relationship comparing loading and unloading in a continous measurement, for each tape spring configuration in d70. Where nj indicates the number of layers and n_tj the thickness of one layer, with $j = 1, 2, 3$. Spring w1 is a tape spring of 12.7mm width, spring w2 is a tape spring of 15.5mm width.*

F

Force values

.

F.1. Spring geometry

The table below illustrates the difference in elevation force between springs of different dimensions. The tape spring with largest dimensions will in generally yield the largest elevation force. However, spring $n2, n_t2$ (two fixed layered spring) shows a decrease in elevation force when the tape spring becomes larger.

Table F.1: *Mean absolute increase (mean abs) and mean relative increase (mean rel) in steady state elevation force between springs of two different dimensions. The number after n indicates the number of layers and the number after n_t indicates the number of fixed layers.*

	d70		d60		d50	
Spring	mean abs [N]	mean rel [%]	mean abs [N]	mean rel [%]	mean abs [N]	mean rel [%]
$n1, n_t1$	0.068	18.7	0.055	12.4	0.090	15.5
$n2, n_t1$	0.097	12.7	0.104	11.1	0.156	13.4
$n2, n_t2$	0.377	22.8	-0.231	-9.5	-0.203	-7.0
$n3, n_t1$	0.206	17.7	0.205	14.5	0.233	13.7
$n3, n_t3$	0.344	14.1	0.929	26.9	0.677	16.7

F.2. Number of spring layers

The relative and absolute increase in elevation force for different spring layers can be seen below. Table F.2 shows the elevation force increase in free stacked tape spring layers. The force increase can be explained by superposition and induced strain in the fold. Table F.3 shows the elevation force increase in fixed stacked tape spring layers. The force increases can be explained by superposition, induced strain in the fold and induced bending strain in the thickness of the tape spring.

Table F.2: *Mean relative increase (mean rel) and mean absolute increase (mean abs) in steady state elevation force between different number of free spring layers. Where 2-1 means the increase between the two and one spring layer(s) configuration etc.*

Free layers		d70		d60		d50	
		mean rel [%]	mean abs [N]	mean rel [%]	mean abs [N]	mean rel [%]	mean abs [N]
w1	2-1	103.27	0.41	117.45	0.50	110.43	0.62
	3-2	113.82	0.40	119.98	0.51	107.69	0.59
	3-1	217.09	0.81	237.43	1.01	218.13	1.21
w2	2-1	97.72	0.44	96.81	0.55	141.41	0.70
	3-2	106.64	0.51	105.09	0.60	140.96	0.68
	3-1	204.36	0.95	201.90	1.15	282.37	1.38

Table F.3: *Mean relative increase (mean rel) and mean absolute increase (mean abs) in steady state elevation force between different number of fix spring layers. Where 2-1 represents the increase between the two and one spring layer(s) configuration etc.*

Fixed layers		d70		d60		d50	
		mean rel [%]	mean abs [N]	mean rel [%]	mean abs [N]	mean rel [%]	mean abs [N]
w1	2-1	367.87	1.63	419.04	1.89	442.08	2.41
	3-2	235.94	1.08	181.64	0.82	132.84	0.72
	3-1	603.80	2.71	600.68	2.71	574.92	3.13
w2	2-1	398.58	1.79	303.54	1.55	336.00	2.12
	3-2	176.43	0.76	399.93	2.04	247.05	1.56
	3-1	575.00	2.55	703.46	3.58	583.05	3.68

F.3. Fold distance

The distance between the fold and the symmetry axis has a large impact on the magnitude of the elevation force. For each tape spring configuration, three fold distances where investigated. Table F.4 shows the mean elevation force at every value of h in steady state.

Table F.4: *Mean steady state elevation force for all measurements in N. Bold values are the maximum force in their row. Cells containing NaN already experienced snapback and are considered as outliers. The number of layers is indicated as the number before x, the number of fixed layers is indicated as the number after t. For example $n2, n_t2$ means two spring layers, with two layers fixed together.*

			h [mm]				
			0	10	20	30	32.5
w1	$n1, n_t1$	d70	0.349	**0.385**	0.348	0.380	NaN
		d60	0.379	0.489	0.489	0.441	**0.508**
		d50	0.385	0.566	**0.719**	0.583	0.599
	$n2, n_t1$	d70	0.726	0.805	0.747	**0.814**	NaN
		d60	0.804	1.022	1.033	0.930	**1.100**
		d50	0.815	1.169	**1.500**	1.233	1.262
	$n2, n_t2$	d70	**2.332**	2.216	1.759	1.324	NaN
		d60	2.887	**2.964**	2.439	1.630	1.827
		d50	3.057	3.698	**3.757**	2.360	2.005
	$n3, n_t1$	d70	1.109	1.228	1.134	1.235	**1.821**
		d60	1.240	1.573	**1.584**	1.425	NaN
		d50	1.194	1.771	**2.261**	1.863	1.892
	$n3, n_t3$	d70	**4.134**	3.841	3.015	2.125	NaN
		d60	3.847	**4.038**	3.513	2.269	2.187
		d50	3.840	4.500	**4.527**	3.101	2.513
w2	$n1, n_t1$	d70	0.423	0.449	0.423	0.440	**0.535**
		d60	0.449	**0.560**	0.526	0.504	0.543
		d50	0.448	0.708	**0.790**	0.635	0.702
	$n2, n_t1$	d70	0.875	0.901	0.823	0.880	**1.051**
		d60	0.957	**1.180**	1.106	1.016	1.149
		d50	0.941	1.447	**1.671**	1.327	1.373
	$n2, n_t2$	d70	**2.517**	2.506	2.182	1.933	2.058
		d60	2.598	**2.734**	2.216	1.448	1.318
		d50	2.862	**3.502**	3.485	2.191	1.823
	$n3, n_t1$	d70	1.381	1.430	1.311	1.409	**1.646**
		d60	1.533	**1.830**	1.696	1.583	1.764
		d50	1.430	2.173	**2.464**	2.022	2.055
	$n3, n_t3$	d70	3.924	3.672	3.161	2.136	2.123
		d60	5.415	5.473	4.453	2.710	2.447
		d50	4.533	5.319	5.329	3.494	2.994

G

Including peak force in the force bandwidth

One more tape spring configuration would be applicable when the peak force is included the average elevation force. It was assumed that the force would remain constant throughout the correction when the lower force boundary was determined. Therefore, the influence of the peak force was not considered for the lower boundary. As long as the peak force remains lower than the upper force boundary, the peak force can aid in increasing the correction rate after snap back.

After snap back, the peak force first causes a small instantaneous displacement (δ_{peak}). However, the elevation force does not stay constant, but decreases linearly from the F_{peak} to zero. As a result, the tape spring mechanism finds force equilibrium (F_{eq}) at an equilibrium position (h_{eq}) with the reaction force from the stiffness of the chest wall. The equilibrium position is the point where the FDR in Figure G.1 intersects the line h_{eq}.

$$h_{eq}(F_{eq}) = h_{peak} + \delta_{peak}(F_{eq}) \tag{G.1}$$

Because both F_{eq} and h_{eq} are still unknown, Equation G.1 is solved graphically. For F_{eq} is taken as a vector containing the decreasing force values from F_{peak} to zero. The equilibrium position is then the point where the FDR intersects the curve of h_{eq} in Figure G.1.

For example, spring w2 with three fixed layers has a peak force of $F_{peak} = 19.96N$ at $h_{peak} = 35mm$. Using Equation G.1, The equilibrium force equals $F_{eq} = 6.3N$ at $h_{eq} = 38.5mm$ (Figure G.1). Therefore the SCARPE implant makes a correction of $3.5mm$ "instantaneously", caused by the peak force of snap back.

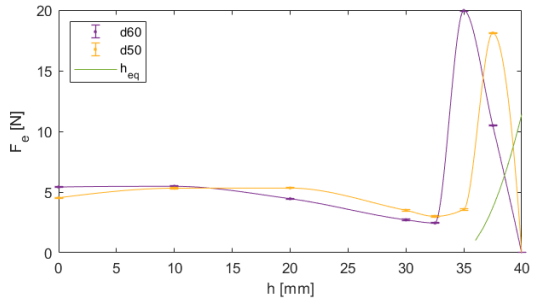

Figure G.1: *Spring w2 with three fixed layers for force distance d60 and d70. The intersection of line h_{eq} is the equilibrium height reached by the SCARPE implant after instantaneous displacement caused by the peak force.*

as a result of the peak force, the final part of the deformity is corrected faster. we assume the last five millimeters of the deformity is will be corrected in ten days. This implies that the remaining 35mm can take 720 days and still adhere to the maximum correction time of two years. We can now re-evaluate

the lower force boundary from Equation 2.7 with $d_{max} = 35mm$ and $n_{day} = 720$ days.

$$F_{min} = a_1 \frac{d_{max} * CR}{n_{day}} + a_2 \left(\frac{d_{max} * CR}{n_{day}} \right)^2 \tag{G.2}$$

The new lower force boundary, that is minimally required in steady state, is 3.61N. The slight decrease of the lower force boundary makes one more spring configuration applicable for use in the SCARPE procedure. Spring w1 with three fixed layers in d50 had an average elevation force in steady state of 3.70N. This tape spring configuration meets the lower force boundary requirements, but only by 0.09N.

H

Alternative load case

H.1. Alternative concept design

In an alternative concept we present the design of a tape spring mechanism where the spring is actuated directly. The alternative concept is schematically shown in Figure H.1. The fold lever has a fixed position and is rigidly connected to the bar-end. The length of the fold lever can only be changed during surgery to apply a patient specific entrance point. The spring used in this mechanism is a custom spring. A custom spring should be produced with a constant transverse curvature on one side and zero transverse curvature on the other side. The side with transverse curvature functions as a tape spring, used for continuous correction. After the tape spring section, the transverse curvature gradually disappears and the tape spring becomes a flexure. The flexure side is compliant in order to be placed along the bar-end curvature.

The custom tape spring can be driven by a linear actuator in the box to translate the entire spring. The proposed actuator is a spool with a magnetic ratchet mechanism. A transcutaneous magnetic pulse attracts a magnetic lever in the box and moves up one tooth of the ratchet. Retracting the custom tape spring reduces the effective length between the fold and the middle segment. Thereby increasing the perpendicular force. Moreover, the fixed fold lever causes the bending angle to decrease as well. So, both the perpendicular force and the contribution factor increase the total elevation force of the tape spring. In addition, retracting the spring will raise the sternum. Therefore this alternative concept implements both gradual correction and continuous correction.

To increase the correction rate, the sternum is imposed to a displacement step, dependent on the step size of the actuator. As a result of the displacement, the reaction forces of the sternum (F_{st}) increase. In response to the reaction forces, the pulling force of the actuator (T) loads the custom spring in tension. Figure H.2 shows a free body diagram (FBD) of the middle segment. Perpendicular force $F_{\perp}$ and T both contribute to maintain force equilibrium with F_{st} in the y-direction. The forces due to bending of the flexure itself are considered negligible. In a symmetric situation horizontal force equilibrium is automatically satisfied. The vertical force equilibrium yields:

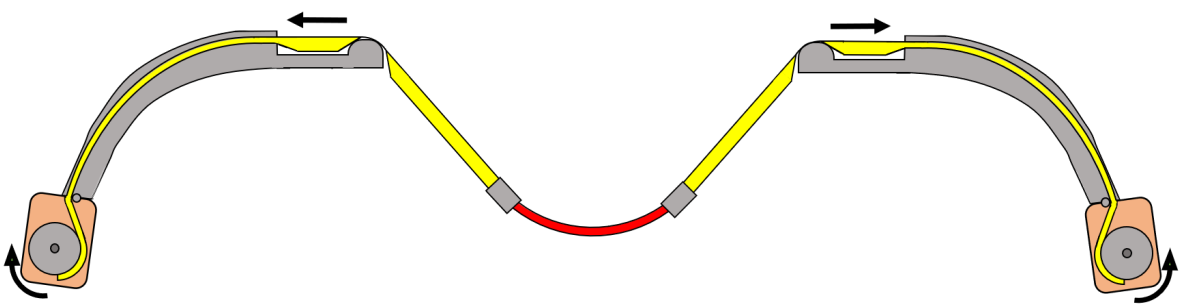

Figure H.1: *Alternative concept for changing the effective length of a custom tape spring (yellow) by actuating the spring at the box (orange) in the extremities of the implant device.*

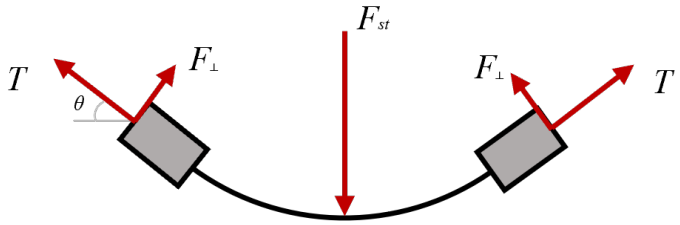

Figure H.2: *Free Body diagram (FBD) of the middle flexure, subjected to tension to raise the sternum.*

$$F_{st} = 2F_\perp cos(\theta) + 2Tsin(\theta) = F_e \tag{H.1}$$

Where θ is the bending angle between the vector T and the horizontal. Only the vertical component of T contributes to the elevation force F_e. As the bending angle decreases during correction, the contribution factor of T decreases.

Equation H.1 is only true if we assume the fold lever functions as a pulley in the system. For low friction values, large internal stresses are prevented. If no forces act on the fold, it is considered as zero stiffness joint. However, to investigate if the fold lever can be considered as a pulley, we evaluate the friction in the fold. The fixed fold lever constrains the fold from moving by imposing a normal force N and frictional force F_f. These force are assumed to be very small compared to T. Figure H.3 shows a FBD of one fold. The friction force can be calculated by $F_f = \mu N$. Where μ is the friction coefficient between two layers of coated spring steel. Normal force N can be calculated by the force equilibrium in the y'-direction:

$$F_f = 2\mu T cos(\alpha), \tag{H.2}$$

$$\alpha = \frac{\pi - \theta}{2}. \tag{H.3}$$

Where α is the angle between the vectors T and N. From Equation H.2 we can conclude the friction force increases for increasing values of T and decreases for decreasing values of θ. Using Matlab (See H.2.1), we found the mean $F_f = 0.33N$ (range, 0.16-0.49N) for $T = 15N$. The friction increased linearly during correction in friction during correction. Nevertheless, the value for F_f remains negligible small compared to T. The fold lever can thus indeed be considered as a pulley.

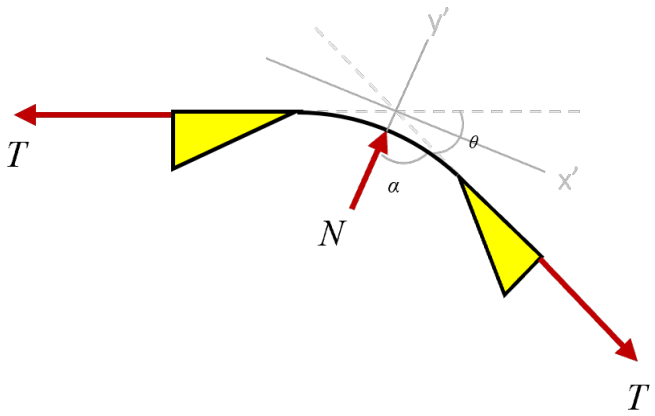

Figure H.3: *Free Body diagram (FBD) of one fold, subjected to tension to raise the sternum.*

At the start of the correction, the required T for the actuator to make one displacement step is of a manageable magnitude. However, as correction progresses, θ decreases. The required T for a step of equal size grows asymptotically. To visualize this, we found a mathematical expression for T. First we rewrite Equation H.1 for T and then substituted Equation 4.9 for $F_\perp$.

$$T = \frac{F_{st} - \frac{2M^* cos(\theta)}{\sqrt{(d-l_s)^2+h^2}}}{2sin(\theta)} \tag{H.4}$$

The reaction force on the sternum F_{st} was calculated using Equation 2.2. In a separate Matlab function, F_{st} was calculated for every displacement step in the correction (See H.2.2). The load case was selected of a 16-year-old male. Moreover, a steady state moment M^* of 40 Nmm was assumed. That is equivalent to spring w1 with three free layers. Variables l_s, h and d dimensional properties dependent on the correction. The required tension T to raise the sternum one step was calculated according to Equation H.4 and plotted in Figure H.4.

The yellow dashed line in Figure H.4 represents a hypothetical actuator that can apply maximum force of 15N to one tape spring. With one actuator per tape spring, the deformity can be corrected up to 10-15mm from the desired correction (dependent on the step size of gradual correction step). Even if high power actuators are applied the asymptotic nature of this FDR makes it effectively impossible to achieve full correction purely on gradual correction.

The benefit of this concept lies thus in the combination of gradual correction with continuous correction. The gradual correction can increase the correction speed by manually raising the chest wall, but only until the tension matches the maximum actuation force of the actuator. After the maximum actuation force is reached, the remaining deformity has to be corrected by continuous correction. The bending moment causes a constant elevation force until self-locking at the final position. The bending moment also benefits from a increased correction rate and small effective length at the end of the correction.

The alternative design presented here is a conceptual idea and has not been tested on feasibility. I invite future researchers to grasp the idea of this concept, and validate the working principle in future research. .

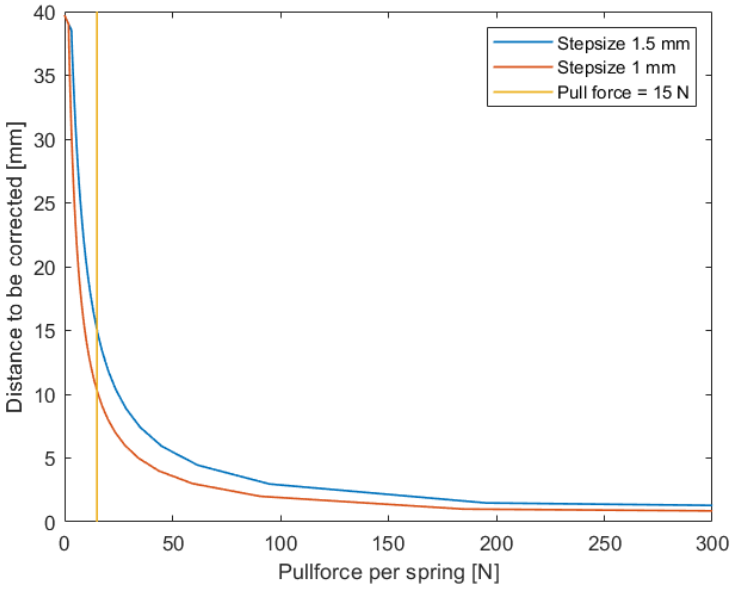

Figure H.4: *Tension required for gradual elevation of the sternum for two different step sizes. The yellow dashed line represents a hypothetical actuator with 15N pull force. The intersection between the dashed and solid line is the maximum height possible for gradual correction.*

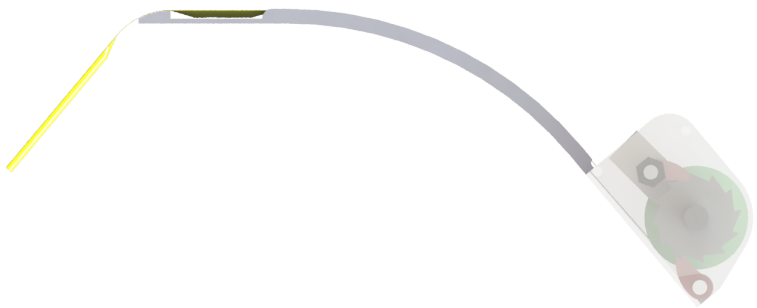

(a) *Side view*

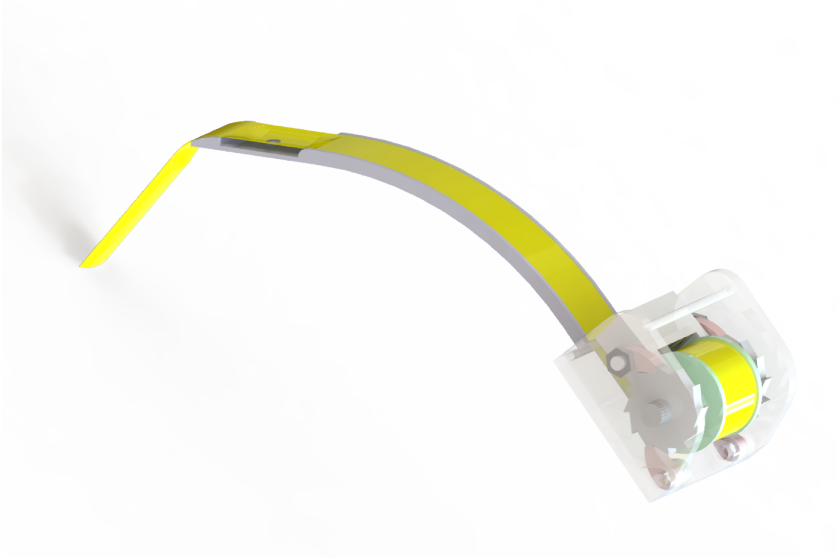

(b) *Orthogonal view*

Figure H.5: *Renders of a design proposal of one side of the alternative concept*

H.2. Matlab scripts

H.2.1. Pulltech.m

```
%% Berekeningen_pulltech
% Determination of tension in one wire pull tecnique
% Bas Ackermans
% 04-03-2022

clear all
close all

%% variables
d = 70;                     %    horizontal distance from highest point [mm]
ls = 17.5;                  %    Half of the sternum width
h = 40;                     %    pectus depth [mm]
hlin = linspace(h,0);       %    vertical distance vector [mm]
phi = atand((d-ls)./hlin);  %    tension angle
stepsize = [1.5, 1];        %   [mm]
```

```
n_step = h./stepsize;        %    number of steps
M = 20;                      %    steadystate moment [Nmm]
[F, F_step, a] = ForcesBoia16m(stepsize,h);

%% Tension in one "wire" (stepforce)

h_step = [linspace(h,0,(round(n_step(1))+1)), zeros(1,round(n_step(2)-n_step(1))) ; linspace(
    h,0,n_step(2)+1)];
phi_step = atand((d-ls)./h_step);

for jj = 1:length(n_step)
    for ii = 1:length(F_step)
    T_cont(jj,ii) = (F_step(jj,ii)-((2*M*sind(phi_step(jj,ii))) / (sqrt((d-ls)^2+h_step(jj,ii
    )^2)))) / (2*cosd(phi_step(jj,ii)));
    end
end
T_cont(isnan(T_cont))=0;
T_cont(isinf(T_cont))=10000;
%
maxF = 15;

%% Plot tension vs height

figure
plot(T_cont(1,:),h_step(1,:))
hold on
plot(T_cont(2,:),h_step(2,:))                        %Forcexdisplacement
plot((maxF*ones(1,21)),[0,1:20])
xlabel('Pullforce per spring [N]')
ylabel('Distance to be corrected [mm]')
legend('Stepsize 1.5 mm', 'Stepsize 1 mm', 'Pull force = 15 N' )
xlim([0 500])
```

H.2.2. ForcesBoia16m.m

```
%% ForcesBoia16m
% Gradual step force according to Boia et al. 2005 for a 16 yo male
% Bas Ackermans
% 07-04-2022

% Input:
% stepsize in mm. IF INPUT IS VECTOR --> biggest to smallest
% Height   in mm. Distace to correct.

% Output:
% F_fit i in N. total forces at each correction distance
% F_zeros in N. forces per step
%%
function[Fmax, F_zeros, a] = ForcesBoia(stepsize,height)
%% Fit data

x = [0 5 7.5 10 12.5 15 17.5 20 22.5 25 27.5 30 32.5 35]';
F = [0 1.8 2.8 3.8 5.0 6.5 7.8 9.3 10.5 12.5 14.3 15.93 17.8 20]'*9.8066;
a = fit(x,F,'poly2');

%% Measurings
n_step = height./stepsize;
x_fit = zeros(length(n_step),n_step(length(n_step))+1);

for j=1:length(n_step)
    x_fit(j,1:(round(n_step(j))+1)) = linspace(0,height,round(n_step(j))+1)';     %
    Displacement values [mm] for each step
    F_fit(j,:) = feval(a,x_fit(j,:));                                  % Instataneous force
    required for each displacement value
end
 F_fit(F_fit <= 0.1) = 0;

 F_step = zeros(length(n_step),n_step(length(n_step)));
 for jj=1:length(n_step)
    for ii=1:n_step(length(n_step))
        F_step(jj,ii) = F_fit(jj,ii+1) - F_fit(jj,ii);          % Force required per step [N]
```

```
35      end
36  %       Fmax(jj) = F_step(jj,(n_step(jj)));
37   end
38   Fmax = max(F_step,[],length(n_step));
39  F_step(F_step <= 0) = 0;
40  F_zeros = cat(2, zeros(size(F_step,1),1), F_step);
41
42  end
```